Reliability Based Design Optimization on Quay Walls by re-evaluating Eurocode/ re-calculating partial factors

A Dissertation

Submitted in partial fulfillment of the requirements
for the degree of

Master of Science in Geo-Engineering
by
Petros Zakynthinos

Supervisor:

Dr. ir. Luca Flessati
Dr. ir. Bram van den Eijnden
Dr. ir. Alfred Roubos
Dr. ir. Evangelos Kementzetzidis
MSc. ir. Camille Habets

Civil Engineering Department
Delft University of Technology

December 2023

To my Family

Acknowledgements

Foremost, my deepest gratitude goes to my primary supervisor, Professor Luca Flessati. His mentorship, unwavering dedication, and guidance have not only set the course for this research but have also played a pivotal role in my academic development.

I must also express my sincere appreciation to the members of the thesis committee, Professors Bram van den Eijnden and Evangelos Kementzetzidis, whose insightful feedback enhanced the rigor and comprehensiveness of this work.

Additionally, I offer my profound gratitude to Professor Alfred Roubos, whose mentorship and profound expertise in the field have been invaluable assets throughout the development of this thesis.

Special recognition is reserved for Camille Habets from Royal Haskoning DHV. His collaboration and support provided practical insights, access to essential resources, and real-world relevance, greatly enriching the research. My gratitude extends to Jelle van der Zon for his invaluable contributions as well. Furthermore, I would like to extend my appreciation to the company for their support throughout the thesis completion process.

I also want to acknowledge the invaluable assistance of Rob Brinkman from Deltares, whose immediate support with the Probabilistic toolkit software was pivotal to the successful execution of this research.

Lastly, I want to express my deepest appreciation to my friends and family. Their unwavering support, love, and encouragement have been the bedrock upon which my academic pursuits stand. Their belief in me has been a constant source of motivation.

Petros Zakynthinos
Delft University of Technology
January 6, 2024

Abstract

In the years to come, the Netherlands will face a substantial challenge as over 1,500 kilometers of aging quay walls and sheet pile walls approach the end of their technical lifespan. Infrastructure managers anticipate that the necessary replacements will necessitate investments amounting to billions of euros. Moreover, this task carries a significant environmental footprint, notably in terms of CO_2 emissions. The construction work required for these replacements will also result in disruptions and reduced accessibility, inconveniencing users.

This study addresses two pivotal aspects. Firstly, it focuses on enhancing the design aspects of new structures and optimizing costs, with a specific focus exploring how these enhancements can ease the financial challenges faced by infrastructure managers. Secondly, it investigates the safety of existing structures and explores ways to maximize their load-bearing capacity while maintaining safety standards. The expected outcomes of this study promise improved design aspects, cost-efficiency, and enhanced safety measures.

Quay walls can fail due to various mechanisms. This research investigates three primary causes: yielding of soil, yielding of quay wall and anchor yielding. Quay walls illustrate the complexities of soil-structure interaction. To address this, models were developed in both Plaxis and D-Sheet Piling. D-Sheet Piling was the preferred choice due to its computational speed. The reliability analysis was conducted with Probabilistic Toolkit. Considering the calculation methods, First Order Reliability Method (FORM) was employed, emphasizing in efficient computational results in contrast to the Monte-Carlo approach.

In the first aspect, the partial factors were recalculated and compared them with the existing EC partial factor approach. To optimize the current design methodology, the retaining height of the structure was adjusted based on its reliability index. Additionally, the maximum anchor force required was re-evaluated for the structure. This procedure has been conducted for two scenarios, considering and not considering model uncertainty. Furthermore, an analysis was conducted to understand how altering the retaining height can lead to reduced steel usage, subsequently impacting costs and CO_2 emissions.

In the second aspect, it was pursued to enhance the structure's performance by introducing a factor "n" across four distinct scenarios: 1. Simultaneously increasing all

loads. 2. Increasing the surcharge loads on the terrain. 3. Increasing the bollard load. 4. Raising the final excavation level in front of the quay wall.

While this study aligns with the extensive body of research in the field of civil engineering, It seeks to offer a new and sustainable approach on understanding quay wall design, focusing specifically on the designers' viewpoint. Through the exploration of innovative design frameworks and approaches, this research seeks to make a valuable contribution to the long-term sustainability of quay wall structures. It aims to redefine our approach to accessibility and safety in these crucial structures. The comprehensive investigations conducted throughout this study provide an enhanced comprehension of quay wall design, reliability, and the optimization of performance.

Table of Contents

List of Figures

List of Tables

1

Introduction

Quay walls refer to earth-retaining structures where ships can berth, typically equipped with bollards serving as anchor points for mooring and fendering systems that absorb impacts from the vessels (Figure 1.1).

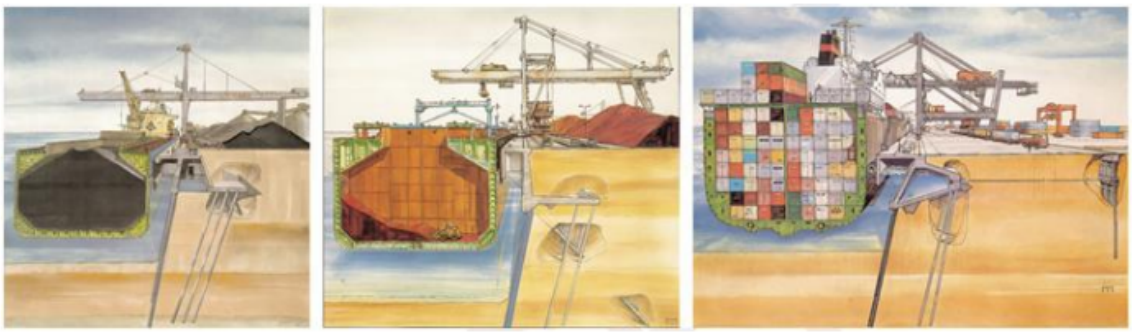

Figure 1.1: Typical quay walls in the Port of Rotterdam. Source: Adapted from Post et al. (2021).

Quay walls are used for commodities transshipment by cranes or heavy equipment, which are moving alongside the ship. This superstructure must be robustly constructed and must meet a variety of constraints imposed by soil conditions, water levels, ship size and loads. Alongside the construction of the quay wall, it is common to install a rail system to facilitate crane operations, as well as channels for the cables that provide power to the cranes. The foundation must ensure adequate safety and stability to support all the earlier considerations. (De Gijt and Broeken, 2013) .

1.1 Significance of Reliability Analysis

Probabilistic reliability analysis offers a multitude of benefits for evaluating geotechnical structures, applicable to both the design of new structures and the evaluation of pre-existing ones:

- Ensuring a consistent approach in addressing various uncertainties.
- Enhancing precision by integrating supplementary data.
- Adequately addressing system-level reliability considerations.

Utilizing these methodical advantages results in more precise reliability evaluations and facilitates cost-effective designs for new structures. Moreover, it enables the potential extension of the service life for existing structures and justifies modifications in their functional use. A specific area where these benefits are applicable is the assessment of quay walls, particularly existing ones. In the field of quay-wall engineering, addressing various uncertainties is essential to ensure the safe and efficient serving of vessels throughout their operational lifespan (Post et al., 2021). While the development of new port infrastructure continues, the emphasis is now shifting towards the maintenance, repair, rehabilitation, and adaptation of existing structures within fully operational terminals (Roubos, 2019).

In the coming years, many quay walls worldwide will need to be assessed for potential extended service life. Existing simplified design methods often suggest that extending the life of these structures is not possible. However, experts in marine structures believe that there could be hidden safety in the failure modes of quay walls. Identifying and utilizing this potential remains a challenge. One solution is to assess critical structural components using reliability-based methods (Phoon and Retief, 2016).

The current reliability level of the majority of existing quay walls remains uncertain. This is primarily due to the limited practical implementation of reliability-based assessments in quay-wall engineering and the absence of a suitable probabilistic framework tailored to their unique risk characteristics. As time progresses, the need for these advanced analyses is expected to rise, especially as numerous quay walls require reassessment and computation times continue to decrease (Post et al., 2021). In the near future, the anticipated second generation of Eurocode 7 is expected to incorporate more explicit reliability-related elements compared to its predecessor (ERTC10: Evaluation of Eurocode 7, 2021).

1.2 Previous Research on Quay Wall Reliability

Due to their complexity, which includes retaining walls, anchors, soil, and marine environment, quay walls pose complex soil-structure interaction challenges. Especially, given the uncertainties associated with crucial assumptions in geotechnical engineering, such as the characteristic strength properties of soil (Fenton et al., 2016). In such cases, structural and geotechnical evaluations are typically conducted using semi-probabilistic methods, frequently relying on finite element modeling. However, a more organized approach to address uncertainties can be conducted with reliability based assessments (Phoon and Retief, 2016). However, integrating reliability assessments based on finite element methods into quay wall engineering encounters challenges in terms of efficiency and robustness. Particularly, establishing a robust connection between probabilistic techniques and finite element models remains a complex task, given the complex and nonlinear nature of soil behavior. While some studies (Adel, 2018) ; (Schweckendiek et al., 2012) ; (Teixeira et al., 2016) ; (Wolters, 2012) ; (Rippi and Texeira, 2016) ; (Roubos et al., 2020) ; (Wel, 2018) exhibiting favorable results for quay walls and other soil-retaining structures, many of these studies opt for simplified models to ease computational demands.

1.3 Research Questions

This thesis aims to assess the accuracy of the current design approach for quay walls, which accounts for soil uncertainty and other forms of uncertainty using partial factors. The objective of the thesis is to analyze the impact of soil parameter uncertainties and partial factors on quay wall design, with the ultimate goal of improving design efficiency, safety, and sustainability while minimizing costs.

The objective of this thesis is to investigate target reliability values for a quay wall structure in the Eurocode framework. The following set of questions has been formulated as part of the research to be conducted:

1. How can reliability-based analysis be used to optimize a modern Quay Wall design, and what are the key considerations in reliability-based design?

2. How can a semi/full probabilistic design approach be implemented in the Eurocode framework.

3. How do the results obtained from the probabilistic design approach compare to the current EC partial factors approach, and what are the differences in the design results obtained from the two approaches?

4. How can we improve the current design during the design phase to achieve cost optimization? Furthermore, what alternatives are available for further refining the existing structure to maximize optimization potential?

In order to understand completely the topic, the following sub-questions should be also answered:

a. How were the partial factors derived in the Eurocode for quay walls, and what simplifications were used in the derivation process?

b. Which parameters have the most significant influence on the design, and how are they correlated?

c. What practical improvements can be implemented in engineering practices to enhance reliability in quay wall designs?

d. To what extent can the design be enhanced to provide more sustainable solutions?

1.4 Outline

In the current sub chapter the outline is going to be introduced. The structure of the thesis is depicted in Figure (1.2).

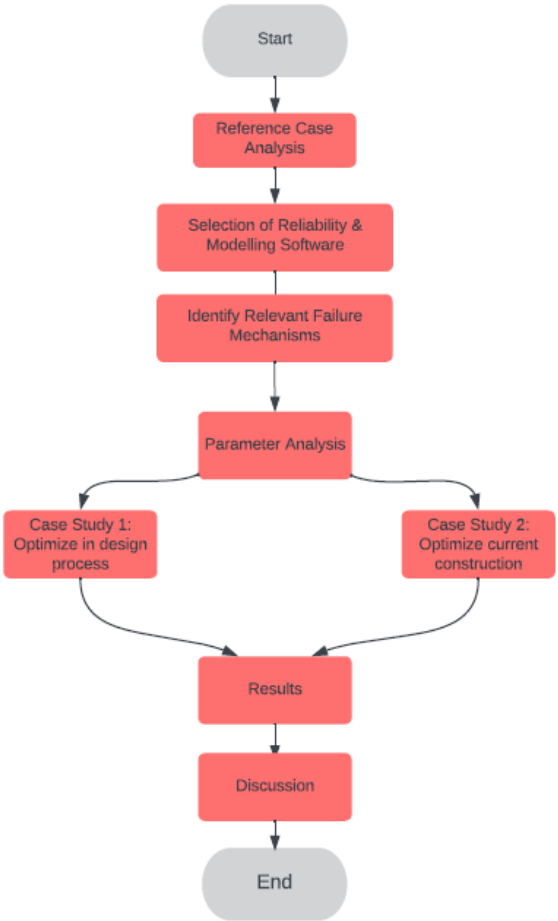

Figure 1.2: Research Methodology Flowchart

Chapter 1 serves as the foundation for this thesis, providing an introduction to quay walls in civil engineering. Emphasizing their significance, it explores the need for reliability analysis and reviews prior research on quay wall reliability. The chapter sets up the core research questions of the thesis.

Chapter 2 delves into the theoretical framework, focusing on quay walls in the Port of Rotterdam. Their functions, classifications, and structural components are been examined. The chapter covers design methodologies and finishes with an analysis of limit states.

Chapter 3 explores the theoretical basis of reliability-based design, introducing levels of design and uncertainties in geotechnical Engineering. It addresses the concept of partial factors in Load and Resistance Factor Design (LRFD), failure probability, reliability indices, and computational methods, namely First Order Reliability Method (FORM). It also introduces design codes, including Eurocode and Dutch Standards.

In Chapter 4 the main design aspects of the case study are been introduced, considering soil parameters, hydraulic conditions, loadings, and structural components. Then the modelling process of the structure is been compared for two modelling software, Plaxis and D-Sheet Piling to determine the optimal choice for the research.

Chapter 5 provides the research methodology, explaining how partial factors are derived and introducing the limit state equations. Then the distribution functions and the correlations are been established. The chapter ends by establishing the final model, which will be subjected on the reliability analysis.

Chapter 6 explores optimization in the quay wall in the design as well in post-construction performance phase.

Chapter 7 concludes the thesis, providing recommendations for future studies.

2

Theoretical Background on Quay Walls

This chapter delves into the prevailing understanding of quay walls, encompassing their design features and potential failure mechanisms. To enhance comprehension of the case study, we will engage in a brief discussion on the evolution of quay walls within the port of Rotterdam. This will be accompanied by a concise overview of the primary structural elements and the methods utilized for calculations as well as a brief analysis on the limit states.

2.1 Port of Rotterdam- Development and Challenges

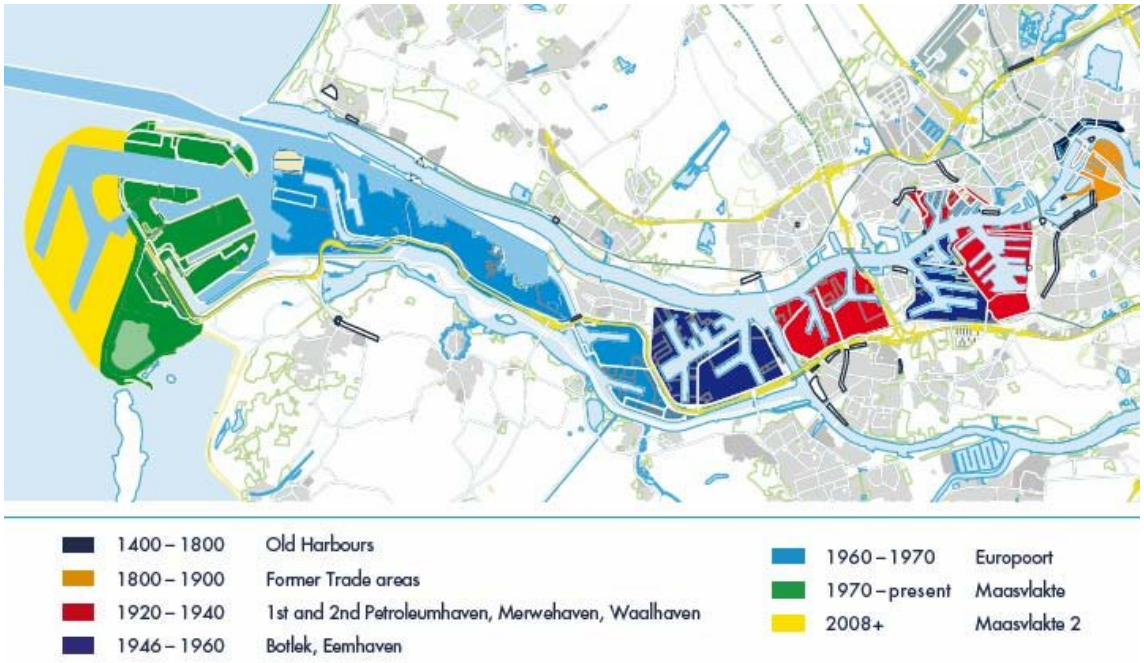

Figure 2.1: Historical Development of Rotterdam Port and its industrial complex. Source: Adapted from De Gijt et al. (2010).

The Rotterdam port and industrial complex Figure (2.1) holds immense economic significance. As of 2021, the Rotterdam-Rhine Estuary seaport region contributed approximately €24.40 billion in added value, encompassing indirect backward effects. This substantial contribution accounts for about 2.8% of the entire Dutch GDP, supporting 183.004 full-time equivalent employments within the Rotterdam-Rhine Estuary seaport sector. Notably, the complex is actively committed to expediting sustainability efforts across various fronts, including the reduction of carbon emissions, promotion of circular practices, and enhancement of air quality throughout both project planning and operational phases (Port of Rotterdam, 2023). Consequently, optimizing structure designs emerges as a pivotal necessity.

To keep the natural expansion possible it is necessary to adapt the design of port facilities, quay walls, and the loading and unloading facilities to these changing requirements (De Gijt, 2010). The magnitude of ships destined to utilize the port significantly shapes the design considerations for its existing and new quay walls structures. It is natural that the deeper the draught of the ships, the higher the retaining height of the quay walls. Whereas, the usage of bigger ship's engines would conclude in higher erosion in the front of quay walls, during its mooring. Nevertheless, the loads and transshipment methods also change through the years. Consequently, the cumulative effect has been a progressive escalation in the demands placed on both quay walls and terminal zones. This reality prompted the ongoing deepening of the Port of Rotterdam and necessitated the shifting of the port area seawards to accommodate these increasing demands (De Gijt and Broeken, 2013).

In Figure (2.2) it is illustrated the significant correlation between ship size expansion and the notable augmentation in water depth,

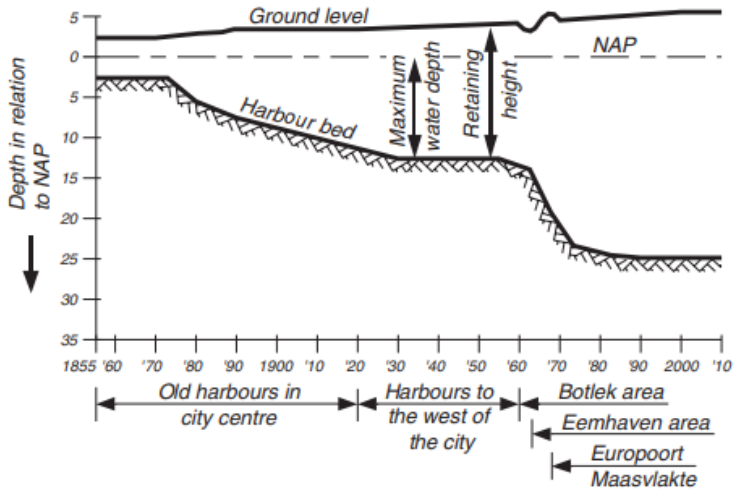

Figure 2.2: Progressive Evolution of Water Depth in the Port of Rotterdam over time. Source: Adapted from De Gijt (1999).

consequently resulting in a considerable rise in the required height of quay walls. While historical city harbors of the 19th century rarely exceeded depths of 10.00 m, the Botlek harbors, established during the 1960s, underwent dredging operations reaching depths as profound as NAP - 16.00 m. The creation of Europoort and the Maasvlakte involved excavations that reached even greater depths, further increasing to NAP - 23.00 m (De Gijt and Broeken, 2013).

In order to get a better representation for the maximum draught which should be implemented an illustration is shown in Table (2.1).

Table 2.1: Max draught of container ships development. Source: Adapted from De Gijt and Broeken (2013).

Name	Period in Years	Max Draught (m)
1st generation	End '60	9.00
2nd generation	'70ies	10.50
3rd generation	Begin '80ies	11.50
4th generation	Mid '80ies	12.50
Post Panamax	After '90	13.50
6th generation	End '90ies	14.52
New Panamax	After 2010	15.20
CMA Marco Polo	2012	16.00
Maersk Triple E	July 2013	14.50
Future	After 2013	16.50

2.2 Quay Walls - Functions and Main Types

2.2.1 Quay Wall Functions

- **Freight Handling Function:** : A quay wall should provide accessibility and efficient freight handling. The cranes, trains, and trucks should be able to approach the vessel with ease, simplifying the process of cargo management. To accelerate freight handling, the design incorporates both existing and potential considerations. These encompass: the demand for future uses, the demand of local conditions, nautical demands, whereas also the future development in cargo storage, transshipment techniques, navigation and vessel dimensions.

- **Retaining Function:** : The quay wall establishes a clear distinction between the soil and water. It provides an option in order to save space when compared to a slope, since it can create a big surface level difference between the two sides. This imposes a substantial horizontal load on the quay structure to retain the soil mass. In addition, it can be part in water retention and play a role in flood protection systems, during periods of elevated water levels.

- **Load Bearing Function:** : Along the face of the quay wall, continuous port activities such as vessel loading, unloading and adjacent goods storage are in progress. This predominantly gives rise to vertical loads applied to both the quay structure and the adjacent soil. The quay wall is required to effectively support these applied loads, ensuring the safety and integrity of port operations.

2.2.2 Quay Wall Main Types

- **Gravity walls**: This type of structure relies on its own weight, often involving the soil mass above, to achieve its retaining purpose. Noteworthy examples include block walls, L-walls, caisson walls, cellular walls, and reinforced earth structures.

- **Sheet pile walls**: Characterized by soil pressure and anchoring systems, sheet pile walls have a soil retaining function, along with resisting bending moments and lateral forces. Varieties constitute of anchored sheet piles, combined walls, diaphragm walls, and cofferdams.

- **Structures with relieving platforms**: Essentially an extension of sheet pile wall concept, these structures incorporate relieving platforms to significantly reduce forces on the underlying retaining wall and tensile stresses within the foundation. Such structures can be categorized based on the presence of either a high relieving platform or a deep relieving platform.

- **Open berth quays**: Similar to jetties, these structures consist of a deck supported by piles, extending across a slope.

In the process of designing a quay wall, the designer needs to select the most suitable structure type. This is influenced by a variety of influential factors, among which the most significant include:

- Geological characteristics
- Retaining height of structure
- Imposed structural loads
- Feasibility of construction

Due to the specific local boundary conditions, particularly the presence of weak soil layers within the Rotterdam region, a sheet pile wall type of quay wall emerges as the most favorable choice. Furthermore, by coupling it with grout anchors to mitigate horizontal loading on the sheet pile wall, the system proves to be cost-effective and relatively easy to install. However, challenges arise with larger retaining heights (>15.00

m) and heavier surcharge loads. These issues include concerns about constructability, resistance to bending moments, and the vertical bearing capacity of sheet piles. Figure (2.3) presents a comprehensive overview and visual representation of the potential failure modes associated with a sheet pile quay wall. The ability to drive sheet piles is limited to around

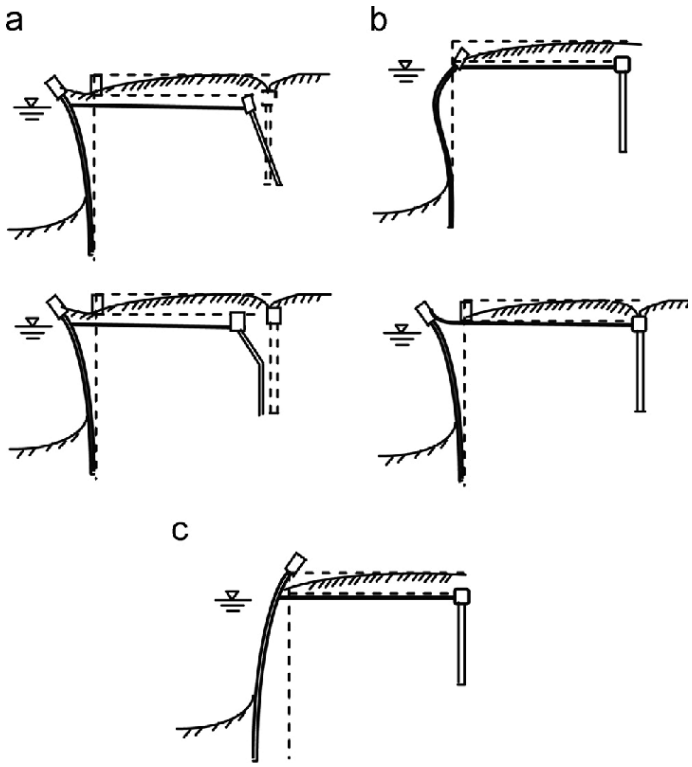

Figure 2.3: The modes of failure for a sheet pile quay wall, (a) deformation or failure at the anchor, (b) failure at the sheet pile wall or tie-rod, and (c) failure at the embedment. . Source: Adapted from Zekri et al. (2014).

30.00 - 35.00 m, beyond which the risk of interlocking failure and sheet pile damage increases significantly (Korff, 2018). To address these challenges, a solution involves using combined-walls, coupled with already mentioned grout anchors. Important to keep in mind, is that combi-walls have also their limitations, particularly for retaining heights exceeding 20.00 m, whereas a much more complex structure would need to be implemented, that of a combi-wall with a relieving platform.

2.2.3 Sheet pile wall components

2.2.3.1 Combined Wall

A combined wall consists of robust primary elements that are deeply embedded in the underlying soil at a specified intervals. These principal elements transfer forces to the anchoring system and subsoil. Between these main elements, a seal composed of standard steel sheet piles, which are interconnected through welding, is introduced. These intermediate sheet piles may have shorter lengths compared to the main elements, as soil

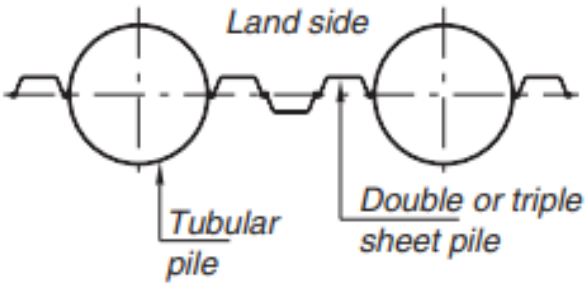

Figure 2.4: Cross-section of a tubular pipe combined wall. Source: Adapted from De Gijt et al. (1993).

pressure is transmitted to the main elements through an arch action. As also illustrated in Figure (2.4) in this system circular, open, high-quality steel tubular piles are employed as the main elements. Tubular piles are advantageous both in terms of construction and cost-effectiveness. The use of these piles became feasible thanks to advancements such as welding interlocks onto them. Additionally, the ability to produce tubular piles from steel coils through automated spiral welding further enhanced their applicability. An alternate approach involves constructing the main elements using sections of tubular piles that have been welded together, with wall thickness adapted to moment distribution. This construction method presents economic viability. The open tubular piles can be relatively easily be installed through vibration or driven through compact sand layers. The dimensions of intermediate piles are determined not only by the applied loads but also by the forces generated during the vibration or pile driving process (De Gijt and Broeken, 2013).

2.2.3.2 Grout anchor system

Grout anchors serve as essential tension elements, comprising a steel rod or a bundle of wires encased in a high-pressure grout cover. These prestressed anchorages consist of an anchor head and a tendon, with a portion bonded to the ground through injected pressurized grout (De Gijt and Broeken, 2013). Grout anchors must undergo pre-stressing, as the substantial stress levels in the anchor rod could otherwise lead to significant deformations in the sheet pile wall. The pre-stressing process is conducted incrementally until the force aligns with the design value (Korff, 2018). Designing anchors requires accounting for ground corrosion influenced by factors like soil acidity, salinity, and the anchorage position relative to the phreatic level. Except for high-strength prestressed steel, the primary method to protect anchors from corrosion involves adding extra steel thickness, termed 'corrosion allowance' for typical rods or employing double corrosion protection for high tensile steel strand anchors. Tensile strength derives from the interaction between the grout body and soil, relying on friction (De Gijt and Broeken, 2013). In cases where the tube's lower end

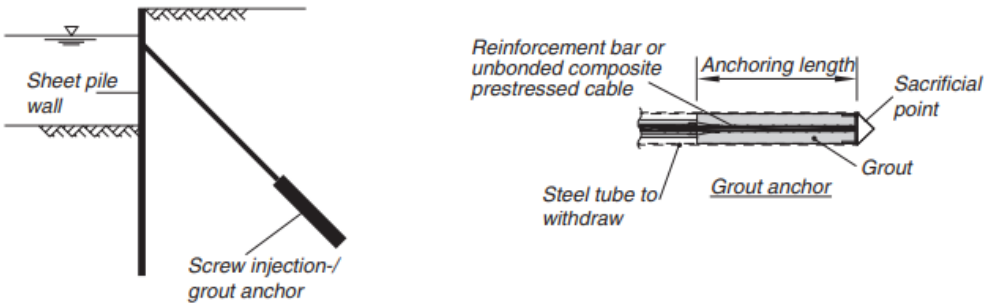

Figure 2.5: Cross-section of an anchor with grout body. Source: Adapted from De Gijt and Broeken (2013).

lies within a sand layer experiencing elevated water pressures, precautions are taken to prevent upward grout displacement upon tube removal. This can significantly decrease the density of the sand layer , potentially affecting the maximum bearing capacity.

Grout anchors can be installed through either driving or drilling methods, each impacting the extraction force of the anchor (Korff, 2018). Additionally, the specific requirements are outlined in Figure (2.6).

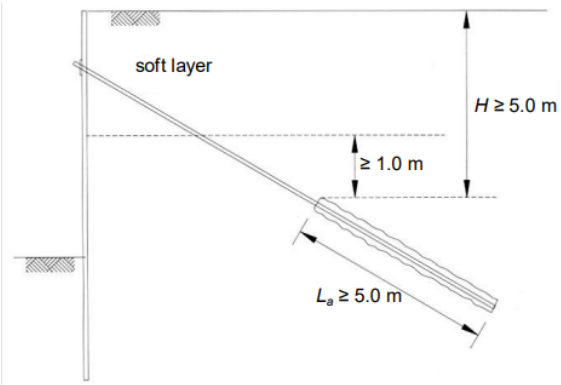

Figure 2.6: Specifications regarding the depth of the grout body. Source: Adapted from CUR (2012).

2.3 Quay Walls Calculation Methodologies

Various approaches are available for computing the theoretical response of quay walls in consideration of soil-structure interaction. This section outlines three primary methodologies: analytical modelling, spring models, and finite element modeling (FEM).

2.3.1 Analytical Modelling

The most widely used analytical model for analyzing retaining walls is the Blum method (Blum, 1931). Blum's approach is employing a conceptual framework related

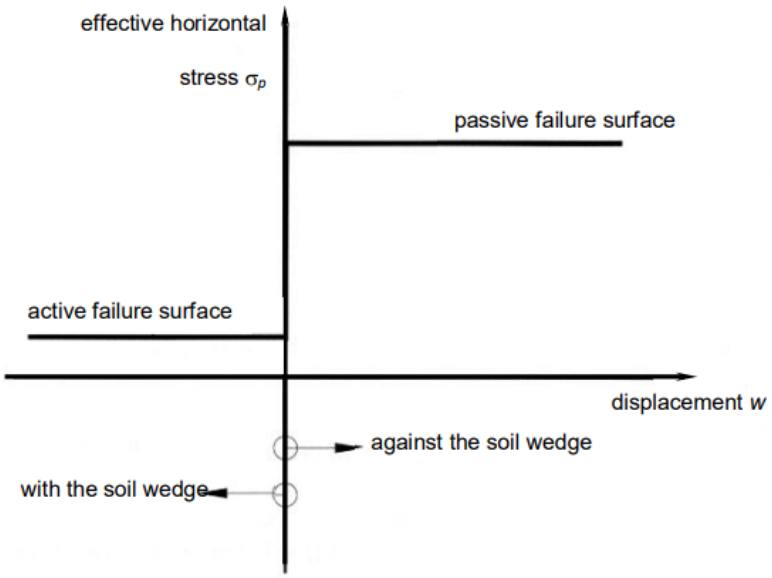

Figure 2.7: Soil pressure-displacement diagram in accordance with Blum. Source: Adapted from Blum (1931).

in beam theory, where a retaining wall and the surrounding soil is represented. This conceptualization establishes a statically defined system and a calculation approach, in which limit equilibrium around the retaining wall is assumed. The limit equilibrium of the retaining wall is established through the straight failure surfaces found in both the active and passive zones. In areas of activation, the retaining wall is subjected to soil pressure, while in passive zones, the soil reacts to the structure's pressure. Coulomb's theory is employed to determine the earth pressures in these zones. The lateral distribution of active and passive earth pressures governs the wall's displacement and deflection, ultimately leading to a distribution of bending moments or rotation around the base. Blum's method offers several advantages due to its simplicity and extensive validation. It serves as a valuable tool for comprehending the mechanics of retaining walls and conducting rapid preliminary calculations to estimate penetration depth. However, the method has limitations, including its inability to accurately predict displacements and deformations. It also disregards the influence of construction phases. Consequently, it is not typically applied in final design stages, where most sophisticated calculation methods allow for the consideration of additional factors, leading to enhanced designs and optimization opportunities.

2.3.2 Spring Method Modelling

Spring-supported beam methods find primary application in the analysis of simple quay walls. This model characterizes soil behavior through uncoupled (non)-linear springs. In this framework, piles are depicted as beams supported by springs, where its initial development can be attributed to Winkler and Zimmerman (Hetényi and Hetbenyi, 1946).

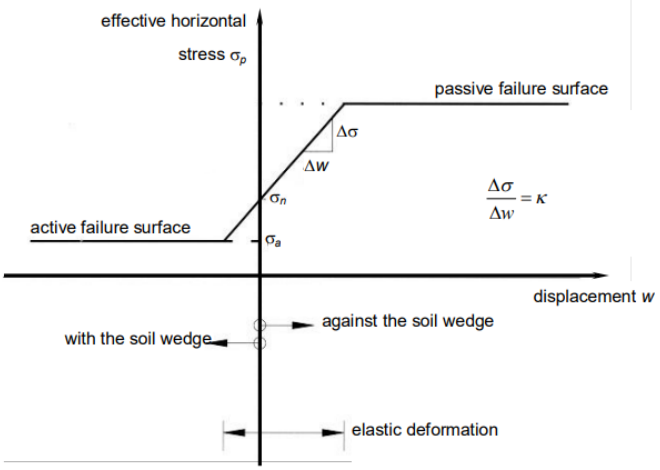

Figure 2.8: Soil pressure-displacement diagram in accordance with spring supported beam. Source: Adapted from Korff (2018).

These models are attributed in Equation (2.1).

$$E\frac{\partial^4 w}{\partial x^4} + k(x,w)\cdot w = f(x) \tag{2.1}$$

This equation establishes a connection between lateral deflection and the position of the structure, taking into account factors such as the beam's rigidity (bending stiffness), the response of the elastic foundation or soil (including the modulus of subgrade reaction), the presence of spring supports (earth springs and elastic anchors), and the influence of external loads.

Non-linear behavior and also heterogeneous soil can be modelled through the utilization of the p-y curve. In Figure (2.9) such a schematization is depicted. In this curve, 'p' represents the soil reaction per unit length, while 'y' indicates the displacement between the pile and the soil. Each spring has its own p-y curve, the value of which are dependent on factors such as depth, soil properties, and dimensions of the pile (Hemel et al., 2022).

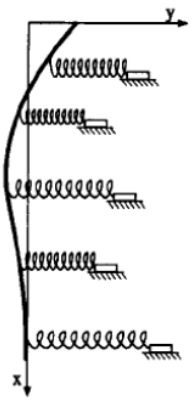

Figure 2.9: Model depicted as elastic line. Source: Adapted from Perumalsamy et al. (2015).

Employing this method confers several primary benefits (De Gijt and Broeken, 2013), including reduced computational times, a user-friendly interface, fully integrated safety approaches, clear soil profile representation and results that are readily verifiable. Also in its advantages this approach enables the incorporation of construction phases, can accommodate multiple anchors, offers an understanding of the normal forces exerted on the retaining wall, and establishes a heightened accuracy in the relationship between soil reaction and pile displacement. This improved precision is a result of the earth pressure envelope deriving from the elastic phase of the spring characteristic, which is influenced by the deformations and deformation direction of the sheet pile wall (HTG, 2015).

In its limitations the connection between earth pressure on the sheet pile wall and the wall's elastic displacement relies on the horizontal coefficient of subgrade reaction. This connection is commonly assumed to be linear within the elastic interval. So the soil's behavior is depicted using unlinked springs, simplifying the actual soil behavior considerably. Since the springs in the soil are assumed unlinked, the effects of arching, as described in HTG (2015) are not automatically taken into account. The horizontal coefficient of subgrade reaction is influenced by the loaded area's size, which inherently relates to the sheet pile wall's flexural rigidity and stress level. Also, calculation outcomes are primarily influenced by the layer system across the sheet pile wall's height. If there are weaker layers beneath the wall's toe, overall stability of both the wall and the soil mass requires evaluation through a slip failure calculation (Korff, 2018). For both simple quay wall structures and initial drafts of more intricate quay walls (ones that employ relieving platforms), it is highly recommended for this method to be employed (De Gijt and Broeken, 2013).

2.3.2.1 D-Sheet Piling

D-Sheet Piling is a valuable tool for designing sheet pile walls, diaphragm walls, and horizontally loaded piles comprehensively. The software accommodates various structural elements and loads, such as anchors, struts, surcharges, forces, and moments. It also considers phases of construction.

The methodology used by D-Sheet Piling involves the subgrade reaction method, treating the soil as a system of uncoupled springs. This means that soil layers do not interact with each other. The software offers options for elastic or elastoplastic modeling of soil springs, allowing for the consideration of nonlinear deformations that occur along with the deformation of the soil retaining structure. Unlike the Blum Method, which assumes immediate yielding of soil, D-Sheet Piling introduces a linear transition between passive and active soil behaviors. This transition results in a gradual change in soil pressure and displacement as illustrated in Figure (2.10).

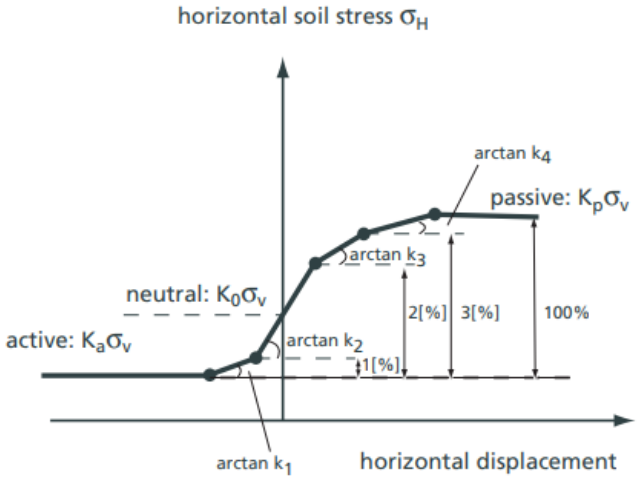

Figure 2.10: Stress-strain diagram of soil as per the subgrade reaction method, illustrating the mechanical response of soil under loading conditions. Source: Adapted from Deltares (2020).

The calculation approach relies on the Bernoulli assumption, suggesting that the cross-sections of the beam (or retaining structure) stay straight and have perpendicular orientation to the beam axis (Deltares, 2020).

2.3.3 Finite Element Modelling

2D finite element modeling offers the capability to simulate very complex geometries. This approach is utilized to examine the interaction between soil stress/strain distribution and structural components. It encompasses a comprehensive representation of complex

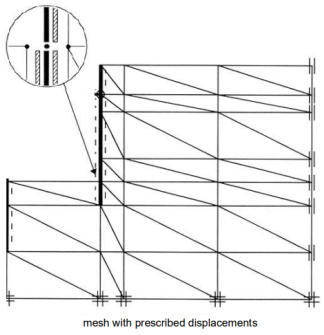

Figure 2.11: Element mesh with border supports and representation of sheet pile walls, interface elements, and soil elements. Source: Adapted from Korff (2018).

soil-structure interaction, advanced soil behavior, structural elements, and the stress history through the construction phases (including the "as-built" condition) through one model.

The characterization of the soil involves establishing equilibrium by considering stress-strain-deformation relationships and forces, which are expressed through a system

of partial and ordinary differential equations. At the interface of the soil and structural elements, sliding behavior can be defined. These interconnected equations form a system with node displacement as the unknown. Finite elements, often triangular or rectangular, connected by corner nodes, divide the soil into smaller sections known as elements. These elements collectively form a mesh, representing the soil. The relative displacement of nodes with respect to each other describes the stress-strain conditions within an element, relying on the material properties (Korff, 2018). The nonlinear nature of soil behavior is captured by selecting from various constitutive models, each defining a unique set of soil parameters (Brinkgreve, 2005).

The model's output is influenced by the geometry and dimensions of the soil-structure model, the accurate representation (modelling) of construction stages, the selected constitutive models along with their corresponding soil parameters, as well as mesh size and discretization. A finer mesh provides more precise results (mesh quality), with the drawback lying at the cost of more computational time.

The application of this method offers significant advantages, including absence of geometry restrictions, comprehensive soil-structure interactions across all elements, consolidation analysis, assessment of undrained/drained soil behavior and deformation in front or in behind the sheet pile walls. Furthermore, it facilitates the analysis of geotechnical failure mechanisms, sectional forces within structural elements, and the comprehensive assessment of stability and deformations in quay walls. Also in the state of art FEM program outputs alongside the numerical data, there exists the capability to generate graphical depictions of the computed displacement field, stress distributions, and plastic zones to better understand soil behavior. Furthermore, it facilitates the analysis of geotechnical failure mechanisms, sectional forces in structural elements, and overall stability and deformations of quay walls since checking of the mechanism of total stability loss is expressed implicitly in the method (Korff, 2018). The main drawbacks primarily involve a requirement for a deeper understanding of soil behavior and complexity. Also the verification methods as well as the integration of safety approaches. Furthermore, the higher accuracy comes to the cost of higher computational times.

When contrasted with alternative calculation methods for sizing a sheet pile wall, such as Blum's method or the spring method the finite element method inherently includes the mutual shear stress transformation between the soil layers (Korff, 2018). Moreover, the phenomenon of arching on the active side of an anchored sheet pile wall arises from the internal transformation of shear stresses within the soil mass. So Blum's method cannot directly include this interaction in its calculation and the spring method is not so accurate and consequently, these analytical methods, tend to overestimate bending moments and anchor forces (Korff, 2018).

2.3.3.1 Plaxis

PLAXIS (2D/3D) is a commonly employed finite element software in geotechnical applications. This software enables the calculation of deformations and stresses in structural elements and geotechnical sections, assisting in the assessment of global stability for both the structure and the soil mass. In PLAXIS, soil behavior relies on different constitutive models that account for how soil stiffness is influenced by stress state changes. In this particular case study, the Hardening Soil (HS) model is employed to accurately depict the unloading and reloading characteristics that occur throughout various stages of construction (Schanz et al., 2019).

In general, a more-simplistic widely used model is the Mohr-Coulomb model, as linear elastic perfectly-plastic, this model is primarily utilized for initial (first-order) approximation calculations and it does not incorporate diverse stiffness moduli. In order to address the incorporation of different moduli corresponding to various soil stress states and stiffness, the Hardening-Soil (HS) model has been formulated. In this model, soil stiffness is more accurately described by incorporating three different input stiffness parameters, including E_{50}^{ref}, E_{oed}^{ref}, and E_{ur}^{ref}.

Hardening soil model characteristics is firstly characterized by a broader stress-dependent stiffness behavior, employing a power-law formulation. In the context of axial compression, the stress-strain relationship follows a hyperbolic pattern. Notably, the model involves generation of plastic deviatoric strains by mobilizing the material's internal friction, a phenomenon termed as 'shear hardening.' Simultaneously, it undergoes the generation of plastic volumetric strains in primary compression, denoted as 'compaction hardening'. Furthermore, the model exhibits elastic behavior during unloading and reloading phases. Its failure mechanism aligns with the Mohr-Coulomb failure criterion, introducing two distinct yield contours: shear hardening and compaction (cap) hardening. Shear hardening characterizes irreversible strains resulting from primary deviatoric loading, while compaction (cap) hardening accounts for irreversible plastic strains induced by primary compression in both Oedometer and isotropic loading scenarios (Brinkgreve, 2022). A summary of the model parameters for the Hardening-Soil (HS) model can be found in Table (2.2).

Table 2.2: Description of Parameters

Parameter Symbol	Description
E_{50}^{ref}	Secant soil stiffness for a reference stress in triaxial test
E_{oed}^{ref}	Tangent stiffness for a reference stress in oedometer test
E_{ur}^{ref}	Unloading-reloading stiffness for a reference stress
m	Rate of stress dependency in stiffness behavior
v_{ur}	Poisson's ratio in unloading/reloading
c'	Effective cohesion
ϕ'	Effective friction angle
ψ	Dilatancy angle
γ_{sat}	Saturated soil weight
γ_{unsat}	Unsaturated soil weight
R_{int}	Interface strength ratio

One way of estimating the parameters is by applying the correlation equations below:

- E_{50}^{ref} : The value is determined based on the parameter Q_c.

$$\text{For sand: } Q_c \leq 10\,\text{MPa: } 4 \cdot Q_c \cdot \left(\frac{100}{\sigma_v'}\right)^{0.5},$$

$$\text{For sand: } Q_c > 10\,\text{MPa: } 20 + 2 \cdot Q_c \cdot \left(\frac{100}{\sigma_v'}\right)^{0.5}.$$

(Lunne and Christophersen, 1983)

$$\text{For clay: } Q_c > 2\,\text{MPa: } 2 \cdot Q_c \cdot \left(\frac{100}{\sigma_v'}\right).$$

(Sanglerat, 1972)

Where Q_c is the cone tip resistance of a CPT test, whereas $\sigma_{v'}$ is the effective vertical stress.

- E_{oed}^{ref} : Ratio between E_{50}^{ref} / E_{oed}^{ref} is assigned a value of 1 for sand layers and a value of 1.25 for clay layers (Bentley Advancing Infrastructure, 2022).

- E_{ur}^{ref} : Ratio between E_{ur}^{ref} / E_{50}^{ref} is 2.00 - 5.00. A value of 5 is selected for sand and a value of 4.00 is selected for clay (Gouw, 2014).

- m : The value is 0.50 for sand layers and 1.00 for clay layers (Gouw, 2014).

- v_{ur} : The value of the parameter lies between 0.10 to 0.20. Therefore a value of 0.20 was selected (Bentley Advancing Infrastructure, 2022).

- ψ : For sand, ψ can be calculated as $\psi = 30 - \phi$. For clay the value is 0. (Brinkgreve, 2022)

- R_{int} : The value is approximately 0.67 (Bentley Advancing Infrastructure, 2022).

Furthermore, the user has the option to choose between the types of material behavior in the analysis:

Drained Behavior: In this mode, no excess pore pressures are generated. This is applicable for dry soils and well-drained soils characterized by high permeability and/or a low rate of loading. This option is also suitable for simulating long-term soil behavior.

Undrained Behavior: This setting is employed when there is a full development of excess pore pressures. The user needs to input the effective elastic parameters (E' and Φ'). Additionally, PLAXIS automatically incorporates bulk stiffness for the water and distinguishes between effective stresses and excess pore pressures. Undrained (A) is typically selected for the clay layers, while Drained for the sandy soil layers (Bentley Advancing Infrastructure, 2022).

2.4 Limit States

2.4.1 Theory Behind Limit States on Quay Walls

Probabilistic safety verifications assess whether a structure's main function or a component meets failure or non-failure criteria. This analysis evaluates the structure's response to different load combinations, using design values for properties like soil, loads, geometry, strength, and stiffness. When the limit state is not exceeded, the function meets the necessary conditions. Eurocodes distinguish between Ultimate Limit States (ULS) and Serviceability Limit States (SLS). In the Ultimate Limit State (ULS), the following aspects need to be examined:

- **EQU (Equilibrium)**: Associated with the loss of equilibrium in the structure or a segment treated as a rigid body, which does not consider soil strength as a contributing factor.
- **STR (Structural)**: Relates to internal failure or or exceptional deformations of the structure, including shallow and pile foundations. The assessment is guided by the strength of construction materials.
- **GEO (Geotechnical)**: Involves subsoil failure or exceptional deformations where soil strength governs the required resistance.
- **FAT (Fatigue)**: Deals with structure failure due to fatigue.
- **UPL (Uplift)**: Associated with structure or subsoil failure caused by upward forces from water pressure or other vertical loads.

- **HYD (Hydraulic)**: Relates to hydraulic soil failure resulting from internal erosion due to concentrated groundwater flow (piping) in the subsoil caused by hydraulic gradients.

Figure (2.12) demonstrates various failure mechanisms, while on Table (2.3) the various failure mechanisms related to the sheet pile wall structure can be identified.

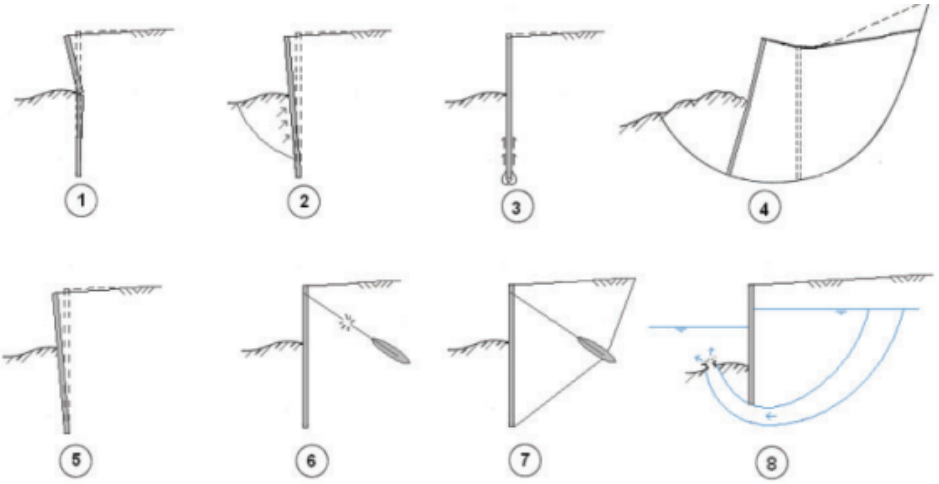

Figure 2.12: Failure mechanism on relevant case study of sheet pile structure. Source: Adapted from De Gijt and Broeken (2013)

Table 2.3: Failure mechanisms, limit states, and their relevance to current case study of retaining walls. Source: Adapted from De Gijt and Broeken (2013)

Failure Mechanism	Limit State	Sheet Pile Wall Structure
Vertical Bearing Force on Subsoil	GEO	x
Vertical Pile Bearing Capacity (Compression)	GEO	x
Vertical Pile Bearing Capacity (Tension)	GEO/UPL	
Horizontal Bearing Force on Subsoil	GEO	x
Horizontal Soil Resistance	GEO	x
Vertical Soil Fracture (Heave)	GEO/UPL	x
Tension Resistance (Anchorage)	GEO/UPL	x
Local Stability/High Sliding Plane (e.g. Kranz)	GEO	x
Overall Stability	GEO	x
Overturning	EQU	x
Structural Strength of Anchorage	STR	x
Structural Strength of Wall	STR	x
Structural Strength of Piles	STR	x
Structural Strength of Other Elements	STR	x
Failure through Very Large Deformations	STR	x
Under and Back Seepage and Piping	HYD	x
Internal Erosion	HYD	x

3

Reliability-based Design Method

This chapter provides a comprehensive background on reliability-based design approaches. It begins by delving into the essential concepts of reliability-based methods, offering a concise classification of these approaches. Moreover, the chapter explores the inherent uncertainty that characterizes geotechnical engineering. Finally, the practical application of both the Eurocode and the Dutch standards, CUR166 and CUR211 for the assessment of designs are been examined, whereas the fault trees incorporated within these two latter design codes are been presented.

3.1 Introduction

"Structure Reliability" has a broad definition, as the ability of the structure to meet design performance criteria within a specified time period. In a narrower context, it signifies the likelihood that a structures will avoid reaching their ULS (ultimate limit state) throughout their operational life. The relation between failure probability and reliability is described by the equation "Failure probability = 1 - Reliability." (Thoft-Christensen and Baker, 1982). Reliability analysis quantifies uncertainty in core model variables affecting structural performance through probabilistic distributions, ultimately calculating failure probabilities. Reliability-based design, a derived methodology, extracts outputs from reliability analysis into design considerations (OCDI, 2020). The global adoption of the reliability-based design method is evident in its incorporation into major international standards. Specifically, the Structural Eurocodes (a European uniform standard) (Low and Phoon, 2015), along with AASHTO (North American standard) (AASHTO, 1993) and "Technical Standards and Commentaries for Port and Harbour Facilities in Japan (OCDI, 2020)" have embraced and put into practice on full scale, the reliability-based design approach. Currently, it is widely acknowledged as the sole method capable of effectively addressing the inherent uncertainties that arise in structural design. It stands out as the

singular approach capable of addressing various uncertainties inherent in structural design (ISO, 1998).

3.2 Classification of the Reliability-Based Design Methods

An overview of various levels of reliability-based design methods will be provided, concentrating specifically on Level 2 methods. The focus will primarily be on the First Order Reliability Method (FORM), as it holds relevance for the subsequent analyses covered in the following chapters.

1. **Level IV Reliability-Based Design Method (Risk Based)**

   Level IV method consider failure consequences (costs), using risk (consequence × failure probability) for reliability evaluation. This enables cost-effective design comparisons, accounting for uncertainty, costs, and benefits (Jonkman et al., 2018).

2. **Level III Reliability-Based Design Method (Numerical)**

   Level III methods directly calculate failure probability using variable distributions. For P_f (Probability of Failure), the probabilistic formulation is determined through analytical expressions, numerical integration, or Monte Carlo simulations. Analytical solutions work for simple scenarios, while numerical integration is more suitable for a limited number, n, of basic variables (Jonkman et al., 2018).

3. **Level II Reliability-Based Design Method**

   Level II methods utilize mean values and first and second-order moments (covariance matrix) of basic variables to assess reliability index, β. The joint probability density function is simplified, and computational effort is reduced via linearization of the limit state function. This is commonly achieved using the First Order Reliability Method, where the function is linearized at the design point—the highest probability density point on g(X) = 0, where failure is most probable (Jonkman et al., 2018). Performance is validated by ensuring that the reliability index, β ($\beta \geq P_f$), meets or exceeds the specified limit value (OCDI, 2020).

4. **Level I Reliability-Based Design Method**

   Level I methods introduce partial factors, $(\gamma' s)$, for uncertain parameters, into the performance verification equation to ensure a safety margin through deterministic validation. This partial factor method, substitutes characteristic values for basic variables in the equation. The partial factor is established using Level 3 or 2 reliability-based design methods (code calibration) (Jonkman et al., 2018).

5. **Level 0 Reliability-Based Design Method**

   Level 0 deterministic methods that rely on nominal values of basic variables and a single (empirical) global safety factor. (Jonkman et al., 2018).

3.3 Uncertainty in Geotechnical Engineering

The uncertainties addressed in geotechnical engineering can be categorized into three main categories, as illustrated in Figure (3.1) :

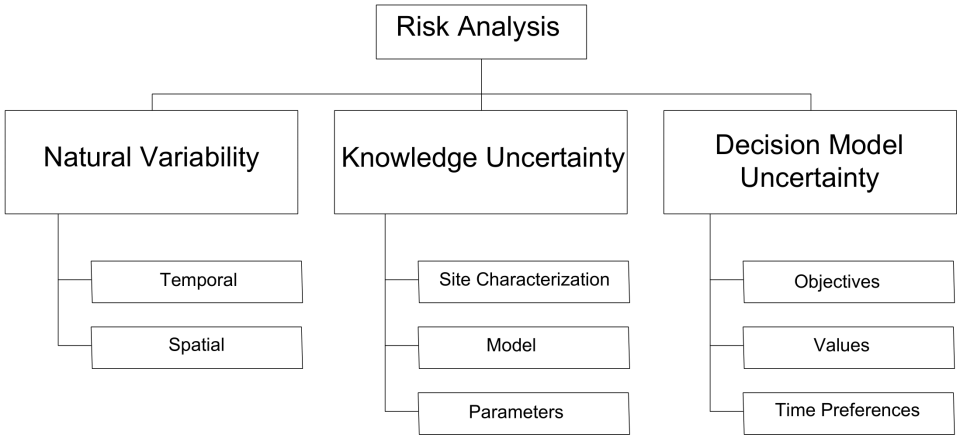

Figure 3.1: Varieties of uncertainty encompassed within risk analysis in geotechnical engineering. Source: Adapted from Baecher and Christian (2003).

1. Natural variability: Related to the inherent stochastic nature of natural processes, demonstrating temporal variation for events occurring at a single location (temporal variability), spatial variation for events across different locations but in a single time (spatial variability), or combined temporal and spatial variation. This inherent variability is approximated through mathematical models, which may or may not accurately represent natural phenomena. Ideally, these models provide accurate approximations that closely match natural phenomena.

2. Knowledge uncertainty: Originates due to inadequate data, restricted knowledge of events and processes, or partial comprehension of physical laws, limiting our capacity to simulate reality via modeling. This encompasses three geotechnical sub-categories:

(a) Site characterization uncertainty, model uncertainty, and parameter uncertainty. Site characterization uncertainty pertains to the reliability of interpretations concerning subsurface geology, stemming from uncertainties in data and exploration: (i) measurement errors, (ii) inconsistencies or non-uniformities in data, (iii) errors in data handling and transcription, and (iv) inadequate representation of data samples due to temporal and spatial constraints.

(b) Model uncertainty pertains to the extent to which a selected mathematical model faithfully replicates the actual world. This type of uncertainty arises from a model or design approach's inability to precisely capture a system's genuine physical behavior, or from our challenge in identifying the optimal model, which might be subject to changes in ways that are not well understood over time. The models we apply to naturally varying phenomena must be tailored to these processes by observing their mechanisms, measuring significant attributes, and statistically estimating model parameters (Baecher and Christian, 2003). Even in Finite Element Method simulations, the margin of inaccuracy is typically within the range of $\pm 30.00\%$ (De Gijt and Broeken, 2013).

(c) Parameter uncertainty concerns the accuracy of estimating model parameters. It arises due to our inability to precisely determine parameter values using test or calibration data, and is compounded by a scarcity of observations and the consequent statistical imprecision.

3. Decision model uncertainty: These pertain to the practical execution of designs and the economic considerations involved in benefit-cost evaluations. These uncertainties can be categorized into two main types: operational uncertainties, which encompass factors such as construction, manufacturing, degradation, maintenance, and human-related aspects not considered in engineering performance models; and decision uncertainties, which stem from our limited understanding of social objectives, prescribed social discount rates, planning horizon duration, preferred trade-offs between current consumption and future investment, and societal risk aversion (Baecher and Christian, 2003).

3.4 Partial Factors through LFRD method

Load and Resistance Factor Design (LRFD) is a design approach that incorporates safety margins in performance verification. Through applying a partial factor to the calculated resistance value, which is based on a characteristic value. On the load side, a similar partial factor is used to multiply the corresponding load value, effectively increasing the applied load. LFRD method often combines resistance values, but there is also a proposed format that breaks them down into multiple terms, which also happens on the load side. Both forms are described below:

$$\gamma_R R\left(x_{k1},\ldots,x_{kn}\right) \geq \sum_j \gamma_{Sj} S_j\left(x_{k1},\ldots,x_{kn}\right) \tag{3.1}$$

$$f_R\left(\gamma_{R1}R_{1k}\left(x_{1k},x_{pk}\right),\ldots,\gamma_{Rm}R_{mk}\left(x_{1k},x_{pk}\right)\right) \geq f_S\left(\gamma_{s1}S_{1k}\left(x_{1k},x_{pk}\right),\ldots,\gamma_{Sn}S_{nk}\left(x_{1k},x_{pk}\right)\right) \tag{3.2}$$

Where:

γ_R **or** γ_{R_i}**:** Represents a partial factor used to adjust resistance values, which we'll call the 'resistance factor.'

γ_{S_i}**:** Represents another partial factor used to adjust load values, known as the 'load factor.'

R **or** R_i**:** Refers to the resistance values themselves.

S_i**:** Stands for the load or effect values.

According to Eurocode (NEN, 2019), a design is deemed adequately safe when the design value of resistance, R_d, exceeds the design value of the action effect, S_d, while also accounting for the model factor uncertainty. These two values are specified as:

$$\begin{aligned} S_d &= S\left(F_{d;i}, a_{d;i}, \theta_{d;i}\right) \\ R_d &= R\left(X_{d;i}, a_{d;i}, \theta_{d;i}\right) \end{aligned} \tag{3.3}$$

Where:

S_d : Design value of the action effect.

S : Action effect.

R_d : Design value of resistance.

R : Resistance.

$F_{d:i}$: Design value of load property for i.

$X_{d:i}$: Design value of material property for i.

$a_{d,i}$: Design value of geometric property for i.

$\theta_{d,i}$: Design value of model uncertainty for i.

In quay-wall engineering, it is noteworthy that certain material properties in soil layers, such as soil strength and weight density, can serve dual purposes by acting both as resistance and as a load. Consequently, the formulation of the action effect definition needs to be adjusted as: $S_d = S\left(F_{d;i}, X_{d;i}, a_{d;i}, \theta_{d;i}\right)$, incorporating the design values of these material properties in both load and resistance considerations.

The reasons to adopt this method can be concluded in the following:

1. Designers can utilize LRFD to assess structures throughout the final design phase, gaining a comprehensive understanding of the structure's expected behavior. LRFD computes designs based on the characteristic values of crucial variables. This method enhances the application of sound engineering judgment, ensuring a more robust and informed design process.

2. When designing structures with complex interactions with the ground, a reduction in key basic variables, such as in material factor design, may not act on enhancing structural design safety.

3. If there are evident uncertainties in the design calculation model, drawn from real failures in full-scale structures or a database of test results closely resembling full-scale behavior, these uncertainties encompass various influencing factors. By incorporating these uncertainties, we can realistically identify uncertainties observed in existing structures, leading to the determination of the resistance factor applied to calculated resistance values.

3.5 Probabilistic Design Approach

3.5.1 Failure Probability and Reliability Index

The evaluation of system reliability involves a comparison between two stochastic quantities: the system's resistance, denoted as R, and the applied load (or solicitation) S (Benjamin and Cornell, 1970).

The primary objective is to minimize the probability of both a low resistance and a very high load occurring simultaneously. If the probability density functions of resistance (R) and load (S) are known, the failure probability (P_f) can be determined as the probability that the applied load (S) exceeds the system resistance (R). The formulation can be represented symbolically as follows:

$$P_f = P(S > R) \tag{3.4}$$

The same problem can be approached using the concept of a limit state. In this approach, a limit state represents a condition where the structure or a component of the structure no longer meets its required performance criteria. The limit state Z can be evaluated by considering the resistance R and the loads S:

$$Z = R - S \tag{3.5}$$

Failure occurs when $R < S$, which translates to $Z < 0$. The probability of failure (P_f) is calculated as $P[Z < 0] = P[S > R]$ (Jonkman et al., 2018).

When dealing with a limit state function that encompasses various solicitation and resistance variables, the failure probability is indicated by the limit state function $Z(X)$ being negative. In this context, X represents the vector of all stochastic variables, and $f_X(x)$ signifies the joint probability density function:

$$P(Z(X) < 0) = \int_{Z(X)<0} f_X(x)\,dx \tag{3.6}$$

In Figure (3.2) it is illustrated the bell-shaped simultaneous probability density function with contours, simplifying the performance function $Z = g(R,S)$ to a linear $R-S$ relation. The limit state plane, separating the safe and failure ranges, indicated as non-destruction and destruction, forms a positive 45-degree line from the origin. A probability density function of the safety margin Z can be derived from the volume of the simultaneous probability density function at $Z = z$, perpendicular to the limit state plane. The failure probability corresponds to the area where Z is not positive in the probability density function.

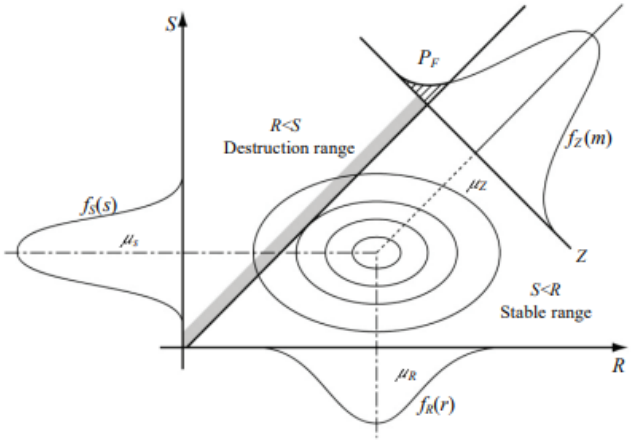

Figure 3.2: PDF of Safety Margin, $Z = R - S$ Source: Adapted from OCDI (2020))

The average and variance of the safety margin Z are $\mu_Z = \mu_R - \mu_S$ and $\sigma_Z^2 = \sigma_R^2 + \sigma_S^2$, respectively, where the average of R is μ_R, the standard deviation is σ_R, the average of S is μ_S, and the standard deviation is σ_S.

Figure (3.3) depicts an alternate representation of the probability density function for the safety margin, denoted as Z. Within the context of the reliability-based design approach, a reliability index can be employed, denoted as β, as an alternative to the failure probability, P_f.

The reliability index is defined using the average and variance of the safety margin:

$$\beta = \frac{\mu_z}{\sigma_z} = \frac{\mu_R - \mu_S}{\sqrt{\sigma_R^2 - \sigma_S^2}} \tag{3.7}$$

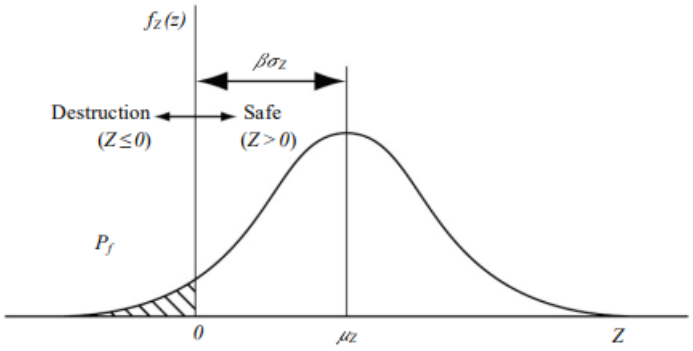

Figure 3.3: Distribution of the Safety Margin Z and the Reliability Index β Source: Adapted from OCDI (2020)

The reliability index, denoted as β, serves as a measure to gauge the magnitude of the safety margin's average in relation to its standard deviation. Additionally, β can be directly related to the failure probability P_f and is expressed by the following equation when the safety margin Z follows a normal distribution.

$$P_f = \Phi(-\beta) = 1 - \Phi(\beta) \tag{3.8}$$

Φ represents the cumulative standard normal probability distribution function, while the relationship between β and P_f is depicted in Figure (3.4) and summarized in Table (3.1).

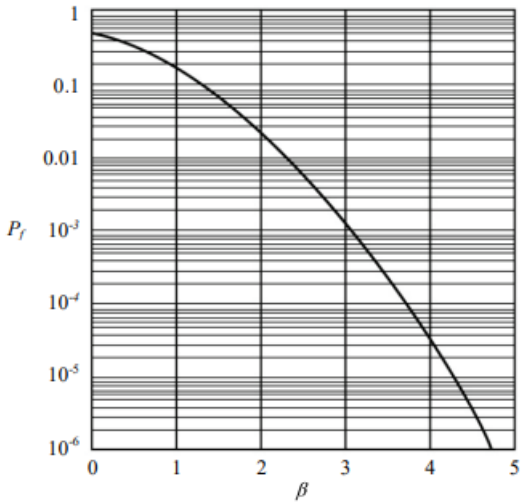

Source: Adapted from OCDI (2020))

Figure 3.4: Correlation of the Reliability Index, β, and the Failure Probability, P_f

3.5.2 Calculation Method for Partial Factors using the Design Value Method

Ensuring a balanced and consistent level of reliability across all conditions poses a considerable challenge. This complexity is further pronounced by the need to design

Table 3.1: Reliability Index β for various different Failure Probabilities P_f. Source: Adapted from OCDI (2020)

P_f	10^{-1}	5×10^{-2}	10^{-2}	10^{-3}	10^{-4}	10^{-5}	10^{-6}
β	1.28	1.64	2.32	3.09	3.72	4.26	4.75

structures of the same type under diverse circumstances. For instance, achieving uniform reliability for quay walls with varying water depths becomes challenging when utilizing identical partial factor combinations.

The core idea of the design value method involves determining factors related to load values, resistance values, and basic variables in relation to design points and characteristic values. Design points, are points on a plane where the likelihood of a certain event happening is the highest. This plane represents a situation where the performance function (a mathematical representation of the system's behavior) equals zero. These points exist within a space defined by various load and resistance values.

Figure (3.5) depicts the design points $(S(x^*), R(x^*))$ situated on the plane characterized by load values, $S(x)$, and resistance values, $R(x)$. This depiction highlights that the

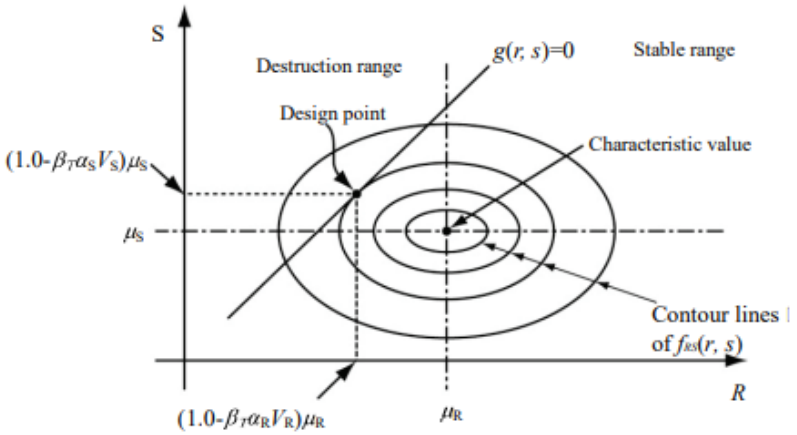

Figure 3.5: Conceptual Diagram of Design Points Source: Adapted from OCDI (2020)

design point signifies the most plausible location to encounter the limit state amidst the combinations of load and resistance values on the limit state plane.

Through the design value method, the load factor, γ_S, and the resistance factor, γ_R, are determined utilizing the subsequent equation:

$$\gamma_S = \frac{S(x^*)}{S(x_k)} \tag{3.9}$$

$$\gamma_R = \frac{R(x^*)}{R(x_k)} \tag{3.10}$$

where x_k represents the characteristic value vector of the basic variable (OCDI, 2020). Figure (3.6) provides a visual overview of different methods used to calibrate partial factors

from NEN-EN 1990 (Gulvanessian, 2001). In terms of probabilistic calibration procedures for partial factors, they can be categorized into two main classes: full probabilistic methods (Level III) and first-order reliability methods (FORM) (Level II). In terms of probabilistic calibration procedures for partial factors, they can be categorized into two main classes: full probabilistic methods (Level III) and first-order reliability methods (FORM) (Level II). Eurocodes primarily utilize method a, while method c or equivalent approaches are employed in further Eurocode development.

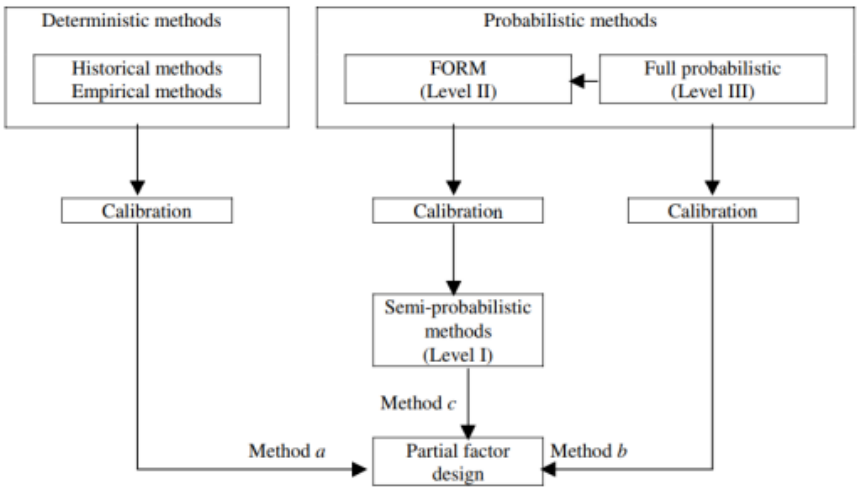

Figure 3.6: Approaches for Determining Partial Factors Source: Adapted from Gulvanessian (2001)

3.5.3 First Order Reliability Method (FORM)

In this thesis, a Level II method is employed, primarily assuming that the variables follow a normal distribution. However, the current analysis involves the presence of lognormal distribution variables within the material property parameters and Gumbel distribution variables within the load property parameters. To ensure compatibility with the analysis method, appropriate transformations are applied to bring these non-normal distributions into a format suitable for Level II methodology. The parameters are represented by their mean values and standard deviations, simplifying the joint probability density. The limit state function is linearized, often employing the First Order Reliability Method (FORM), which streamlines the joint probability density function and increases computational speed.

FORM is a commonly employed technique in reliability analysis to determine the likelihood of structural failure. FORM method is rooted in the assumption that the limit state function—marking the boundary between safe and failure regions within the input variable space—can be approximated using a linear function centered around a designated design point Figure (3.7). This chosen design point aims to maximize the probability of failure. The linear approximation is achieved by applying a first-order Taylor series expansion to the limit state function (Jonkman et al., 2018).

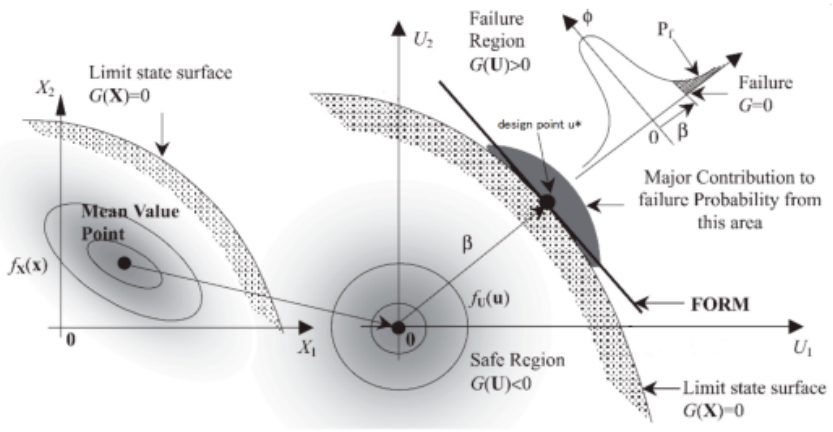

Figure 3.7: Schematic representation of FORM. Source: Adapted from Mahmood et al. (2022)

The FORM procedure commences from a user-defined initial point within the parameter space. It then aims to identify a point that is closer to the design point by following the gradient of the Z-value within the parameter space. The Z-value serves as an indicator of potential failure, as determined by the failure criterion. After a series of steps, the point approaches the design point sufficiently, prompting the calculation to conclude. The associated probability of failure is then determined based on this calculation and given by Equation (3.8) (Deltares, 2023).

Given that the design point corresponds to the combination of parameters with the highest probability density for $Z = 0$, the linearized and normalized limit state function resulting from the FORM analysis can be expressed as:

$$Z = \beta - \sum_{i=1}^{n} \alpha_i u_i \tag{3.11}$$

Where:

β: Reliability index

α_i: Influence coefficient of stochastic variable X_i

u_i: Normalized value of stochastic variable X_i involved in the limit state function

The influence coefficient, denoted as α, it is a measure for the relative importance of the standard deviation of a stochastic variable in relation to reliability index and, consequently, the probability of failure. By squaring this coefficient, we determine the portion of the variable's variance associated with the linearized and normalized limit state function. It is crucial to note that the sum of the squares of all influence coefficients should add up to 1 (Kanning et al., 2017).

The FORM method can handle complex models and thoughtfully incorporate input parameters and assumptions. Its sensitivity to these factors enables an analysis of system

behavior across various conditions. Additionally, FORM is computationally efficient when compared to alternatives like the time-consuming and resource-intensive Monte Carlo simulation method (Diermanse et al., 2016).

3.6 Design Codes

3.6.1 Eurocode

NEN-EN 1990 (Gulvanessian, 2001) has introduced in the past three reliability classes, each with different safety levels represented by a reliability index. These classes define the maximum allowable probability of failure or safety margin, valid for the designated design lifespan. It is important to note that the reliability classes (RC) do not have any separate distinctions than consequence classes (CC).

In the latest additions from NEN-EN 1990 structures must be categorized into a consequence class based on the following criteria, which can be located on Table (3.2).

Table 3.2: Consequence Classes and Descriptions. Source: Adapted from NEN (2019)

Consequence class	Description
CC 3	Major consequences with respect to loss of life, or very large economic or social or environmental consequences (Maritime structures, quay walls that are part of a primary water barrier or a main waterway)
CC 2	Medium impact with respect to loss of life, or significant economic, social, or environmental consequences (Maritime structures, such as quay walls, jetties, breakwaters, and bollards, without functional redistribution capacity)
CC 1 (further subdivided into:)	
CC 1b	Minor impacts with respect to loss of life and minor or negligible economic or social or environmental impacts (Maritime structures, such as quay walls, jetties, breakwaters, and bollards, with functional redistribution capacity)
CC 1a	Virtually excluded loss of life and very minor or negligible economic or social or environmental impacts (Bollards with exclusively secondary nautical functions)

If the structure being assessed serves multiple purposes, the objective is to establish the appropriate consequence class for each individual function. Once the consequence class has been determined for all functions, the highest consequence class among them should be applied to the entire structure. An essential point to emphasize is that in situations involving functional load redistribution capability, the failure or impairment of the underlying maritime or structural element should not lead to full failure of the structural system.

Given the subject of the thesis and the goal of achieving a robust comparison among the outcomes to be computed in the forthcoming chapters, it is essential to incorporate

Table 3.3: Reliability Minimum values for β for quay wall structures. Source: Adapted from NEN (2019)

Reliability class RC	Minimum values for β	
	1-year reference period	50-year reference period
RC3	5.20	4.30
RC2	4.70	3.80
RC1	4.20	3.30

the existing partial factors utilized in the design process. The values in respect to the construction can be located in Table (3.4) in the column of RC1/CC1. Also in a similar manner the values of the partial factors in respect to the loads can be located in Table (3.5) in the column of RC1/CC1.

Table 3.4: Partial factors for soil parameters (Y_M) following the specifications of Table A.4b in NEN 9997-1:2012 and NEN 9997-1+C2:2017 are applicable to basic quay walls, resembling an anchored sheet pile wall with a coping. Source: Adapted from De Gijt and Broeken (2013), NEN (2017)

Soil Parameter	Symbol	Combination			
		M1	M2		
			Sheet Pile Wall (Simple quay wall)		
			RC1/CC1	RC2/CC2	RC3/CC3
Angle of internal friction	$\gamma_{\phi'}$	N/A	1.150	1.175	1.200
Angle of shearing resistance	$\gamma_{\delta'}$	N/A	1.150	1.175	1.200
Effective cohesion	$\gamma_{c'}$	N/A	1.150	1.250	1.400
Undrained shear strength	$\gamma_{cu'}$	N/A	1.500	1.600	1.650
Unconfined compression strength	$\gamma_{qu'}$	N/A	1.500	1.600	1.650
Density	$\gamma_{\gamma'}$	N/A	1.100	1.100	1.100
Subgrade reaction modulus	$\gamma_{kh'}$	N/A	1.300	1.300	1.300

Table 3.5: Load partial factor parameters for different reliability/consequence classes on geotechnical loads. Source: Adapted from NEN (2017)

Load Parameter	RC1/CC1	RC2/CC2	RC3/CC3
Permanent, $_{unfavourable}$	1.00	1.00	1.00
Variable, $_{unfavourable}$	1.00	1.10	1.25

3.6.2 Dutch Guidelines

In the Dutch guidelines (Meijer, 2006), Handbook Quay Walls, CUR 166 , failure mechanisms for limit states are depicted using fault trees. These trees outline the potential failure mechanisms that can arise in specific structures. When a fault tree is applicable to multiple structure types, the failure mechanisms tend to be more generalized. The reliability index values, represented as β, for the failure mechanisms illustrated in both fault trees, are provided in Table (3.6). In Figure (3.8), CUR 166 is depicted and was

initially developed for a sheet pile structure, encompassing failure mechanisms relevant to such structures. This design is adaptable to both building pits and quay walls (CUR, 2012).

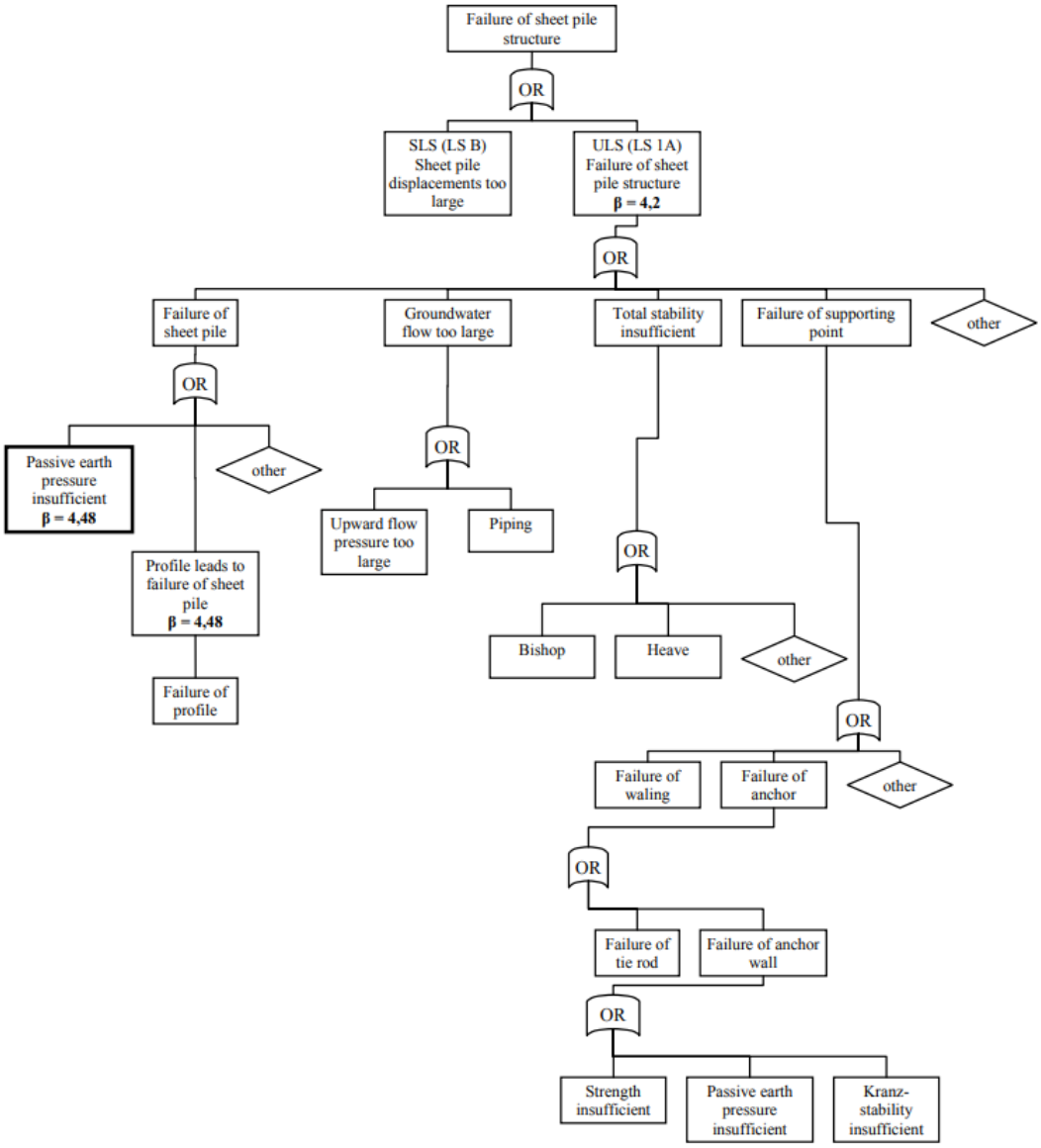

Figure 3.8: Fault tree representation of the failure mechanisms for sheet pile structures in CUR 166. Safety factors based on "Passive Earth Pressure Insufficient". Source: Adapted from Meijer (2006)

The safety level for quay walls (sheet pile structure) in CUR 166 adheres to level III, featuring a β-value of 4.2.

Table 3.6: Reliability Index and Probability of Failure for Failure Mechanisms in CUR 166 and Handbook Quay Walls. Source: Adapted from Meijer (2006)

Failure Mechanism	Reliability Index (β)		Admissible Probability of Failure	
	Handbook Quay Walls	CUR 166	Handbook Quay Walls	CUR 166
Quay Walls structure fails	3.40		$3.37 \cdot 10^{-4}$	
Sheet pile structure fails		4.20		$1.34 \cdot 10^{5}$
Failure of sheet pile	3.707	4.39	$1.05 \cdot 10^{-4}$	$5.57 \cdot 10^{-5}$
Failure of sheet pile profile	3.872	4.48	$5.39 \cdot 10^{-5}$	$3.71 \cdot 10^{-6}$
Passive earth pressure insufficient	4.396	4.48	$5.39 \cdot 10^{-6}$	$3.71 \cdot 10^{-6}$
Failure of tensile element/support	3.828	4.44	$6.47 \cdot 10^{-5}$	$4.45 \cdot 10^{-6}$
Insufficient total stability	4.247	4.48	$1.08 \cdot 10^{-5}$	$3.71 \cdot 10^{-6}$
Groundwater flow too large	4.247	4.48	$1.08 \cdot 10^{-5}$	$3.71 \cdot 10^{-6}$

The quay walls in Handbook Quay Walls operate at a safety level II, featuring a β-value of 3.40.

Most safety factors are established with consideration of a typical structure's service life, often around 50 years. This safety level must be maintained and it depends on the specific limit state.

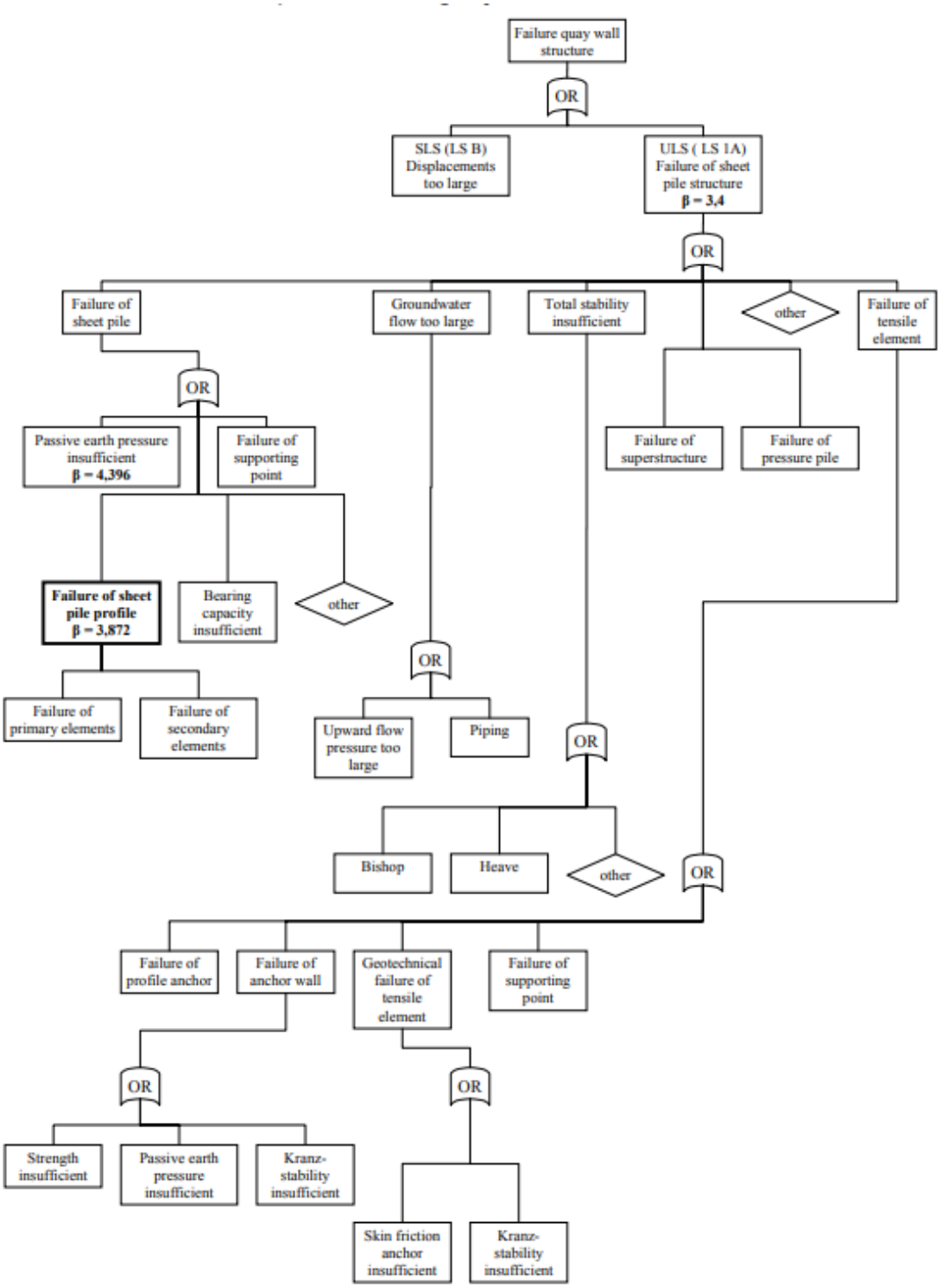

Figure 3.9: Fault tree representation of the failure mechanisms for quay walls in Handbook Quay Walls (CUR 211). Safety factors based on "Failure of Sheet Pile Profile". Source: Adapted from Meijer (2006)

4

Case Study Design Aspects

In this chapter the case study is introduced. It starts with the design itself, followed by a breakdown of the construction sequence (as build) until the final construction. To enhance comprehension, we delve into the key design parameters that played a pivotal role. This encompasses an in-depth understanding of soil parameters, hydraulic conditions and the process of determining water levels using hydrometer data. Furthermore, the procedure of establishing combination loadings derived from variable actions such as bollard loads and crane/container loads is been introduced. Then the modelling process of the structure is been compared for two modelling software, Plaxis and D-Sheet Piling to determine the optimal choice for the research.

4.1 Introduction

The Maasvlakte is a significant part of the harbor and industrial zone in Port of Rotterdam. Formed in the 1960s through land reclamation from the North Sea, sand for the expansion mainly came from the North Sea and Lake of Oostvoorne (Meulen, 2016).

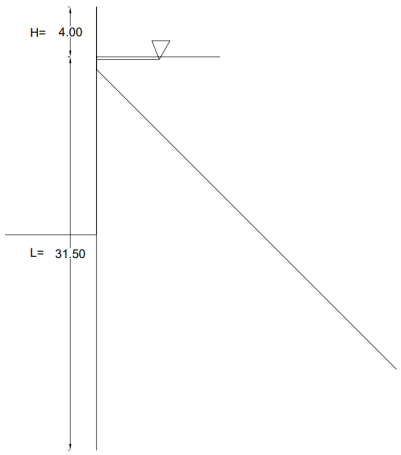

Figure 4.1: Simplified cross-section of the quay wall

The case study will examine a quay wall built in Maasvalte. The quay wall has been designed in 2016, where the original design was according to CC2 / RC2, but according to new guidance in (NEN, 2019) and considering the nature of the construction and by administered expertise on the subject, the final category of the structure is CC1b. So under the consideration that CC1 is the category of the structure, the value of β in respect to 50-year reference period is 3.30 which can be identified in reliability class RC1 in Table (3.3).

The structure is composed of a combi-wall featuring a concrete cap and supported by two S.I. (Screw Injection) anchors per tubular pile. The total height of the wall is 35.50 meters and can be easily identified as 'H + L' in Figure (4.1). While the total retaining height, is 18.25 m, which is concluded by the final excavation of -14.25 m NAP, plus +4 m NAP of the top level of the quay wall. Also in Figure (4.2) a top view of the combi-wall is represented.

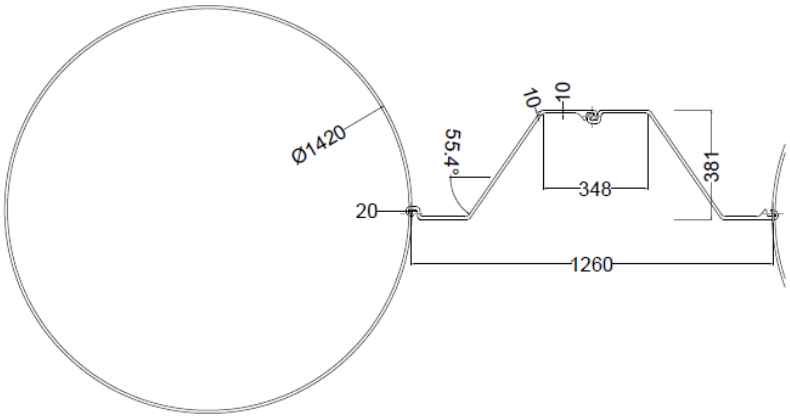

Figure 4.2: Schematic representation of the combi-wall. Source: Adapted from ArcelorMittal (nd)

4.2 Construction Sequence

Before the construction:

As previously mentioned in the introduction, the Maasvlakte is a reclaimed land harbor. To accurately model soil-structure interaction during the construction process, it is crucial to start at the initial phase, before the dredging. The natural consolidation of the soil, is primarily influenced by the geological history of the area. In this stage, the soil state has been identified as normally-consolidated. Though, Given the natural consolidation process that occurred from the 1960s, when the dredging works began until the start of construction, it's reasonable to infer that the soil profile prior to construction initiation is still in normally-consolidated state. Though, the soil in front of the quay wall, will have some degree of over-consolidation, which can be attributed to the significant loading and compaction resulting from the reclamation process, which involves dredging large

amounts of soil from the seabed or nearby areas for use as fill material. This is the basic requirement for precisely understanding the changes in soil behavior, often referred to as the "soil history". The representation of the stage is illustrated in Figure (4.3).

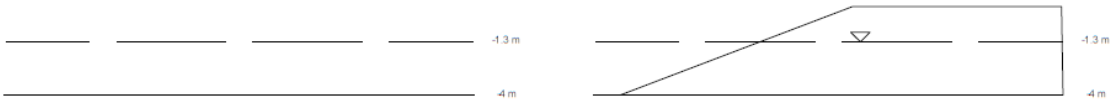

Figure 4.3: Schematic representation of area before and after reclamation.

Initial Stage:

To initiate the construction of the quay, a brief excavation was carried out. This excavation aimed to establish a level surface in the soil, facilitating access for workers and machinery to the designated area. Furthermore, this preliminary groundwork provided the necessary foundation for the subsequent installation of anchors to secure the construction.Additionally, on the seaside of the construction site, a temporary sheet pile wall was erected. The purpose of the temporary sheet pile wall was to create a dry working area during all tidal levels. This is illustrated in Figure (4.4).

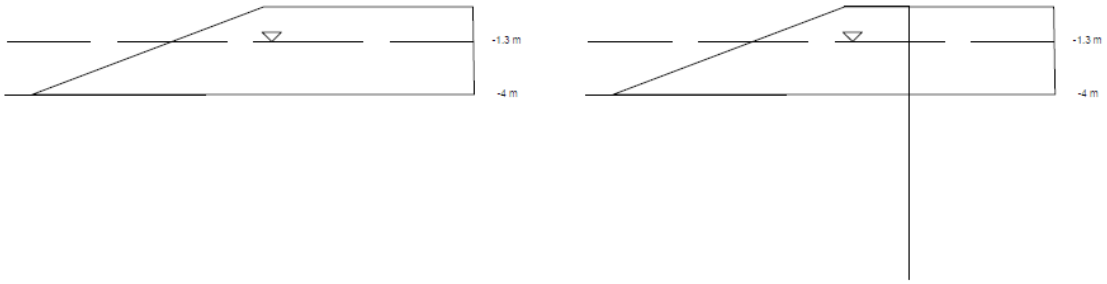

Figure 4.4: Schematic representation of area before and after installation of temporary sheet pile wall.

Installation Quay Wall:

At this point, the construction of the quay wall has been finalized, and the combined wall has been installed up to a depth of -18.25 m NAP using S355 quality steel double sheet pile AZ 18-10-10 and tubular piles of X70 steel quality with an external diameter of 1420 mm and thickness of steel equal to 20 mm. Simultaneously, the tubular piles of X70 steel quality have been successfully driven to their ultimate depth of -31.50 m NAP. This phase concludes with the installation of prestressed S.I. grout anchors. Additionally, during this final step, the pile cap is put into place. This can be identified in Figure (4.5).

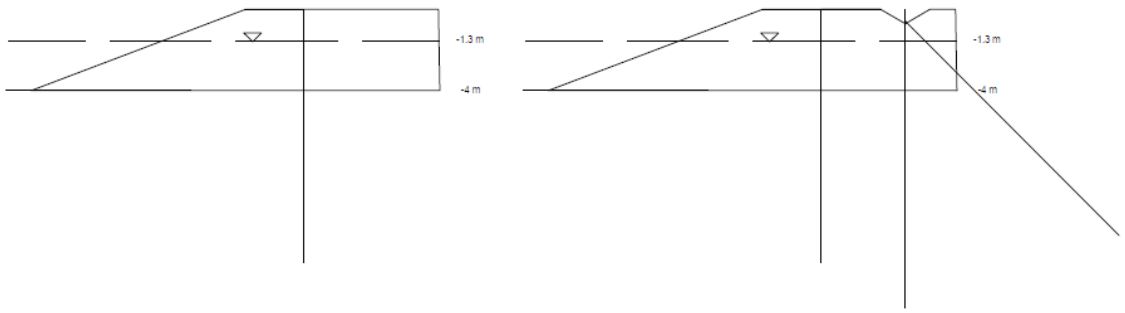

Figure 4.5: Schematic representation of area before and after installation of quay wall.

Dredging and load application:

Finally, the dredging process has been carried out in front of the quay wall, reaching a final depth of -14.25 m. A layer of rocks has been placed to maintain the appropriate bottom depth, serving as scour protection along the quay wall. Additionally, the construction is now subjected to various loads, with significant ones including crane loads, bollard loads, and terrain loads, as designed. The schematic cross-section is illustrated in Figure (4.6). In Figure (4.7) the final cross-section of the construction is depicted.

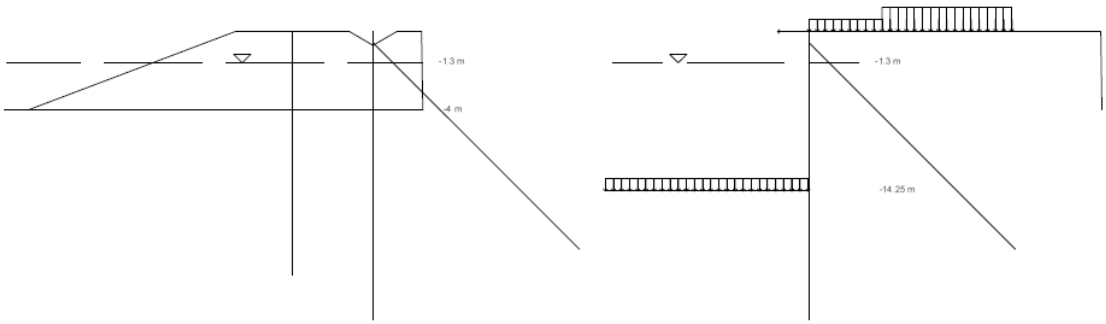

Figure 4.6: Schematic representation of area before and in the final stage.

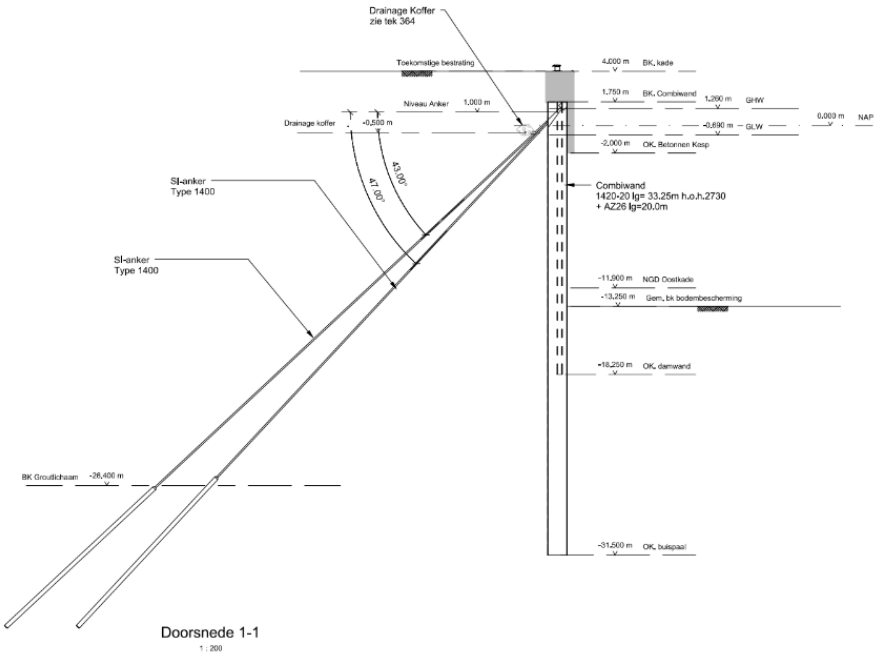

Figure 4.7: Final schematic cross-section of the quay wall

4.3 Design Parameters

4.3.1 Soil Parameters

In the initial phase of the analysis, the soil profile needed to be examined. The soil layers were classificated based on the most critical Cone Penetration Test (CPT) profile (worst-case scenario) provided in the Appendix (A) and specifically Figures (A.1), (A.2), (A.3) contains further details about the CPT profile.

Table 4.1: Soil Layers Identification

Layer Depth (m NAP)	Layer Name
4	Medium clean **sand**
-4	Loose clean **sand**
-16	Soft little sandy **clay**
-20	Loose clean **sand**
-21.5	Medium little sandy **clay**
-23.5	Loose clean **sand**
-24.5	Medium little sandy **clay** 2
-26	Dense clean **sand**

After defining the different soil layers, the main geotechnical parameters of the soil layers have been defined based on Table 2-b of NEN (2016), as depicted in Figure (A.1) . In order to avoid confusion regarding the extensive description over the names of the soil layers, for the Sand layers, **Sand** clean medium is going to be replaced with **Sand** 1, **Sand**

clean loose with **Sand** 2, **Sand** clean dense with Sand 3. Considering now the Clay layers, **Clay** little sandy soft will be replaced with **Clay** 1, **Clay** little sandy medium with **Clay** 2 and **Clay** little sandy medium 2 with **Clay** 3. As represented in Table (4.2).

Table 4.2: Geotechnical Parameters of Soil Layers

Layer Depth (m NAP)	Layer Name	γ_{unsat} (kN/m^3)	γ_{sat} (kN/m^3)	c (kN/m^3)	ϕ (°)
4	Sand 1	18	20	0	32.5
-4	Sand 2	17	19	0	30
-16	Clay 1	17	17	2.5	22.5
-20	Sand 2	17	19	0	30
-21.5	Clay 2	17	17	5	22.5
-23.5	Sand 2	17	19	0	30
-24.5	Clay 3	17	17	5	22.5
-26	Sand 3	19	21	0	35

Except the geotechnical parameters described in Table (4.2) though, additional soil parameters should be incorporated for the accurate modelling process, with separate considerations tailored for both Plaxis and D-Sheet Piling analyses. The Plaxis parameters that are not included in Table (4.2) have been derived from equations described in Subsubsection (2.3.3.1). In contrast, for D-Sheet Piling, the stiffness parameters have been chosen in accordance with the guidelines outlined in CUR (2012).

Table 4.3: Plaxis Soil Layer Properties

Layer Name Units	Layer Depth [m NAP]	Q_c [MPa]	γ_{unsat} [kN/m³]	γ_{sat} [kN/m³]	c' [kN/m²]	ϕ' [°]	ψ [°]	$E'_{50;ref}$ [MPa]	$E'_{oed;ref}$ [MPa]	$E'_{ur;ref}$ [MPa]	m [-]
Sand 1	4	15	18	20	0	32.5	2.5	58.93	58.93	235.70	0.50
Sand 2	-4	10	17	19	0	30	0	31.13	31.13	124.50	0.50
Clay 1	-16	4	17	17	2.5	22.5	0	6.92	5.54	34.61	1.00
Sand 2	-20	7.5	17	19	0	30	0	18.93	18.93	75.71	0.50
Clay 2	-21.5	4	17	17	5	22.5	0	6.05	4.84	30.25	1.00
Sand 2	-23.5	7.5	17	19	0	30	0	18.07	18.07	72.28	0.50
Clay 3	-24.5	4	17	17	5	22.5	0	10.37	8.30	51.87	1.00
Sand 3	-26	15	19	21	0	35	5	24.42	24.42	97.69	0.50

Table 4.4: D-Sheet Piling Soil Layer Properties

Layer Name Units	Layer Depth [m NAP]	γ [kN/m³]	γ_{sat} [kN/m³]	c' [kPa]	ϕ' [°]	$k_{h1;low}$ [kN/m³]	$k_{h2;low}$ [kN/m³]	$k_{h3;low}$ [kN/m³]
Sand 1	4	18	20	0	32.5	20000	10000	5000
Sand 2	-4	17	19	0	30	12000	6000	3000
Clay 1	-16	17	17	2.5	22.5	4000	2000	800
Sand 2	-20	17	19	0	30	12000	6000	3000
Clay 2	-21.5	17	17	5	22.5	4000	2000	800
Sand 2	-23.5	17	19	0	30	12000	6000	3000
Clay 3	-24.5	17	17	5	22.5	4000	2000	800
Sand 3	-26	19	21	0	35	40000	20000	10000

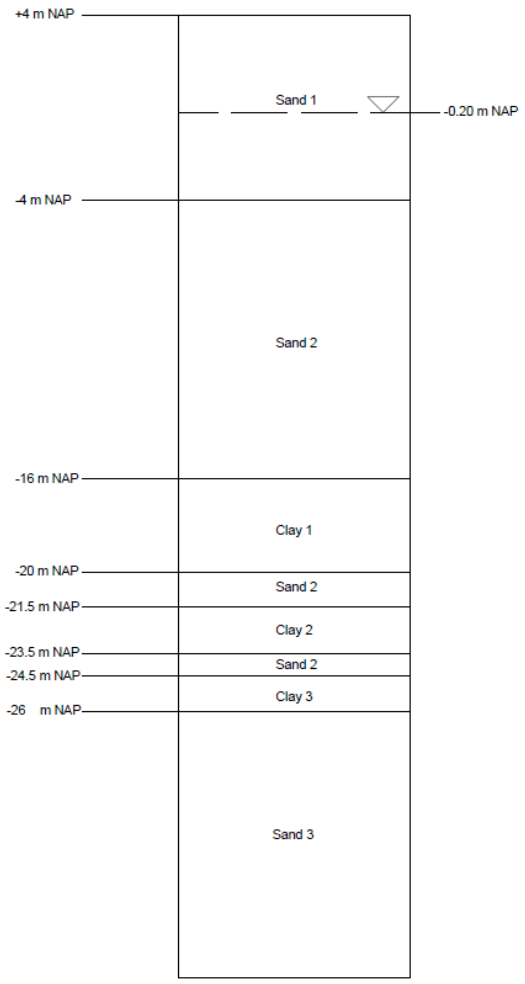

Figure 4.8: Representation of soil profile identified.

4.3.2 Hydraulic Conditions

4.3.2.1 Measured Water Levels

To determine the water levels with respect to NAP (m), it is necessary to establish the measurements of the water level. Considering that the structure of the quay wall is a part of east quay wall design, the focus should be established in the final column of Table (4.5).

Table 4.5: Measurement of Water Levels with Respect to NAP

Water Level	Hydrometeo 3	Hydrometeo 4	South Quay Design	East Quay Final Design
MHW	+1.26 m	+1.26 m	+1.15 m	+1.26 m
MLW	-0.68 m	-0.39 m	-0.66 m	-0.69 m
ALAT		-0.92 m		-1.00 m
HW 1%	1.66 m		1.90 m	1.90 m
HW 50%	0.95 m		1.09 m	1.09 m
HW 90%	0.63 m		0.75 m	0.75 m
LW 1%	-1.25 m		-1.32 m	-1.32 m
LW 50%	-0.72 m		-0.69 m	-0.69 m
LW 90%	-0.36 m		-0.41 m	-0.41 m
1 in 250-year event				-2.29 m
1 in 1-year event				-1.50 m

- **MHW / MLW (Mean High / Low Water):** Average height of the high / low tide over a specified period.
- **ALAT (Average Lowest Astronomical Tide):** Average level of the lowest tide during a specific period, often averaged over a long time frame.
- **HW / LW (High Water / Low Water):**The mean of the highest / lowest water levels determined over a span of several years. Source: Adapted from De Gijt and Broeken (2013)

4.3.2.2 Serviceability limit state and Ultimate Limit State

The quay wall has a drainage system at a level of NAP -0.50m, and it is expected to operate under both Serviceability Limit State (SLS) and Ultimate Limit State (ULS) conditions.

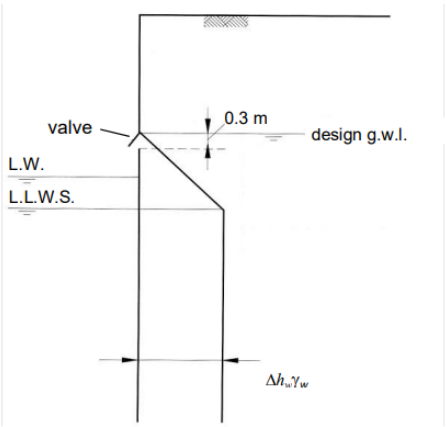

Figure 4.9: Computed groundwater pressures resulting from significant variations in external water levels, influenced by tides, and featuring a drainage mechanism with a valve. Source: Adapted from Korff (2018) ; CUR (2012).

In accordance with Part 2 of CUR166 (CUR, 2012), an additional 0.30 m is added here to account for the water level behind the quay, as shown in Figure (4.9); Table (4.6) below. For the representative groundwater level, NAP -0.20 m is considered. Regarding the design water level at the waterfront, the Lowest Low Water Spring (L.L.W.S.) is not utilized as per CUR166 (CUR, 2012) and CUR211 (CUR, 2005). Instead, the 1% Low

Water (LW 1%) of NAP – 1.32 m is used. The L.L.W.S. (approximately NAP -0.90 m) is not deemed representative for this design in terms of low water levels.

Table 4.6: Fundamental hydraulic pressure variation Δh with drainage. Source: Adapted from Roubos and Gijt (2013)

Drainage				
Water level fluctuations	**Soil conditions**	**OWL**	**GWL**	**Δhmin**
Minor	–	MLW	$h_{drainage} + 0.3$ m	>0.5 m
Major (rivers)	–	OLW/OLR	$h_{drainage} + 0.3$ m	>0.5 m
Tidal conditions	–	LLWS	$h_{drainage} + 0.3$ m	>0.5 m

4.3.2.3 Accidental water pressure

According to the handbook for quay walls (De Gijt and Broeken, 2013) three ALS (*Accidental Load Situations*) should be considered as per Table (4.7) below (relieving floor is not relevant):

1. Flooding
2. Extreme low water
3. Failure drainage

Table 4.7: Accidental hydraulic pressure variation Δh with drainage, in OWL (Outer Water Level) and GWL (Ground Water Level). Source: Adapted from De Gijt and Broeken (2013)

Drainage					
Accidental actions	**Water level fluctuations**	**Soil conditions**	**OWL**	**GWL**	**Δh_{min}**
Flooding	Minor	–	–	–	–
	Major	–	GL-2$\Delta h_{outer;day;1\times year}$	GL-1.5*$\Delta h_{outer;day;1\times year}$	–
	Tidal conditions	–	GL-2$\Delta h_{tide;mean}$	GL-1.5*$\Delta h_{tide;mean}$	–
Extreme low water	–	–	$LW_{1\times 250year}$	$h_{drainage}$+0.3m	–
Relieving floor	–	–	$LW_{1\times 250year}$	$LW_{1\times 250year}$	–
Failure drainage	Minor	Impermeable	$LW_{1\times year}$	$LW_{1\times year}$ $+\Delta h_{outer;month;1\times year}$	>1.0 m
		Permeable	$LW_{1\times year}$	$LW_{1\times year}$ $+\Delta h_{outer;day;1\times year}$	>0.5 m
		Permeable	MHW	MHW $+\Delta h_{outer;day;1\times year}$	>0.5
	Major	Impermeable	$LW_{1\times year}$	$LW_{1\times year}$ $+\Delta h_{outer;month;1\times year}$	>1.5 m
		Permeable	$LW_{1\times year}$	$LW_{1\times year}$ $+\Delta h_{outer;day;1\times year}$	>1.0 m
		Permeable	MSL	MSL $+\Delta h_{outer;day;1\times year}$	>0.5
	Tidal conditions	Impermeable	$LW_{1\times year}$	MSL	>1.5 m
		Permeable	$LW_{1\times year}$	MSL	>1.0 m
		Permeable	MSL	MSL + 0.5*$\Delta h_{tide;spring}$	>0.5

After carefully examining the hydraulic differences presented in Table (4.7), it has become imperative to reevaluate the scenarios involving accidental loads. This reassessment is detailed in Table (4.8), where the impact of the hydraulic differences on accidental load situations is documented.

Table 4.8: Accidental Load Situations and Water Levels

Load Case	**OWL NAP (m)**	**GWL NAP (m)**	**Δh (m)**
Flooding	$GL - 2\Delta h_{\text{tide;mean}} = 4.00\,\text{m} - 2.00 \times (1.26\,\text{m} - (-0.69\,\text{m})) = 0.10\,\text{m}$	$GL - 1.5\Delta h_{\text{tide;mean}} = 4.00\,\text{m} - 1.50 \times (1.26\,\text{m} - (-0.69\,\text{m})) = 0.76\,\text{m}$	0.66 m
Extreme Low Water	$LW_{1\text{x}250\text{year}} = -2.29\,\text{m}$	$h_{\text{drainage}} + 0.30\,\text{m} = -0.50\,\text{m} + 0.30\,\text{m} = -0.20\,\text{m}$	2.09 m
Failure Drainage	$LW_{1\text{xyear}} = -1.32\,\text{m}$	$MSL = (1.26\,\text{m} - (-0.69\,\text{m}))/2.00 = 0.29\,\text{m}$	1.79 m

4.3.2.4 Final Water Load

Based on the analysis conducted in the preceding sections, the Table (4.9) presents the ultimately determined water levels for the design.

Table 4.9: Load Situations and Water Levels

Load Case	**OWL NAP (m)**	**GWL NAP (m)**	Δh
Fundamental water level difference between SLS and ULS	-1.32 m	-0.20 m	-1.12 m
Accidental limit state	-2.29 m	-0.20 m	-2.09 m

4.4 Combination Loadings from Variable Actions

The loadings that have been considered in the current design as the most dominant, also indicated in Table (4.10) are :

1. **Bollard Load**: A horizontal line load is applied at the uppermost level of the quay wall, precisely at a height of +4 meters. This load configuration simulates the lateral forces exerted on the quay wall, typically arising from mooring operations and vessel interactions. The characteristic value of is calculated as 155 kN / m' (**Variable Load**).

2. **Crane Load**: Characterized as a surcharge load, the crane load is spanning from x values of 0 to 20 meters along its length. It represents the vertical forces imposed by crane operations during cargo handling, impacting the structural integrity of the quay wall in these regions. It accounts as a characteristic value of 40 kN/m^2 (**Variable Load**).

3. **Crane and Terrain Loads**: This scenario combines the effects of crane and terrain loads, concentrated within a specific section of the quay wall, spanning from x values of 20 to 100 meters. It considers the dynamic interaction between cranes and the varying weight distribution of cargo, crucial for evaluating the quay wall's response to dynamic loading conditions during cargo handling operations. It accounts as a characteristic value of 100 kN/m^2 (**Variable Load**).

4. **Scour Protection**: The bottom protection load is represented as a uniform load pattern. It is applied at the dredged depth of the quay wall, specifically at the construction depth of -14.25 meters. This load simulates the consistent forces that the quay wall may experience at its submerged base, aiding in the assessment of its stability and long-term structural integrity. The load, in the form of rocks, has a favorable effect in stabilizing the quay wall at the designated final depth. The characteristic load is 8 kPa. (**Permanent Load**).

5. **Crane and Pile Self-Weight**:The crane and pile self-weight load is introduced as a constant axial force over the full height of the wall. This distribution ensures stability and even weight distribution during crane operations. The characteristic

Table 4.10: Loads Adjusted to a 2D Construction with Coordinates (X1, Y1) and (X2, Y2)

Load Type	Magnitude	X1 (m)	Y1 (m)	X2 (m)	Y2 (m)
Horizontal Line Load	155 (kN/m')	0	4		
Surcharge Load	40 (kPa)	0	4	20	4
Surcharge Load	100 (kPa)	20	4	100	4
Uniform Load (Left Side)	8 (kPa)	-50	14.25	0	−14.25
Crane and Pile Self-Weight	533 (kPa)	0	4	∞	−31.50

load is 533 kPa at -31.50m, though it is subjected to changes, when the quay wall toe level changes and the value is reduced. (**Permanent Load**).

The design incorporates three distinct combination loadings that have been adjusted according to factors, which are depicted on Table (4.11).

Table 4.11: Recommended Values for Ψ-Factors for Combination of Variable Actions acting on Quay Walls. Source: Adapted from De Gijt and Broeken (2013)

Action	Combination factor, Ψ_0	Frequent value, Ψ_1	Quasi static value, Ψ_2
Uniform terrain load (cargo: containers, bulk goods)	0.7	0.5	0.3
Ship ramp loads (roll on roll of)	0.7	0.5	0
Traffic loads/actions (port vehicles)	0.6	0.4	0
Crane loads (crane for cargo handling)	0.6	0.4	0
Mooring loads (bollard pull/hawser load)	0.7	0.3	0
Ship berthing loads (reaction force fendering)	0.7	0.3	0
Earth pressures	1.0	1.0	1.0
(Ground) water pressures	1.0	1.0	1.0
Differential settlement	1.0	1.0	1.0
Environmental/Meteorological loads (wind, waves, current, temperature, ice)	0.7	0.3	0

Three load combinations have been considered in the case study, as presented in Table (4.12). The combination of loads A, B are the normative, while combination C represents an extreme case (accidental load case). In this case, aside from the significant difference in water levels, the presence of bottom protection is also deactivated. The two surchage loads indicated in Table (4.10) contribute to the terrain load and for the Ψ-factors chosen they are represented as a group in "terrain loads".

An important distinction and point to note is that in cases A and C of Table (4.12), the bollard load serves as the secondary momentary load, whereas the "terrain loads" take on the primary role. This is why the factors of 0.7 and 1 are used, signifying this relative significance. Conversely, in the case of B, the opposite scenario takes place.

Table 4.12: Combination Factors, Bollard Loads, Terrain Loads, Soil Protection, OWL, and GWL

Comb. Loads	**OWL (m)**	**GWL (m)**	**Bollard ψ**	**Bollard Load (kN/m')**	**Terrain ψ**	**Terrain Loads (kN/m^2)**	**Scour Protection (kN/m^2)**
A	-1.32	-0.20	0.7	110	1	40-100	Yes
B	-1.32	-0.20	1	155	0.7	28-70	Yes
C	-2.29	-0.20	0.7	110	1	40-100	No

4.5 Structural Components

4.5.1 Retaining Wall

In Table (4.13) the parameters of the tubular piles as well as the combi wall are been represented. The primary parameters governing the deflection of the combined wall in its main carrying direction arise from the interaction between the tubular pile and the intermediate sheet piles. This deflection behavior can be comprehensively determined by combining the respective bending stiffnesses using the following equation. The depiction of the construction can be found in Figure (4.2). It is important to emphasize that this relationship holds under the requirement that the sheet piles are symmetrically positioned relative to the centroid:

$$I_{\text{combi}} = \frac{I_{\text{tube}} + I_{\text{n;sheetpile}}}{L} \tag{4.1}$$

$$I_{\text{tube}} = \frac{\pi}{64} \cdot (D_{\text{e}}^4 - D_{\text{i}}^4) \tag{4.2}$$

Where:

$I_{\textbf{combi}}$: Moment of inertia of the combined wall in mm^4/m.

$I_{\textbf{tube}}$: Moment of inertia of the tubular pile (primary element) about the main neutral axis in mm^4.

$I_{\textbf{n;sheetpile}}$: Moment of inertia of the sheet pile profiles (secondary element) about the main neutral axis in mm^4.

L : center to center distance of the primary elements in m.

D_e : External tube diameter in mm.

D_i : Internal tube diameter in mm.

The elastic section modulus of the combined wall can be determined using the following formula:

$$W_{\text{combi}} = \frac{I_{\text{tube}} + I_{\text{n;sheetpile}}}{\frac{1}{2} D_e \cdot L} \tag{4.3}$$

where the parameters carry the same meaning (De Gijt and Broeken, 2013).

The total system width has been calculated based on the external diameter of the tubular piles, the width of double sheet piles, and double spacing of 30mm, amounting to a total of 2740 mm.

Important note is that in the calculation of M_{el} for the tubular piles the yield stress of X70 has been multiplied with W_{el}, whereas for the Combi-Wall, M_{el} is a result of the combination of both the primary and secondary elements. An essential parameter to consider is the implementation of a fixed-end anchor at the base of the quay wall in the Finite Element Method. The structural characteristics of this anchor include a stiffness value of $EA = 99.39 \times 10^3$ kN and is supported to be in unplugged conditions. This value has been computed using D-Foundation Calculations. Also it is important to mention that no steel corrosion of the combi-wall parameters. The values, which are used as part of the modelling process for the combi-wall, as well as other crucial factors, which influence the design, such as the diameter of the pile are been represented in Table (4.13).

Table 4.13: Combi-wall Parameters

Parameter	**Tubular Pile**	**Units**	**Combi-Wall**	**Units**
System Length	2740	mm	2740	mm
E	210000000	kN/m^2	210000000	kN/m^2
D	1.42	m	1.42	m
t	0.020	m	0.020	m
corr.	0.00	m	0.00	m
$t_{corr.}$	0.020	m	0.020	m
D_u	1.420	m	1.420	m
D_i	1.380	m	1.380	m
A	0.08796	m^2	0.08816	m^2
EA	18472565	kN	18514109	kN
EA / m	6741812	kN/m	6756974	kN/m
I	0.021556	m^4	0.02227134	m^4
EI	4526702	kNm^2	4676981	kNm^2
EI / m	1652081	kNm^2/m	1706927	kNm^2/m
W_{el}	0.030	m^3	0.031	m^3
f_y	X70-485000	kN/m^2	S355-355000	kN/m^2
M_{el}	14725	kNm	15086	kNm
w	2,956	kN/m/m	2,961	kN/m/m
M_{el}/m	5374	kNm/m	5506	kNm/m

4.5.2 Grout Anchor Parameters

The anchor is affixed at a height of $+1$ m above NAP on the retaining wall. To ensure its stability, a grout body of about 15 m in length is necessary. Consequently, the total length of the anchor amounts to 53 m, whereas, the anchors are installed with an angle of -45 °. The stiffness of the anchor is set at 1.9×10^8 kN/m^2 per anchor, and its cross-sectional area is 4.21×10^{-3} m^2/m' with the centre to centre spacing been 2.74 m.

The specified design yield stress, denoted as $f_{y;d}$, has been established at 470 MPa. During installation, the anchor is pre-stressed to a value of 200 kN/m. An essential differentiation arises in the Plaxis model, employing an Embedded Beam Row. The significance lies in the computation of the axial skin resistance, culminating in a final estimated value of 210 kN/m. For the modelling in D-Sheet Piling, no such action is needed to be taken into account.

4.5.3 Concrete Pile Cap

The pile cap primarily encompasses the upper section of the quay wall. It will only be used in the modelling with the usage of Plaxis, while it is excluded on the modelling of the structure on D-Sheet Piling. The comparison of three significant results in D-Sheet Piling, namely bending moment (M), shear forces (Q), and displacements, reveals that the inclusion of the concrete pile cap has minimal impact on these outcomes as illustrated in Subsection (4.7.1). To ensure accurate depiction and coherent presentation, the relevant parameters are provided in the following Table (4.14).

Table 4.14: Pile Cap Properties

Property	**Value**	**Unit**
Pile Cap Type	C(35/45)	-
Height	1.7	m
$E_{cracked}$ (0.3 x E)	1.02E+07	kN/m^2
A / m	1.7	m^2/m
I / m	0.409	m^4/m
EA / m	1.738E+07	kN/m
EI / m	4.186E+06	kNm^2/m
Weight load per Unit Length (w)	37.5	kN/m/m

The uncracked modulus of elasticity of concrete, E, has been determined using the formula prescribed by the Eurocode (EC2) (CEN, 2004):

$$E = 22 \left(\frac{f_c' \cdot 1000}{1000} \right)^{0.3} \times 10^3$$

Where:

E is the modulus of elasticity of concrete in MPa.

f_c' is the characteristic compressive strength of concrete in MPa.

4.6 Calculation Stages

4.6.1 Plaxis

4.6.1.1 Model Geometry and mesh

For the analysis of the model Plaxis 2D (Version 21.01.00.479) was selected since it could offer a comparison with another modelling software used for the modelling of quay walls. The unit weight of the water is set at 10.25 kN/m^3, considering the saltwater. The contour of the model is identified with x_{min} = -100.00 m, x_{max} = 250.00 m, y_{min} = -150.00 m and y_{max} = 6.00 m. The model is a plain strain model, with the elements been selected as 15-noded triangular ones. The final number of elements located on the model is 4530. Considering the boundary conditions, the water conditions are set at a global level per relevant soil cluster, except the lower clay layer near the toe level of the quay wall, which after on the phase preparation before the installation of the combi-wall is set as interpolate. No boundary lines have been set at any boundary point of the domain. When considering the geometry of the analysis, it is important to be mentioned, since also the land reclamation stage is been calculated, that a polygon, as identified in Figure (4.4), is been created with its points on p_0= (x: 26.00 m y: -4.00 m), p_1= (x: 51.00 m y: 4.00 m), p_2= (x: 250.00 m y: 4.00 m), p_3= (x: 250.00 m y: -4.00 m). The secondary sheet pile, which was used to avoid seepage issues, is depicted as a plate element, with its points at p_1= (x: 62.05 m y: 4.00 m), p_2= (x: 62.05 m y: -26.00 m). The quay wall is located at points, p_1= (x: 72.80 m y: 4.00 m), p_2= (x: 72.80 m y: -31.50 m) and its structural components, the tubular piles and concrete pile cap are modelled as plate elements, whereas at the toe of the quay wall, the toe is fixed with an anchor element. The anchor has been modelled as an anchor element and its grout body as an embedded beam row element. The points of the anchor are p_1= (x: 72.80 m y: 1.00 m), p_2= (x: 100.50 m y: -26.40 m), whereas the points of the embedded beam row p_1= (x: 100.50 m y: -26.40 m), p_2= (x: 113.30 m y: -39.16 m). Also the interfaces are been used as part of the analysis. The model used for the soil material is the Hardening Soil Model since it has been proven to be suitable for modelling retaining wall behaviour (Bentley Advancing Infrastructure, 2022).

4.6.1.2 Loading Calculation Stages

For the case of Plaxis, where the soil history can be better represented compared to D-Sheet Piling, it is important to analyze the phases correctly considering, the importance to the mesh and how the finite element method works. So the construction of the structure is depicted as built. The final number of phases were sixteen.

1. **Stress Initiation:** Where the initial case before the land reclamation began works on the soil model.

2. **Land Reclamation:** Where the soil is deposited on the sea bottom in a way to reclaim the land.

3. **Consolidation of Reclamation:** Where a consolidation calculation type is conducted on the previous phase to fully dissipate the excess pore pressures, which have been build up on previous phases.

4. **Preparation of Construction:** Where the sheet pile is constructed 10 meters away from the structure to create a temporary dry working platform, and excavations for the installation process of the combi-wall.

5. **Installation Combi-Wall:** Where the combi-wall is installed.

6. **Anchor Installation:** Installation of the anchor as well as the application of its prestress.

7. **Take out Sheet Pile Wall:** Where the sheet pile in front of the combi-wall is removed.

8. **Concrete Top Installation:** Where the final part of the concrete top part is installed.

    (a) **Final Excavation Level on Water-Side:** Where the soil is excavated to its final level of -14.25m on the left side of the wall.

        i. **Combination Load A Ignore Undrained Behavior:** Where Combination Load A is applied to the structure, ignoring the undrained behavior (drained condition).

        ii. **Combination Load A No Ignore Undrained Behavior:** Where Combination Load A is applied to the structure, not ignoring the undrained behavior (undrained condition).

    (b) **Final Excavation Level on Water-Side:** Where the soil is excavated to its final level of -14.25m on the left side of the wall.

        i. **Combination Load B Ignore Undrained Behavior:** Where Combination Load B is applied to the structure, ignoring the undrained behavior (drained condition).

        ii. **Combination Load B No Ignore Undrained Behavior:** Where Combination Load B is applied to the structure, not ignoring the undrained behavior (undrained condition).

    (c) **Final Excavation Level on Water-Side:** Where the soil is excavated to its final level of -14.25m on the left side of the wall.

i. **Combination Load C Ignore Undrained Behavior:** Where Combination Load C is applied to the structure, ignoring the undrained behavior (drained condition).

ii. **Combination Load C No Ignore Undrained Behavior:** Where Combination Load C is applied to the structure, not ignoring the undrained behavior (undrained condition).

It should be clarified that in phases 8.(a).i, 8.(b).i, and 8.(c).i, the "ignore undrained behavior" option is chosen, in contrast with 8.(a).ii, 8.(b).ii, and 8.(c).ii where this option is not selected. If the option is chosen, water stiffness is disregarded. Consequently, all undrained soil clusters become drained. While existing excess pore pressures remain, no new excess pore pressures are generated during that specific calculation phase.

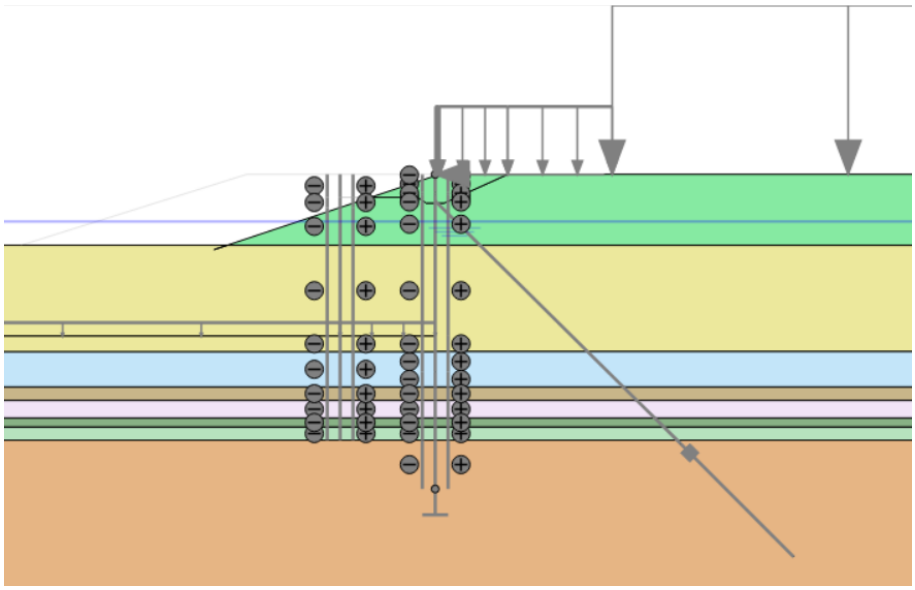

Figure 4.10: Representation of Plaxis soil model.

4.6.2 D-Sheet Piling

For the modelling in D-Sheet Piling(Version 21.1) only four phases are been represented.

1. **Installation of Combi-Wall and Pre-Stress of Anchor:** During this phase, both surface levels (left and right) are maintained at +0 m NAP, and prestress is applied to the anchor.

2. **Final Excavation Level on Water Side and Load Combination A Application:** This phase involves reaching the final excavation level on the water side, accompanied by the application of Load Combination A.

3. **Final Excavation Level on Water Side and Load Combination B Application:** Similar to the previous phase, the final excavation level on the water side is reached, and Load Combination B is applied.

4. **Final Excavation Level on Water Side and Load Combination C Application:** In this phase, the final excavation level on the water side is achieved, and Load Combination C is applied.

In D-Sheet Piling, if the total pore pressure distribution deviates from the hydrostatic distribution, users need to manually input the additional pore pressures for each layer, while in Plaxis this process is calculated automatically. The input of additional pore pressures in this structure applies to the bottom layers of the model at both the upper and lower boundaries. This inclusion of pore pressures is mandatory in enhancing the accuracy of the simulation. By accounting for these pore pressures, we are better able to replicate real-world conditions and the influence of water pressures on the behavior of the quay wall system. Also the value of the unit weight of the water is set at 10.25 kN/m^3 while the calculation behavior is assumed to be elastic.

Table 4.15: Increase in water tension on different water levels after excavation phases (with the values of additional pore pressures at top and bottom) aligning with the respective phases

Layer	Top Level	Water Tension Incr. (kPa) - Ph. 2,3		Water Tension Incr. (kPa) Ph. 4		Water Tension Incr. (kPa) Ph. 1	
	(m NAP)	Ad. pore pr. at top	Ad. pr. at bot.	Ad. pr. at top	Ad. pr. at bot.	Ad. pr. at top	Ad. pr. at bot.
Sand 1	4	0	0	0	0	0	0
Sand 2	-4	0	0	0	0	0	0
Clay 1	-16	0	16.1	0	25.8	0	4.9
Sand 2	-20	16.1	16.1	25.8	25.8	4.9	4.9
Clay 2	-21.5	16.1	16.1	25.8	25.8	4.9	4.9
Sand 2	-23.5	16.1	16.1	25.8	25.8	4.9	4.9
Clay 3	-24.5	16.1	16.1	25.8	25.8	4.9	4.9
Sand 3	-26	16.1	16.1	25.8	25.8	4.9	4.9

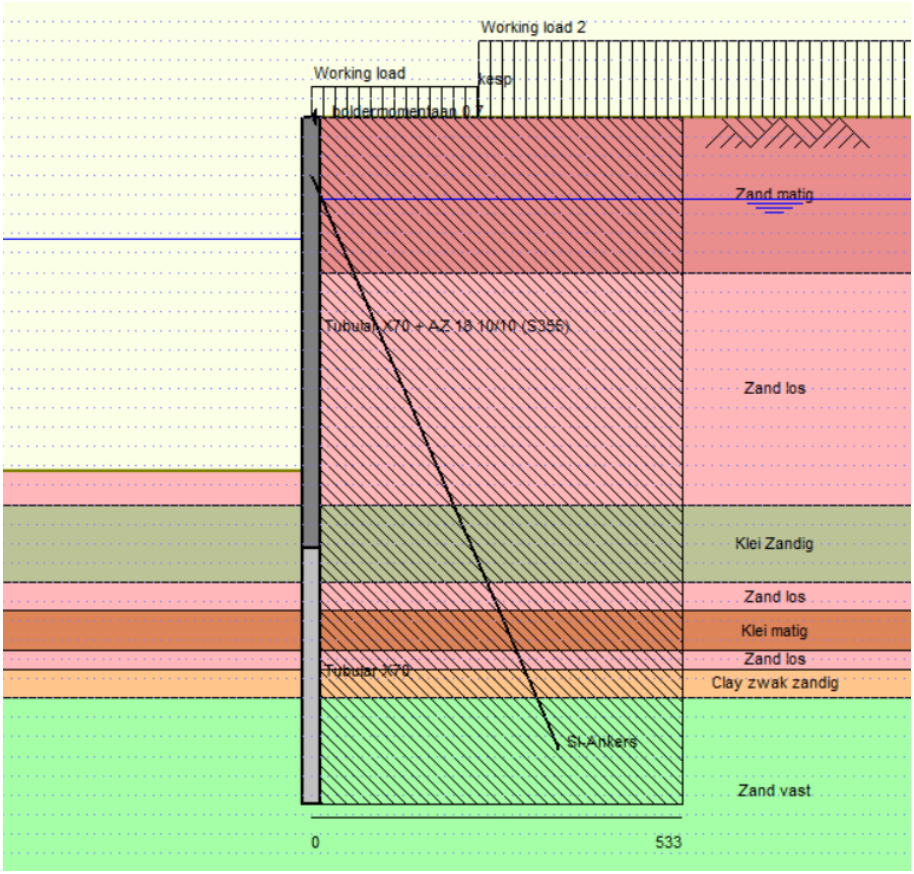

Figure 4.11: Representation of D-Sheet Piling soil model.

4.7 Modelling Software Comparison

Monitoring sensors are installed immediately following the construction of the quay wall. As stated in NEN (2016), monitoring can be implemented, to validate the performance of the predictions made during the design process and to ensure the ongoing performance of the structure meets the required standards after completion.

To gain a more complete understanding of our findings, it is crucial to compare the results we obtained from the Plaxis model with what was observed in the real world. However, we must acknowledge a limitation here. The monitoring data collection stopped three months after the active service period. In simple terms, while this comparison is valuable for evaluating how well our model performed, there is a challenge. We do not have recent monitoring data, so we might not be able to fully assess how accurate our model's predictions are. A crucial distinction lies in the fact that the outcomes detailed in Table (4.16) pertain specifically to a location at the top of the quay wall. This particular point holds significance in terms of the structure's functionality.

Given the results we've obtained, it appears that the measurements closely align with the model's predictions on the y axis, exhibit a significantly higher value. Considering the calculations are based on characteristic values on Plaxis, it is normative that the results of the deformations in Plaxis are higher than monitoring measurements. Additionally, the

Table 4.16: Comparison of deformation measurements between Plaxis (Phase displacement x,y between Phase 8.(a) and 8.(a).i) and a monitoring point on top of quay wall, three months after active use.

Method	X Deformation (m)	Y Deformation (m)
Plaxis Results	- 0.116	- 0.065
Monitoring Measurement	- 0.026	- 0.056

monitoring measurements, as previously mentioned, stop after 3 months. Therefore, it is likely that the deformations have not yet stabilized to their final state. Therefore, we can reasonably conclude that the model is valid.

In the context of validating our model, the next logical step involves transitioning towards simplified modeling approach. This approach aims to assess the model's overall validity for our specific case. Specifically, we plan to compare the structural components' results obtained from the Plaxis model with those derived from D-Sheet Piling. In our case, we want to evaluate how well the D-Sheet Piling model simulates the behavior of structural components in comparison to a specialized software like Plaxis. It is essential to highlight that we consider Plaxis to generally provide more accurate results if calibrated properly. Otherwise we have "accurate fiction". However, it is worth noting that there is a recognized margin of inaccuracy associated with Plaxis, typically falling within the range of plus or minus 30%.

In order to decide, the validity of the results a comparison of the results has been made between Plaxis and D-Sheet Piling. For each of the three load applications the results are been depicted below. In the starting phase a comparison between the two slip surfaces for the validity of the two models is been presented, which is correct and is been presented in Figure (4.12).

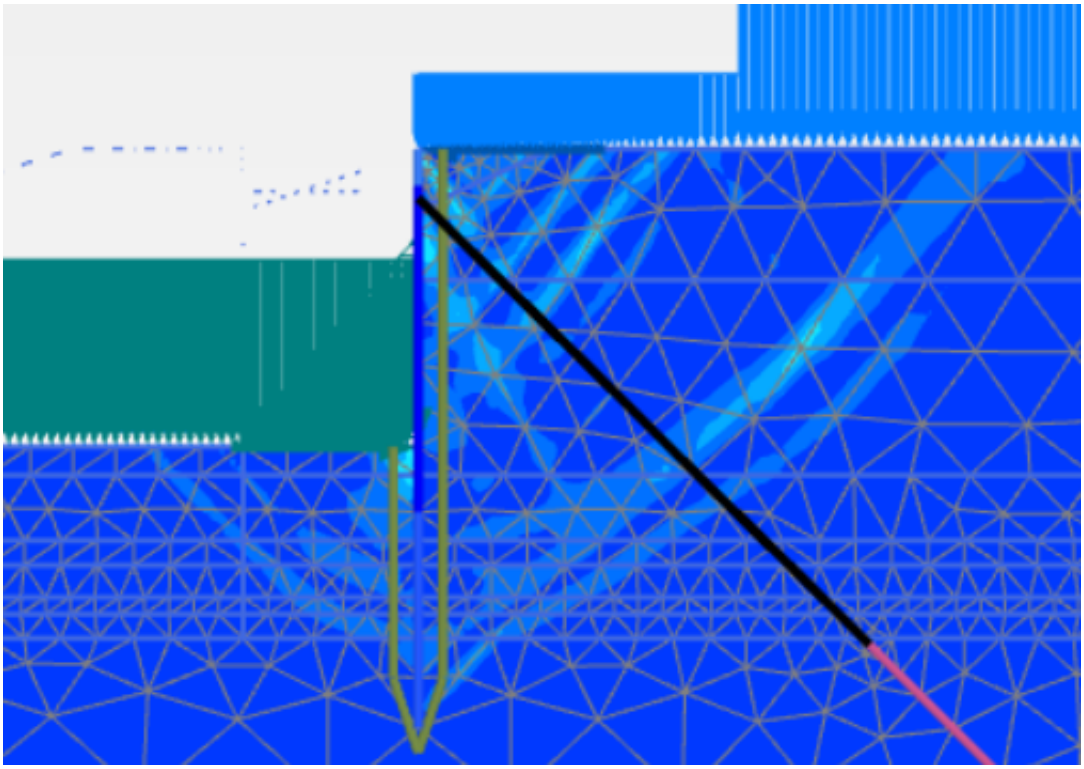

(a) Slip surface line adapted from Plaxis results for load combination A.

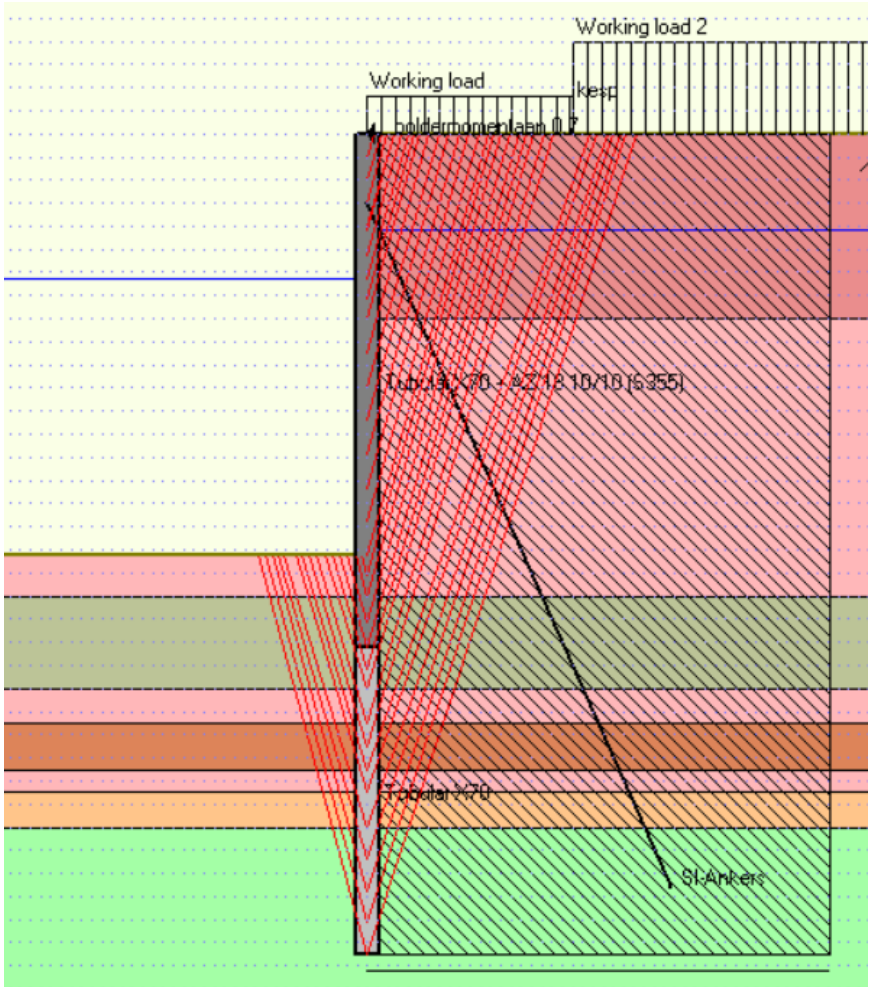

(b) Slip surface line adapted from D-Sheet Piling results for load combination A.

Figure 4.12: Comparison of slip surface lines for load combination A.

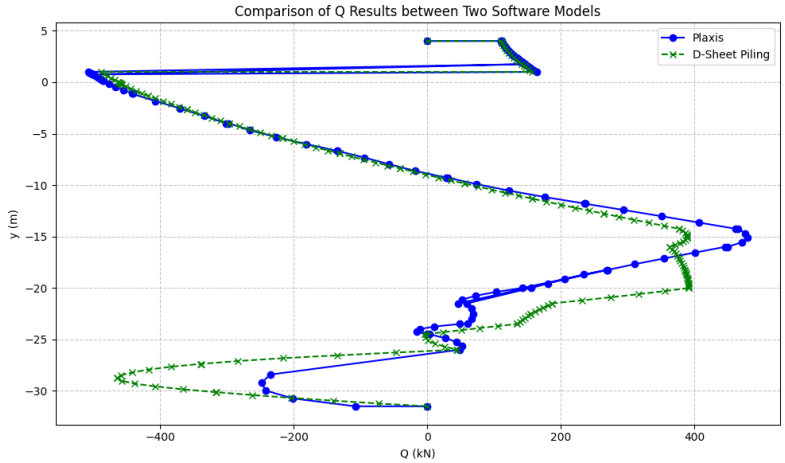

(a) Comparative results for Q for load combination A for D-Sheet Piling and Plaxis.

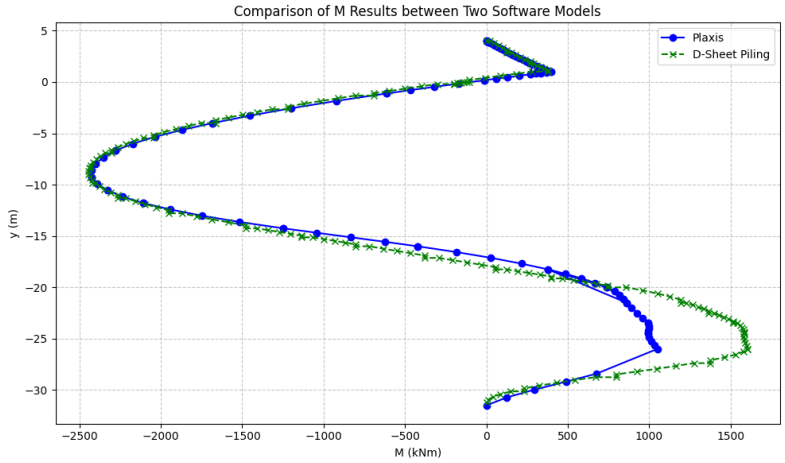

(b) Comparative results for M for load combination A for D-Sheet Piling and Plaxis.

Figure 4.13: Comparison of structural components of quay wall for load combination A.

Table 4.17: Comparison of Maximum and Minimum Values

Comb. A	**Plaxis**		**D-Sheet Piling**	
	Max Value	**Min Value**	**Max Value**	**Min Value**
Q	478.96	-507.64	391.81	-488.12
M	1050.24	-2425.91	1602.31	-2445.19
Comb. B	**Plaxis**		**D-Sheet Piling**	
	Max Value	**Min Value**	**Max Value**	**Min Value**
Q	447.35	-467.11	366.93	-461.65
M	1064.63	-2034.92	1461.49	-2195.98
Comb. C	**Plaxis**		**D-Sheet Piling**	
	Max Value	**Min Value**	**Max Value**	**Min Value**
Q	453.42	-494.52	617.86	-878.74
M	1093.50	-2409.24	2658.23	-3753.59

In the next phase of the analysis, we will delve deeper into the results obtained from both models, with a specific emphasis on examining the diagrams that portray the bending moment (M) and shear forces (Q). These diagrams hold significant importance in gaining insights into the structural behavior and response of the quay wall system under the influence of applied loads and various environmental conditions. The results from both model have a lot of similarities, especially from y=4 m until y= -20 m, which follows a similar trend and are mostly exaggerated in the case of D-Sheet Piling. For easier representation for the load combination B, C the diagrams are represented in the Appendix (A) and specifically Figures (A.4), (A.5). Also, in Table (4.17) a comparison between the maximum and minimum values is been represented, for clarity, since the results can be also be exerted by Figures (4.13), (A.4), (A.5). While combinations A and B exhibit relatively similar values, combination C, representing the accidental load case, demonstrates a significantly higher difference in both Q and M values for D-Sheet Piling compared to the previous two load combinations.

Based on the comparison with monitoring results it is expected that while Plaxis provides more accurate values, D-Sheet Piling offers results that exhibit a strong correlation with Plaxis results. Therefore, the selection of D-Sheet Piling is primarily based on its exceptional computational speed. This choice aligns with the overarching goal of this thesis, which is to develop a practical method for reliability based design assessments. D-Sheet Piling's efficiency makes it a valuable tool for real-world engineering applications.

In the context of the quay wall case study, D-Sheet Piling emerges as a pragmatic and workable choice. However, it is essential to recognize that in more challenging scenarios, such as when modeling a relieving platform, the minor discrepancies inherent in D-Sheet Piling's results may assume greater significance. Extending on that, the soil is been modelled using horizontal uncoupled springs, making it challenging to accurately model relieving platforms and inclined walls. The spring-supported beam model typically does not incorporate undrained behavior. Considering these factors, De Gijt and Broeken (2013) recommends the usage of spring-supported beam models for simple quay wall structures or in the early stages of complex structure design. For more complex quay walls, which have features such as relieving platforms, combined walls, or inclined walls where the arching effect is significant, Finite Element Method (FEM) modeling provides a more accurate representation. In these situations, the necessity for a higher level of precision could outweigh the advantages of computational speed.

In summary, the selection between D-Sheet Piling and Plaxis hinges on the specific engineering project and its unique requirements. For straightforward designs like the current quay wall, which essentially constitutes a sheet pile wall supported by anchors, D-Sheet Piling offers an efficient and effective solution. Nonetheless, in higher complexity projects (quay wall with relieving platform), the precision provided by Plaxis may be indispensable, even if it entails longer computational times.

4.7.1 Concrete Pile Cap Simplification

In order to simplify more the model, it is going to be assessed, the importance of the pile cap in the design by a comparison of the results for the structural elements. The results are illustrated in Figure (4.15), where it is not easy to discern the difference between the two approaches. So in D-Sheet Piling model, pile cap will not be included.

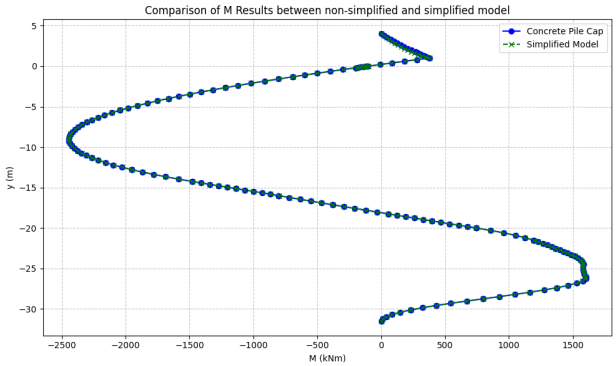

(a) Comparative results of bending moments for load combination A.

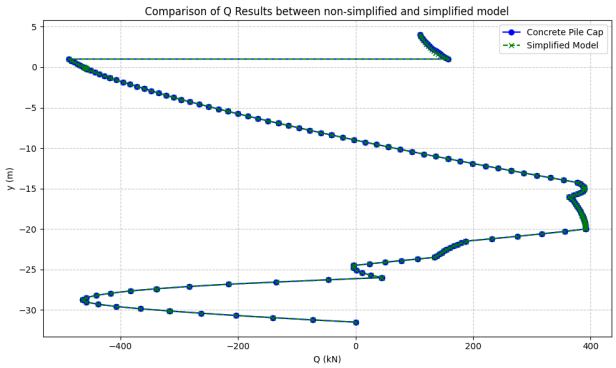

(b) Comparative results of shear forces for load combination A.

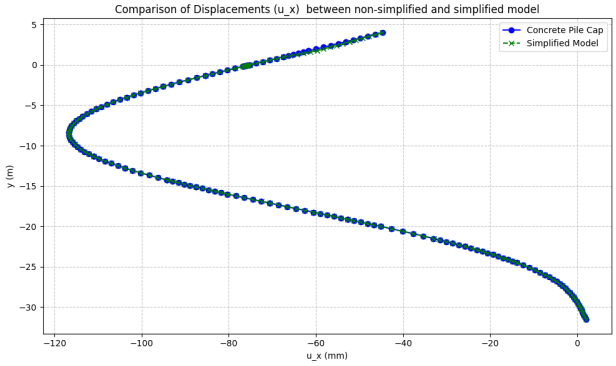

(a) Comparative results of displacements for load combination A.

Figure 4.15: Entire Comparative Results for Load Combination A

5

Research Methodology Background

In this chapter the research methodology that was followed is going to be discussed. After the results of Chapter (4), the simplified modelling software of D-Sheet Piling has been selected as the favorable choice. In this chapter, we will revisit the structure of the methodology. Additionally, a dedicated section on partial factor derivation will be incorporated. Following that, an in-depth examination of the three failure equation mechanisms will be presented, highlighting their significance in the overall structure of the thesis. Subsequently, a comprehensive overview of all stochastic parameters will be provided. This encompasses the stochastic variables, the coefficients of variation (COV), and the correlation parameters, each playing a crucial role in influencing the analysis and its results. The chapter ends by establishing the final model, which will be subjected to the reliability analysis.

5.1 Methodology

In this section the research flowcharts are been depicted in Figure (5.1). It can be depicted that at the base of the methodology D-Sheet Piling as the modelling software exists. Due to easy linkage with Probabilistic Toolkit, also developed Deltares, it will be selected as the reliability software of the analysis. The analysis has been conducted on Probabilistic Toolkit version 2023.0.3055.0) For all 3 failure equation mechanisms then the value of β is going to be estimated, an indication of the probability of failure with FORM method.

Subsequently, upon identifying the dominant combination loading, the focus of the study shifts to two distinct cases: optimization within the design process and the optimization of an existing construction. In the first case scenario, a cost optimization will be undertaken, prioritizing steel conservation while ensuring an optimal design process. This analysis will also encompass the quantification of the unemitted CO_2 emissions within the environment. In the second scenario, the focus will shift towards exploring an optimization of the existing structure.Initially exploring the dredging limits, which

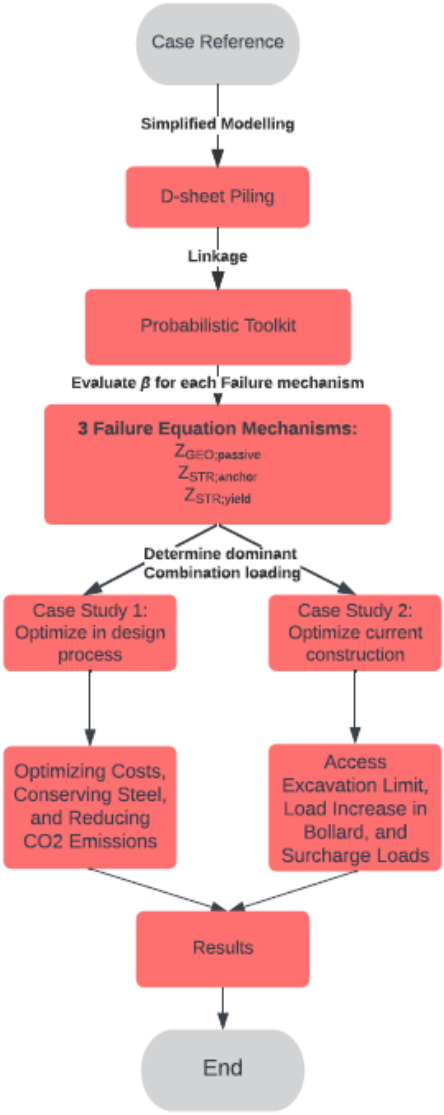

Figure 5.1: Research Structure Flowchart

involves assessing the current combined load conditions within the existing structure while gradually lowering the dredge level in front of the quay wall of the model. Secondly, keeping the same dredge level and incrementally raising the bollard loading and surcharge load of the crane and cargo. Thirdly, these two incremental loading increases are going to be examined simultaneously.

This section is dedicated to the exploration of the potentials and constraints associated with the coupling methodology. Examining the possibilities, one finds it to be a relatively efficient and time-saving approach. The simplicity of utilization, coupled with the abundance of available reliability methods and the option to integrate with Python, makes it a promising avenue. Additionally, users have the flexibility to define their own failure equations. Also an assumption is stated that the behavior of the calculation is set as

elastic (both the behavior of the soil and the wall), with the value of the unit weight of the water is set at 10.25 kN/m^3, due to the area specific case.

The limitations of the research should be acknowledged. The methodology does not consider coupled soil springs, leading to the absence of arching effects. The analysis of soil-structure interaction is constrained (only considers soil-structure interaction between the soil and the front wall), and there is a limited applicability to complex geometries. Additionally, the conclusions drawn are based on a single benchmark case, emphasizing the need for more benchmark cases to enhance the more global conclusion on the findings, so the conclusions are specific to the construction under consideration. Furthermore, the evaluation focuses on only three critical failure equation mechanisms, indicating a scope for broader exploration. Another noteworthy limitation is the no inclusion of the structural stochastic variables in the analysis, where the steel component is important for all the three critical failure equation mechanisms. Though due to the low uncertainty of steel strength it was chosen to not be included. Furthermore, the software is in a relatively developmental stage (beta version(s)), lacking comprehensive manuals or information on usage. Large computations may encounter memory exception errors, adding a layer of complexity to extensive calculations. In addition The lack of additional benchmark cases for the analysis can not lead on the global applicability of the conclusions. The findings are specific to the current case study.

5.2 Limit State Equations

In this thesis report, three distinct failure mechanisms were explored that could lead to failure of a quay structure.

1. **Anchor Force (Yielding of Anchor):** Our analysis includes the assessment of anchor force yielding, which plays a pivotal role in determining the stability and performance of the anchoring system. For this limit state the equation is described in Table (5.1) as Equation (a).

2. **Degree of Mobilization (Yielding of Soil):** In the D-Sheet Piling, the degree of mobilization is defined as the ratio of the mobilized resistance of the passive soil wedge to the maximum resistance. For this limit state the equation is described in Table (5.1) as Equation (b). In the case of a single-supported wall, also the mobilized moment is calculated in Equation (5.1):

$$\frac{\text{Mobilized Resistance} \times \text{Distance from Mob. Res. Force to Support}}{\text{Maximum Resistance} \times \text{Distance from Mob. Res. Force to Support}} \tag{5.1}$$

3. **Degree of Mobilized Moment (Yielding of Sheet Pile Wall):** This mechanism evaluates the potential for the sheet pile wall to yield under load. For this limit state the equation is described in Table (5.1) as Equation (c).

Table 5.1: Failure Equations. Source adapted from Allaix et al. (2022)

Equation	Description
(a)	$Z_{STR;\text{anchor}} = F_{\text{rd;anchor}} - \theta_{m;F} \cdot F_{\text{anchor}}$
(b)	$Z_{\text{GEO;passive}} = 99 - \theta_{m;MobP} \cdot \text{MobPassive}$
(c)	$Z_{\text{STR;yield}} = 99 - \theta_{m;MobM} \cdot \text{MobMoment}$

In the above formulations:

- Variables subject to stochastic variability are visually highlighted in red, denoting their susceptibility to random variations (uncertainty).
- Values characterized by determinism and predictability are represented in green, reflecting their stable nature.
- Outputs generated by the D-Sheet Piling analysis are distinctly highlighted in blue, signaling their derivation from the computational tool's results.

Where:

$Z_{\textbf{STR;anchor}}$: Limit state function for maximum stress in anchor cross-section (kN/m^2)

$Z_{\textbf{GEO;passive}}$: Limit state function for maximum mobilized passive wedge resistance (%)

$Z_{\textbf{STR;yield}}$: Limit state function for maximum mobilized moment of sheet pile wall (%)

$F_{\textbf{rd;anchor}}$: Maximum Anchor force acting as resistance. (kN/m^1)

$F_{\textbf{anchor}}$: Anchor force calculated using D-Sheet (kN/m^1)

$\theta_{m;\textbf{F/MobP/MobM}}$: Factor to account for model uncertainty using D-Sheet (-)

MobPassive : Ratio of Mobilized passive resistance to available passive resistance calculated using D-Sheet (%)

MobMoment : Percentage of the mobilized moment of sheet pile wall, calculated using D-Sheet (%)

While a degree of mobilization of 100 % is permissible for the yielding of soil, it is important to note that if all soil springs yield, this can result in substantial deformations of the sheet pile wall and potential numerical challenges. Therefore, it is advisable to utilize a degree of mobilization less than 100 % where 99 % is used. For the other failure mechanism, there are no known numerical issues. Though for the assessment of the current structure with the quay wall toe level at -31.50 m, it is imporant to clarify that a $F_{\text{rd;anchor}}$ value equal to 99 % x 2000 kN = 1980 kN has been assumed.

5.2.1 Model Uncertainty

In the context of this study, model uncertainty can play a pivotal role, as already elucidated in the equations presented in Table (5.1). This factor encompasses a spectrum of unforeseeable events, that the structure of the quay wall faces, ranging from the randomness of weather conditions to unpredictable variations in loads and most notably in the current research, the coefficient of variation in the soil properties.

It is important to acknowledge that there exists inherent uncertainty regarding how our design models correspond to the actual cross-sectional behavior observed in practical applications. This uncertainty materializes as a disconnect between the calculated outcomes of our models and the empirical data or experimental results, which necessitates the introduction of a model uncertainty factor.

In our case study, we incorporate this model uncertainty factor, denoted as $\theta_{m;\mathrm{F/MobP/MobM}}$, into our probabilistic computations using the Deltares Probabilistic Toolkit. This $\theta_{m;\mathrm{F/MobP/MobM}}$ factor serves as an additional multiplier within the numerator, modifying the output parameters generated by D-Sheet Piling and follows a log-normal distribution (Allaix et al., 2022). This underscores the significant impact of accounting for model uncertainty in our analyses.

5.3 Partial Factor Derivation

This section outlines the derivation process for sensitivity factors and partial factors of safety, considering correlations among prominent stochastic variables. The factor α_i, obtained through a FORM-based reliability assessment, characterizes the sensitivity to variations in random variables concerning the specific reliability index β associated with a given limit state.

5.3.1 Steps for Derivation of Partial Factors

1. **Identify Key Design Variables:**
   Identify the key variables that influence the behavior of the structure, such as material strength, loads, and environmental conditions. In a generic way, it is not directly related with partial factors derivation, but is introduced as a first step, since it is essential for the definition of the model.

2. **Define Limit State Equations:**
   Define the limit states that the structure must satisfy. Limit states are conditions beyond which the structure is considered to be unsafe or not meeting the desired performance criteria.

3. **Determine Mean Values:**
   Determine the mean values of the design variables. These are representative values that account for natural variability and uncertainties.

4. **Determine Characteristic Values:**
   Determine the characteristic values of the design variables. .

5. **Set Target Reliability Levels:**
   Establish target reliability levels for each limit state. Reliability is a measure of the probability that a structure will be "safe" under specified conditions. Where for all the cases a β value of 3.30 has been assumed.

6. **Check Reliability and Adjust Structure:**
   Use reliability analysis methods (FORM) to check whether the structure meets the target reliability level. If the β value is higher than 3.30, modification on the structure should be made in order to get to a value as close as possible to 3.30 with the focus on changing the retaining height.

7. **Establish Partial Factors:**
   Based on the results of the reliability analysis, when β value is close to 3.30 and using the design values that are extracted by the software (FORM method), the partial factors can be established with comparing the design values of the uncorrelated / correlated variables with the characteristic values.

5.3.2 Partial Factors Calculation Equations

5.3.2.1 Material Properties (X_i)

In cases where input variables are uncorrelated, the sensitivity factors in the normalized physical space (U-space), denoted as $\alpha_{u;i}$, can be utilized in analytical expressions to determine the partial material factors γ_m.

For all material properties X with a normal distribution, except ϕ , the characteristic value, $X_{k;i}$, can be calculated as:

$$X_{k;i} = \mu_i - 1.645V_i \tag{5.2}$$

The value of 1.645 corresponds to the standard normal's distribution value at 95% confidence level. Though in the case of ϕ which also has a normal distribution, characteristic value should be calculated :

$$X_{k;\phi} = \mu_\phi - 1.645\frac{V_\phi}{\sqrt{n}} \tag{5.3}$$

The parameter n, indicates the value of samples and is estimated :

$$n = \left(\frac{1.64\sigma_\phi}{\mu_\phi - \phi_{k,\text{low}}} \right)^2 \tag{5.4}$$

Where:

σ_ϕ**:** Standard deviation of material property ϕ.

$\phi_{k,\textbf{low}}$**:** Low characteristic selected value for material property ϕ.

Though the design value, $X_{d;i}$, for the uncorrelated space will be the same for all material properties X and it can be calculated using the equation:

$$X_{d;i} = \mu_i \left(1 - \alpha_i \beta_t V_i\right) \tag{5.5}$$

The partial factor of safety $\gamma_{m;i}$ can then be defined as the ratio of the characteristic value to the design value:

$$\gamma_{\mu;i} = \frac{X_{k;i}}{X_{d;i}} \tag{5.6}$$

Considering the log-normal distribution, the characteristic value, $X_{k;i}$ can be calculated with the following two equations, based on the coefficient of variation of the stochastic variable.

$$X_{\text{k;i}} = \mu_i e^{-\frac{1}{2}\ln\left(1+V_i^2\right)+\Phi^{-1}(p)\sqrt{\ln\left(1+V_i^2\right)}} \quad \text{for } V_i \geq 0.2 \tag{5.7}$$

Where:

$\Phi^{-1}(p)$**:** It describes the inverse of the cumulative distribution function (CDF) of the standard normal distribution.

$$X_{\text{k;i}} \simeq \mu_i e^{\Phi^{-1}(p)V_i} \quad \text{for } V_i < 0.2 \tag{5.8}$$

The design value, $X_{d;i}$, is again estimated based on the value of coefficient of variation.

$$X_{\text{d;i}} = \mu_i e^{-\frac{1}{2}\ln\left(1+V_i^2\right)-\alpha_i\beta\sqrt{\ln\left(1+V_i^2\right)}} \quad \text{for } V_i \geq 0.2 \tag{5.9}$$

$$X_{\text{d;i}} \simeq \mu_i e^{-\alpha_i\beta V_i} \quad \text{for } V_i < 0.2 \tag{5.10}$$

In the presence of correlated variables, applying the following formulas directly may lead to an incorrect physical design point, denoted as X^*. In a First-Order Reliability Method (FORM) approximation, the sequence of correlated random variables significantly affects the sensitivity factor α_u. This is due to correlations influencing the joint probability distribution function of these variables. To address this, sensitivity factors for the correlated normal Y-space, denoted as $\alpha_{y'}$, were derived to accurately represent a model parameter's contribution to the reliability index.

The importance factors α_u^2 and α_y^2 for the uncorrelated U-space and correlated Y-space are defined as follows:

$$\alpha_{u;i}^2 = \frac{u_i^{*2}}{\beta_{HL}^2} \tag{5.11}$$

$$\alpha_{y;i}^2 = \frac{y_i^{*2}}{\|y^*\|^2} \tag{5.12}$$

Where:

u_i**:** Variable related to the uncorrelated normalized U-space.

y_i**:** Variable related to the correlated normalized Y-space.

$\alpha_{u;i}$**:** Sensitivity factor in the uncorrelated normalized U-space $(-)$.

u_i^***:** Normalized value of u_i.

y_i^***:** Normalized value of y_i.

y^***:** Vector containing normalized values related to the correlated Y-space.

$\|y^*\|$**:** Euclidean norm of the vector y^*.

$\alpha_{y;i}$**:** Sensitivity factor in the elliptical/correlated normalized Y-space $(-)$.

β_{HL}**:** Represents the Hasofer-Lind reliability index $(-)$.

The Hasofer-Lind reliability index indicated the in the equation indicated the resulted β by the FORM method. The reliability index β of the design point U^* generally typically deviates from the target reliability level β_t. In order to compare the results with the partial factors employed in the initial design, a slight scaling of the reliability index is necessary. This scaling of the reliability index is related to adjusting the reliability index of the design point (β) to match a target reliability level (β_t). Given the presence of correlated input variables, the direct application of Cholesky decomposition, utilizing matrix L, is employed to transform results from the standard space U^* to the physical space X. Once the results are in the correlated space Y^*, the

transformation to the physical space X is achieved. The transformation is established by the following group of equations. Equation (5.13): calculates the design point U^* in the standard space, incorporating the scaling factor $\sqrt{\alpha_u^2 \beta_t^2}$. Equation (5.14): transforms the design point from the standard space U to the correlated space Y using the Cholesky decomposition matrix L. Equation (5.15): defines the correlation matrix R as the product of the Cholesky decomposition matrix L and its inverse L^{-1}. Equation (5.16): represents the transformation of the normalized variable y_i^* from the correlated space to the physical space X, obtaining x_i^* using the mean (μ_i^N) and standard deviation (σ_i^N) of the original variable x_i in the physical space. The transformation ensures that the design value of a random variable x_i is determined for a specific β_t (Roubos, 2019).

$$U^* = \sqrt{\alpha_u^2 \beta_t^2} \tag{5.13}$$

$$Y^* = LU^* \tag{5.14}$$

$$[R] = [L][L]^{-1} \tag{5.15}$$

$$x_i^* = \mu_i^N + y_i^* \sigma_i^N \tag{5.16}$$

Where:

U^* : Design point, vector of design values, in the uncorrelated standardised U-space

Y^* : Design point, vector of design values, in the correlated normalised Y-space

R : Correlation matrix

L : Lower triangular matrix obtained by Cholesky decomposition of R

x_i^* : Design value of variable i in physical space X

μ_i^N : Mean value of equivalent normal distribution

σ_i^N : Standard deviation of equivalent normal distribution

Additionally, in an uncorrelated space where all variables are orthogonal (uncorrelated) to each other, the squared sensitivity factor is inherently equal to 1. This arises due to the fact that in such a space, the sensitivity factor (also known as the partial derivative or sensitivity coefficient) quantifies the change in the output concerning a change in the input variable. It is normalized by the standard deviation of the input variable.

However, in a correlated space, the squared sensitivity factor does not necessarily hold the value of 1. In a correlated space, variables are not mutually orthogonal, implying that their variations possess some degree of dependence. Consequently,

the sensitivity factor will reflect the extent to which variations in one variable can impact variations in another variable . The sensitivity factor in a correlated space takes into account the correlation between variables, and its value will depend on the specific correlations between the variables involved. If two variables are positively correlated, meaning that an increase in one tends to be associated with an increase in the other, their sensitivity factors might be greater than 1 (Ayyub and McCuen, 2003).

5.3.2.2 *Loads (F_i)*

When going to the part of the actions, an action , F, represents a random variable or a specific action in a mathematical or scientific context. While the Gumbel distribution is a probability distribution used to model extreme value events. It is often employed in various fields, to describe extreme events such as floods. In this case, it will be used to model the actions acting on the structure as well as the hydrological variations. The distribution is characterized by two parameters, location (μ) and scale (c). To find the value c, corresponding to a specific reliability level (probability of failure), the standard approach is to utilize the inverse cumulative distribution function (CDF) of the Gumbel distribution. However, it is important to note that the Gumbel distribution lacks an analytically derived inverse CDF, or quantile function. For this part of the thesis, the automatic values derived by the inputs of the Probabilistic Toolkit have been used, to determine the c value. When dealing with the Gumbel Distribution, the partial factors can be determined using the following equations (Roubos, 2019):

$$F_{k;i} = \mu_i - \frac{1}{c}\ln(-\ln(0.98)) \tag{5.17}$$

$$F_{d;i} = \mu_i - \frac{1}{c}\ln(-\ln(\Phi(-\alpha_i\beta_t))) \tag{5.18}$$

$$\gamma_{f;i} = \frac{F_{d;i}}{F_{k;i}} \tag{5.19}$$

Where:

$F_{k;i}$: Reliability metric for a system or process under constant loading conditions, with i representing the constant load. μ_i is the expected value of the reliability metric, and c is a constant.

$F_{d;i}$: Reliability metric for the same system or process under dynamic loading conditions, with i representing the dynamic load. μ_i is the expected value of the reliability metric, c is a constant, and Φ is the standard normal cumulative

distribution function. α_i and β_t are parameters relevant to the dynamic loading conditions.

$\gamma_{f;i}$**:** Ratio of the reliability metric under dynamic loading ($F_{d;i}$) to the reliability metric under constant loading ($F_{k;i}$), representing the impact of dynamic loading on system reliability. Specifically, it quantifies how the reliability metric changes when the system is subjected to dynamic loading

5.4 Distribution Functions and Correlations

The initial step involved utilizing the spring method modeling in the D-Sheet Piling software developed by Deltares. As highlighted in Chapter (4), this approach not only involved the inherent simplifications offered by the modeling method but also excluded the consideration of the concrete pile cap. Considering the stochastic variables, the focus was primarily on the geotechnical parameters, with structural stochastic variables, regarding materials (steel), being disregarded. Structural stochastic variables are only included as a part of describing the loads acting on the structure. In order to get the mean values for the stochastic variables of the geotechnical parameters, the selection should be based on low and high values, which are indicated in Table (5.2), Table (5.3), Table (5.4) are been presented. Considering the parameter δ, it can be calculated with the relationship $\delta = \frac{2}{3}\phi$.

Table 5.2: Derivation of γ_{unsat}, γ_{sat}, c with the representative low and high values used

Description	SI	$\gamma_{\text{unsat,l}}$	γ_{unsat}	$\gamma_{\text{unsat,h}}$	$\gamma_{\text{sat,l}}$	γ_{sat}	$\gamma_{\text{sat,h}}$	SI	c_{l}	c	c_{h}
Sand 1	kN/m^3	18	18.5	19	20	20.5	21	kPa	0	0	0
Sand 2	"	17	18	19	19	19.5	20	"	0	0	0
Clay 1	"	15	16.5	18	15	16.5	18	"	0	2.5	5
Sand 2	"	17	18	19	19	19.5	20	"	0	0	0
Clay 2	"	18	18	18	18	18	18	"	5	9	13
Sand 2	"	17	18	19	19	19.5	20	"	0	0	0
Clay 3	"	18	19	20	18	19	20	"	5	9	13
Sand 3	"	19	19.5	20	21	21.5	22	"	0	0	0

Table 5.3: Derivation of ϕ with the representative low and high values used

Description	SI	ϕ_{l}	ϕ	ϕ_{h}	δ
Sand 1	°	32.5	33.75	35	22.50
Sand 2	"	30	31.25	32.5	20.83
Clay 1	"	17.5	22.5	27.5	15.00
Sand 2	"	30	31.25	32.5	20.83
Clay 2	"	17.5	22.5	27.5	15.00
Sand 2	"	30	31.25	32.5	20.83
Clay 3	"	17.5	22.5	27.5	15.00
Sand 3	"	35	37.5	40	25.00

Table 5.4: Derivation of $k1$, $k2$, $k3$ with the representative low and high values used

Description	SI	$k1_l$	$k1$	$k1_h$	$k2_l$	$k2$	$k2_h$	$k3_l$	$k3$	$k3_h$
Sand 1	kN/m^3	20000	32500	45000	10000	16250	22500	5000	8125	11250
Sand 2	"	12000	19500	27000	6000	9750	13500	3000	4875	6750
Clay 1	"	4000	6500	9000	2000	3250	4500	800	1300	1800
Sand 2	"	12000	19500	27000	6000	9750	13500	3000	4875	6750
Clay 2	"	4000	6500	9000	2000	3250	4500	800	1300	1800
Sand 2	"	12000	19500	27000	6000	9750	13500	3000	4875	6750
Clay 3	"	4000	6500	9000	2000	3250	4500	800	1300	1800
Sand 3	"	40000	65000	90000	20000	32500	45000	10000	16250	22500

In Table (5.5), the final mean values for the main geotechnical parameters of the soil layers are presented. These parameters have been established according to the specifications outlined in Table 2-b of the NEN 9997-1 standard, as illustrated in Figure (A.1). For the coefficients k_1, k_2, and k_3, the chosen values are derived from the mean values reported in Table 6.18 (De Gijt and Broeken, 2013).

Table 5.5: Mean Geotechnical Parameters for reliability analysis

Depth (m)	Description	γ_{unsat} [kN/m^3]	γ_{sat} [kN/m^3]	c [kPa]	ϕ [°]	δ [°]	k_1 [kN/m^3]	k_2 [kN/m^3]	k_3 [kN/m^3]
4	Sand 1	18.5	20.5	0	33.75	22.5	32500	16250	8125
-4	Sand 2	18	19.5	0	31.25	20.83	19500	9750	4875
-16	Clay 1	16.5	16.5	2.5	22.5	15	6500	3250	1300
-20	Sand 2	18	19.5	0	31.25	20.83	19500	9750	4875
-21.5	Clay 2	18	18	9	22.5	15	6500	3250	1300
-23.5	Sand 2	18	19.5	0	31.25	20.83	19500	9750	4875
-24.5	Clay 3	19	19	9	22.5	15	6500	3250	1300
-26	Sand 3	19.5	21.5	0	37.5	25	65000	32500	16250

5.4.1 Stochastic Variable and coefficient of variations

5.4.1.1 Coefficient of Variation Determination

Taking into consideration expert judgment, an initial set of significant stochastic variables was determined. Notably, certain influential factors like water levels and water bottom levels were deliberately excluded from this selection in order to maintain the case's relative simplicity. Ideally, sensitivity analyses are conducted to pinpoint the most crucial and impactful parameters. No simplification has been employed within the model to ensure the accurate representation of soil parameter reliability. The Table (5.6) provides an overview of the literature (NEN, 2016) ; (JCSS, 2006) ; (Griffiths and Fenton, 2007) ; (Wolters, 2012) ; (Schneider and Schneider, 2013) ; (Roubos, 2019) encompassing the coefficient of variation (COV) values for the given case scenario, along with the specific coefficient of variation (COV) values ultimately chosen, which coincide with the findings of the analysis conducted by Roubos (2019).

Although not explicitly mentioned within Table (5.6), additional influential parameters contribute to the analysis. These variables encompass δ [°], which follows the same distribution characteristics as ϕ, with the relationship $\delta = \frac{2}{3}\phi$. Additionally, the trio of variables, k_1, k_2, and k_3, representing the secant modulus of subgrade reaction, are integrated. The Secant definition relies on the stress-displacement diagram for subgrade reaction, as outlined in CUR 166. This diagram consistently features three branches, intersecting at 50%, 80%, and 100% of the difference between Ka (active earth pressure coefficient) and Kp (passive earth pressure coefficient). Notably, k_1 represents the 50%, while k_2 and k_3 correspond to the 80% and 100% respectively. A distinctive pattern emerges within these parameters, where k_2 is half of k_1, and k_3 is half of k_2. This representation captures better their behavior and influence across different soil surfaces, enhancing the accuracy of the analysis. The values are based on CUR (2012).

Table 5.6: COV Parameter Values by Literature and chosen for analysis

Variable	Distribution	NEN9997	JCSS	Griffiths & Fenton	Wolters	Schneider & Schneider	Roubos	**Thesis**
γ	Normal	0.05	0.05-0.10	0.00-0.10	0.05	0.01-0.10	0.05	0.05
$\tan\phi$	Normal	0.10	0.10-0.20	0.02-0.05	0.20	0.05-0.15	0.10	0.10
c	Lognormal	0.20	0.10-0.50	0.10-0.35	0.80	0.30-0.50	0.20	0.20
k_1, k_2, k_3	Lognormal	0.10	0.20-1.00	-	0.30	0.20-0.70	0.20	0.20

It is crucial to note that, in the context of calculating the coefficient of variation (COV) for $\tan(\phi)$ and subsequently for δ, a transformation to ϕ is essential for accurate results. This transformation process is essential to maintain the validity of COV computations and ensuring the proper interpretation of results. It is a crucial step in accurately assessing the variability of the parameters involved. In order to transform $\tan(\phi)$, the general procedure is analyzed.

Process for determining mean and variance of a function

For any one-parameter function G based on an estimator $G(\hat{\theta})$, the expected value $E[G(\theta)]$ can be approximated as:

$$E[G(\theta)] \approx G(\hat{\theta}) + O\left(\frac{1}{n}\right) \tag{5.20}$$

This approximation holds as the sample size n approaches infinity, where $E(\theta)$ converges to the population parameter q, and $G(q)$ is a function of q. $O\left(\frac{1}{n}\right)$ indicates that the error in the approximation decreases as the sample size n increases.

The variance of $G(\theta)$ can be estimated as:

$$\mathrm{Var}(G(\theta)) = \left(\frac{\partial G}{\partial \theta}\right)^2_{\theta=\hat{\theta}} \mathrm{Var}(\theta) + O\left(\frac{1}{n^{\frac{3}{2}}}\right) \tag{5.21}$$

Variance of friction angle (ϕ) derived from tangent of friction angle ($\tan(\phi)$)

$$f(\phi) = \tan(\phi) \tag{5.22}$$

$$f'(\phi) = \frac{1}{\cos^2(\phi)} \tag{5.23}$$

In the same manner as the previous section, the standard deviation of $\tan(\phi)$ is determined by:

$$\sigma_{\tan\phi} = \frac{1}{\cos^2\phi}\sigma_\phi \tag{5.24}$$

Expressed in terms of coefficients of variation:

$$\mathrm{COV}(\tan\phi) = \frac{\cos\hat{\phi}}{\cos^2\hat{\phi}\sin\hat{\phi}}\mathrm{COV}(\phi)\hat{\phi} = \frac{1}{\cos\hat{\phi}\sin\hat{\phi}}\mathrm{COV}(\phi)\hat{\phi} \tag{5.25}$$

Where $\hat{\phi}$ represents an estimated value.

5.4.1.2 Stochastic Variables Determination

Material Properties (X_i)

Material properties, represented by X_i, play a significant role in structural reliability analysis. In Roubos (2019), it was mentioned that the low characteristic values of soil strength (ϕ or c) and soil stiffness, currently represented as $k_{1,2,3}$, typically correspond to the 5th percentile of layer mean values, while the recommendations for weight density (γ_{unsat}) and (γ_{sat}) usually represent the expected values. Given that previous studies have highlighted the substantial variability in soil strength and its wide range of coefficient variations in the literature, it was crucial to investigate its influence. In log-normal distributions, the characteristic values of the distributions are greater than the mean. This happens because the log-normal distribution is skewed, and the logarithmic transformation affects how the mean and characteristic values relate to each other.

Loads (F_i)

The loads, denoted as F_i, encompass the maximum loads experienced over a lifetime, considered for a reference period spanning 50 years. These loads are determined through the utilization of the Gumbel extreme value distribution function, a common method for modeling extreme events. The characteristic value of terminal loads is often derived from operational limits, reflecting a threshold beyond which a structure should not be stressed. On the other hand, characteristic wind-induced crane loads typically represent events with a specific return period, such as a 50-year recurrence interval. This approach ensures that the structural design accounts for extreme but realistic scenarios, maintaining safety and reliability. As part of this analysis $Q_{surcharge}$ and Q_{crane} will act simutaneously as the dominant loads, whereas $F_{bollard}$ as a non-dominant load. In the analysis, the

values pertinent to the loads for the 50-year reference period (Q_{50}) have been meticulously calculated by utilizing the annual maxima (Q_1) dataset. This choice was made while taking into account a coefficient of variation (COV) for Q1, which has been as assumed to be 0.13. For the $F_{\text{selfweight;i}}$ since it changes for every retaining height, all the values need to be reported.

Geometric Variabilites (a_i)

Geometrical variabilities, represented as a_i, encompasses variations in structural dimensions of the problem. In the current study, no geometric variations were considered in structural components, be it the steel quality or installation depth. Two distinct geometric variabilities were taken into account. The first pertained to variations in water levels, encompassing both the outer water level and the groundwater level. The values of the standard deviation of both the water level variations are very high, which could indicate that the design is over conservative.

The second variability revolved around geotechnical considerations. Initially, an exploration was conducted to assess potential geological variations in soil depositions, for which the standard deviations were set at 0.5 m. The purpose was to determine whether these variations in soil-layer thickness were relevant. It was subsequently determined that geological variations did not impact the study, leading to the conclusion that further investigations into standard deviations were unnecessary. This conclusion was drawn, due to the influence coefficient, α_i, being zero for all the six soil layers.

Model Uncertainty ($\theta_{m;\text{i}}$)

A deliberate choice was made to further investigate model uncertainty influence on the failure equation. The selected coefficient of variation (COV) was set at 0.10, assuming a log-normal distribution, while the mean value is 1. This decision aimed to explore the impact of uncertainty on the failure equation and its associated factors.

As a crucial component of the analysis, the stochastic soil variables will be thoroughly presented. It is important to identify that no structural components of the quay wall, such as steel were introduced in the analysis, thus contributing to a limitation.

Table 5.7: Stochastic Soil Variables (Part 1)

Soil Layer	Variable	SI	$X_{i;k}$	Char. Value	Mean	Distribution	COV (V_x)
Clay 1	γ_{unsat}	kN/m^3	μ_x	16.50	16.50	Normal	0.05
Clay 1	γ_{sat}	kN/m^3	μ_x	16.50	16.50	Normal	0.05
Clay 1	ϕ	$^\circ$	$\phi_{k;\text{low}}$	17.50	22.50	Normal	0.09
Clay 1	c	kPa	$X_{i,5\%}$	2.78	2.50	Log normal	0.20
Clay 1	δ	$^\circ$	$\delta_{k;\text{low}}$	11.70	15.00	Normal	0.09
Clay 1	K_{b3}	kN/m^2	$X_{i,5\%}$	1447.52	1300.00	Log normal	0.20

Table 5.7 – Continued

Soil Layer	Variable	SI	$X_{i;k}$	Char. Value	Mean	Distribution	COV (V_x)
Clay 1	K_{b2}	kN/m^2	$X_{i,5\%}$	3618.79	3250.00	Log normal	0.20
Clay 1	K_{b1}	kN/m^2	$X_{i,5\%}$	7237.57	6500.00	Log normal	0.20
Clay 1	K_{o3}	kN/m^2	$X_{i,5\%}$	1447.52	1300.00	Log normal	0.20
Clay 1	K_{o2}	kN/m^2	$X_{i,5\%}$	3618.79	3250.00	Log normal	0.20
Clay 1	K_{o1}	kN/m^2	$X_{i,5\%}$	7237.57	6500.00	Log normal	0.20
Clay 2	γ_{unsat}	kN/m^3	μ_x	18.00	18.00	Normal	0.05
Clay 2	γ_{sat}	kN/m^3	μ_x	18.00	18.00	Normal	0.05
Clay 2	ϕ	°	$\phi_{k;\text{low}}$	17.50	22.50	Normal	0.09
Clay 2	c	kPa	$X_{i,5\%}$	10.02	9.00	Log normal	0.20
Clay 2	δ	°	$\delta_{k;\text{low}}$	11.70	15.00	Normal	0.09
Clay 2	K_{b3}	kN/m^2	$X_{i,5\%}$	1447.52	1300.00	Log normal	0.20
Clay 2	K_{b2}	kN/m^2	$X_{i,5\%}$	3618.79	3250.00	Log normal	0.20
Clay 2	K_{b1}	kN/m^2	$X_{i,5\%}$	7237.57	6500.00	Log normal	0.20
Clay 2	K_{o3}	kN/m^2	$X_{i,5\%}$	1447.52	1300.00	Log normal	0.20
Clay 2	K_{o2}	kN/m^2	$X_{i,5\%}$	3618.79	3250.00	Log normal	0.20
Clay 2	K_{o1}	kN/m^2	$X_{i,5\%}$	7237.57	6500.00	Log normal	0.20
Clay 3	γ_{unsat}	kN/m^3	μ_x	19.00	19.00	Normal	0.05
Clay 3	γ_{sat}	kN/m^3	μ_x	19.00	19.00	Normal	0.05
Clay 3	ϕ	°	$\phi_{k;\text{low}}$	17.50	22.50	Normal	0.09
Clay 3	c	kPa	$X_{i,5\%}$	10.02	9.00	Log normal	0.20
Clay 3	δ	°	$\delta_{k;\text{low}}$	11.70	15.00	Normal	0.09
Clay 3	K_{b3}	kN/m^2	$X_{i,5\%}$	1447.52	1300.00	Log normal	0.20
Clay 3	K_{b2}	kN/m^2	$X_{i,5\%}$	3618.79	3250.00	Log normal	0.20
Clay 3	K_{b1}	kN/m^2	$X_{i,5\%}$	7237.57	6500.00	Log normal	0.20
Clay 3	K_{o3}	kN/m^2	$X_{i,5\%}$	1447.52	1300.00	Log normal	0.20
Clay 3	K_{o2}	kN/m^2	$X_{i,5\%}$	3618.79	3250.00	Log normal	0.20
Clay 1	K_{o1}	kN/m^2	$X_{i,5\%}$	7237.57	6500.00	Log normal	0.20

Table 5.8: Stochastic Soil Variables (Part 2)

Soil Layer	Variable	SI	$X_{i;k}$	Char. Value	Mean	Distribution	COV (V_x)
Sand 1	γ_{unsat}	kN/m^3	μ_x	18.00	18.00	Normal	0.050
Sand 1	γ_{sat}	kN/m^3	μ_x	19.50	19.50	Normal	0.05
Sand 1	ϕ	°	$\phi_{k;\text{low}}$	30.00	31.25	Normal	0.078
Sand 1	c	kPa	$X_{i,5\%}$	0.0001	0.00	Log normal	1E-05

Table 5.8 – Continued

Soil Layer	Variable	SI	$X_{i;k}$	Char. Value	Mean	Distribution	COV (V_x)
Sand 1	δ	$^\circ$	$\delta_{k;\text{low}}$	20.00	20.83	Normal	0.078
Sand 1	K_{b3}	kN/m^2	$X_{i,5\%}$	9046.97	8125.00	Log normal	0.20
Sand 1	K_{b2}	kN/m^2	$X_{i,5\%}$	18093.93	16250.00	Log normal	0.20
Sand 1	K_{b1}	kN/m^2	$X_{i,5\%}$	36187.87	32500.00	Log normal	0.20
Sand 1	K_{o3}	kN/m^2	$X_{i,5\%}$	18093.93	16250.00	Log normal	0.20
Sand 1	K_{o2}	kN/m^2	$X_{i,5\%}$	36187.87	32500.00	Log normal	0.20
Sand 1	K_{o1}	kN/m^2	$X_{i,5\%}$	6500.00	6500.00	Log normal	0.20
Sand 2	γ_{unsat}	kN/m^3	μ_x	18.50	18.50	Normal	0.05
Sand 2	γ_{sat}	kN/m^3	μ_x	20.50	20.50	Normal	0.05
Sand 2	ϕ	$^\circ$	$\phi_{k;\text{low}}$	32.50	33.75	Normal	0.09
Sand 2	c	kPa	$X_{i,5\%}$	0.0001	0.00	Log normal	1E-05
Sand 2	δ	$^\circ$	$\delta_{k;\text{low}}$	21.68	22.50	Normal	0.09
Sand 2	K_{b3}	kN/m^2	$X_{i,5\%}$	5428.18	4875.00	Log normal	0.20
Sand 2	K_{b2}	kN/m^2	$X_{i,5\%}$	10856.36	9750.00	Log normal	0.20
Sand 2	K_{b1}	kN/m^2	$X_{i,5\%}$	21712.72	19500.00	Log normal	0.20
Sand 2	K_{o3}	kN/m^2	$X_{i,5\%}$	5428.18	4875.00	Log normal	0.20
Sand 2	K_{o2}	kN/m^2	$X_{i,5\%}$	10856.36	9750.00	Log normal	0.20
Sand 2	K_{o1}	kN/m^2	$X_{i,5\%}$	21712.72	19500.00	Log normal	0.20
Sand 3	γ_{unsat}	kN/m^3	μ_x	19.50	19.50	Normal	0.05
Sand 3	γ_{sat}	kN/m^3	μ_x	21.50	21.50	Normal	0.05
Sand 3	ϕ	$^\circ$	$\phi_{k;\text{low}}$	35.00	37.50	Normal	0.074
Sand 3	c	kPa	$X_{i,5\%}$	0.0001	0.00	Log normal	1E-05
Sand 3	δ	$^\circ$	$\delta_{k;\text{low}}$	23.33	25.00	Normal	0.074
Sand 3	K_{b3}	kN/m^2	$X_{i,5\%}$	18093.93	16250.00	Log normal	0.20
Sand 3	K_{b2}	kN/m^2	$X_{i,5\%}$	36187.87	32500.00	Log normal	0.20
Sand 3	K_{b1}	kN/m^2	$X_{i,5\%}$	72375.73	65000.00	Log normal	0.20
Sand 3	K_{o3}	kN/m^2	$X_{i,5\%}$	18093.93	16250.00	Log normal	0.20
Sand 3	K_{o2}	kN/m^2	$X_{i,5\%}$	36187.87	32500.00	Log normal	0.20
Sand 3	K_{o1}	kN/m^2	$X_{i,5\%}$	72375.73	65000.00	Log normal	0.20

Table 5.9: Stochastic Structural Variables with Terrain Loads as Dominant (Load Combination C / Phase 4)

Variable Name	SI	$F_{i;k}$	Char. Value	Mean	Distribution	COV (V_F)
$Q_{\text{surcharge}}$	kN/m^2	$F_{i;TR=50}$	100.00	104.49	Gumbel	0.10

Table 5.9 – Continued

Variable Name	SI	$F_{i;k}$	Char. Value	Mean	Distribution	COV (V_F)
Q_{crane}	kN/m^2	$F_{i;TR=50}$	40.00	41.80	Gumbel	0.10
$F_{bollard}$	kN/m'	$F_{i;TR=50}$	-155.00	-95.97	Gumbel	0.10
$F_{selfweight;31.5}$	kN	$F_{i;TR=50}$	532.88	537.68	Gumbel	0.02
$F_{selfweight;30}$	kN	$F_{i;TR=50}$	527.18	531.98	Gumbel	0.02
$F_{selfweight;29}$	kN	$F_{i;TR=50}$	523.37	528.17	Gumbel	0.02
$F_{selfweight;28}$	kN	$F_{i;TR=50}$	519.57	524.32	Gumbel	0.02
$F_{selfweight;27}$	kN	$F_{i;TR=50}$	515.76	520.51	Gumbel	0.02

Table 5.10: Stochastic Geometry Variables

Variable Name	SI	$a_{i;k}$	Char. Value	Mean	Distribution	STD (Δ_α)
h_{OWL}	m	LLWS	-2.29 m	-2.39 m	Gumbel	0.25 m
h_{GWL}	m	$h_{drainage} + 0.30m$	-0.20 m	-0.21 m	Gumbel	0.25 m

Table 5.11: Stochastic Uncertainty Variables

Variable Name	SI	$\theta_{i;k}$	Char. Value	Mean	Distribution	COV (V_θ)
$\theta_{m;F}$	–	μ_θ	n/a	1.00	Log normal	0.10
$\theta_{m;MobP}$	–	μ_θ	n/a	1.00	Log normal	0.10
$\theta_{m;MobM}$	–	μ_θ	n/a	1.00	Log normal	0.10

5.4.2 Correlation factors

The correlation factor ρ_{pq} between two variables p and q is an indication of how they are related. This correlation coefficient can range from -1, indicating a complete negative correlation, to 0, representing an absence of correlation, and up to 1, signifying a perfect positive correlation. Intermediate values between these extremes suggest varying degrees of partial correlation. The Probabilistic Toolkit employs the Pearson correlation factor. The Pearson correlation factor, utilized within the Probabilistic Toolkit, is computed through the following equation:

$$\rho_{p,q} = \frac{\sum_i u_{p,i} u_{q,i}}{\sum_i u_{p,i} \sum_i u_{q,i}}$$

where: - i is the index number of the observed value; - p, q indicate variables; - $u_{p,i}$ is the u-value corresponding to the observed value x_i (Deltares, 2023).

The values of Table (5.12) have been adopted by Roubos (2019). In the table, all the correlation factors are presented, each varying based on the soil layer definition,

whether it is classified as clay or sand. The statistical determination of these values involved an extensive analysis of a sizable database, which encompassed data from on-site investigations across various projects adjacent to the reference quay walls in the port of Rotterdam.

Table 5.12: Correlation factor between variables for all layers across model. Source: Adapted from Roubos (2019)

No.	Variable	1	2	3	4	5	6	7	8	9	10	11
1	$\gamma_{\text{unsat sand}}$	1.00	1.00	0.50	0.50	0.50						
2	$\gamma_{\text{sat sand}}$	1.00	1.00	0.50	0.50	0.50						
3	ϕ_{sand}	0.50	0.50	1.00	0.25	1.00						
4	$k_1, k_2, k_{3\,\text{sand}}$	0.50	0.50	0.25	1.00	0.25						
5	δ_{sand}	0.50	0.50	1.00	0.25	1.00						
6	$\gamma_{\text{unsat clay}}$						1.00	1.00	0.50	-0.09	0.50	0.50
7	$\gamma_{\text{sat clay}}$						1.00	1.00	0.50	-0.09	0.50	0.50
8	ϕ_{clay}						0.50	0.50	1.00	-0.65	0.25	1.00
9	c_{clay}						-0.09	-0.09	-0.65	1.00	0.12	-0.65
10	$k_1, k_2, k_{3\,\text{clay}}$						0.50	0.50	0.25	0.12	1.00	0.12
11	δ_{clay}						0.50	0.50	1.00	-0.65	0.12	1.00

5.5 Optimal Model Selection for Analysis

Considering the phases which have been indicated in D-Sheet Piling, it can be identified, that except the first one, the other consider the application of each one of the three combination loads, which result from the combination load factors outlined in Table (4.12). In order to determine the correct model for the analysis, the worst-case (dominant) scenario should be identified. This can be done by evaluating the three load combinations against their respective limit values. Considering the results Table (5.13), where no geometry or structural stochastic variables were included in the analysis it is visible the big difference, in the values of β, in the extreme case (accidental limit state water level head on outer water level), denoted as C. For the convergence of the FORM analysis, a relaxation factor of 0.3 was adopted, initializing from a start value of 0.5 while convergence criterion for differential reliability was set at 0.01. The outcomes are presented below:

Table 5.13: Reliability indexes, β, of current design

Combination Load	**Failure Method**	β
A	$Z_{\text{GEO;passive}}$	8.264
"	$Z_{\text{STR; anchor}}$	8.813
"	$Z_{\text{STR; yield}}$	8.261
B	$Z_{\text{GEO;passive}}$	8.672
"	$Z_{\text{STR; anchor}}$	9.270
"	$Z_{\text{STR; yield}}$	8.668
C	$Z_{\text{GEO;passive}}$	6.470
"	$Z_{\text{STR; anchor}}$	6.440
"	$Z_{\text{STR; yield}}$	6.461

Taking into account this, only the fourth phase will need to be evaluated as indicated in Subsection (4.6.2). An attempt was also made to re-evaluate the results of FORM analysis, by using Monte Carlo approaches, though it was concluded to be impractical due to encountered errors, particularly the generation of "not a value" (NAN) results, which made the assessment of failure mechanism equations not possible.

6

Case Study Results & Discussion

In the upcoming chapter will focus on optimizing the structure both during the design phase and after its construction.

6.1 Optimization in Design Phase

For the optimization of the design process, the parameter with the greatest influence will be chosen according to Figure (6.1). In this context, the focus lies on the total wall height, prompting a gradual reduction in the quay section's bottom level. This figure makes it easy to understand what parameter is going to be changed in order to gradually reduce the β value to the target value. This optimization strategy bears implications for both project timelines and material usage, notably steel. The potential reduction in CO_2 emissions will also be quantified.

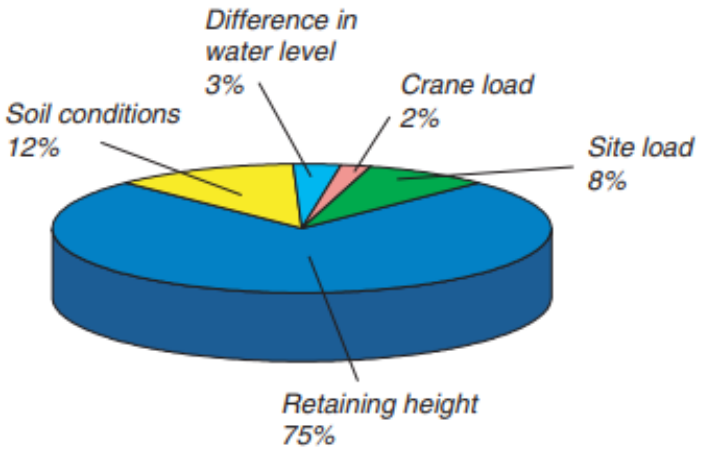

Figure 6.1: Impact of Different Factors on Construction Cost Levels. Source: Adapted from (De Gijt and Broeken, 2013)

6.1.1 Partial Factor determination

As mentioned in the previous chapters, the analysis has been conducted in detail by Probabilistic Toolkit, with FORM method in load combination C.

In this first part the failure mechanisms equations as indicate in Table (5.1) get their output values with $\theta_{m;i}$ parameter as deterministic. In the current design assessments, it is evident that determining partial factors becomes a complex task due to the notably high β values, which ideally should closely align with the target reliability values as indicated for RC1/CC1 category in Eurocode. Considering the current design, it appears to be overly conservative with the current β values be for $Z_{\text{GEO;passive}}$, $Z_{\text{STR; anchor}}$, $Z_{\text{STR; yield}}$ equal to 6.470, 6.440 and 6.492 respectively. In order to evaluate the current Eurocode partial factors, the reliability factor, β, should be as close to the limit value, designated to the current construction, that of RC1. Considering the 50-year reference period as indicated in Table (3.3), this target value is 3.30. Considering the substantial difference and the optimization of the design from an economic perspective, since this is the goal of thesis, the quay section bottom level is been substantially decreased from the starting value of -31.50 m in a way to reach the target value for all failure equation mechanisms. This can be indicated in Figure (6.2), where again all the geometry and structural variables are assumed as deterministic. Regarding Figure (6.2), it is important to highlight the presence of a horizontal line corresponding to a β value of 3.30. This line provides valuable insight into the extent to which we can modify the retaining height while maintaining the desired reliability level. The quay wall toe level is been reduced by -31.50 m to -30.00 m, -29.00 m, -28.00 m and -27.00 m.

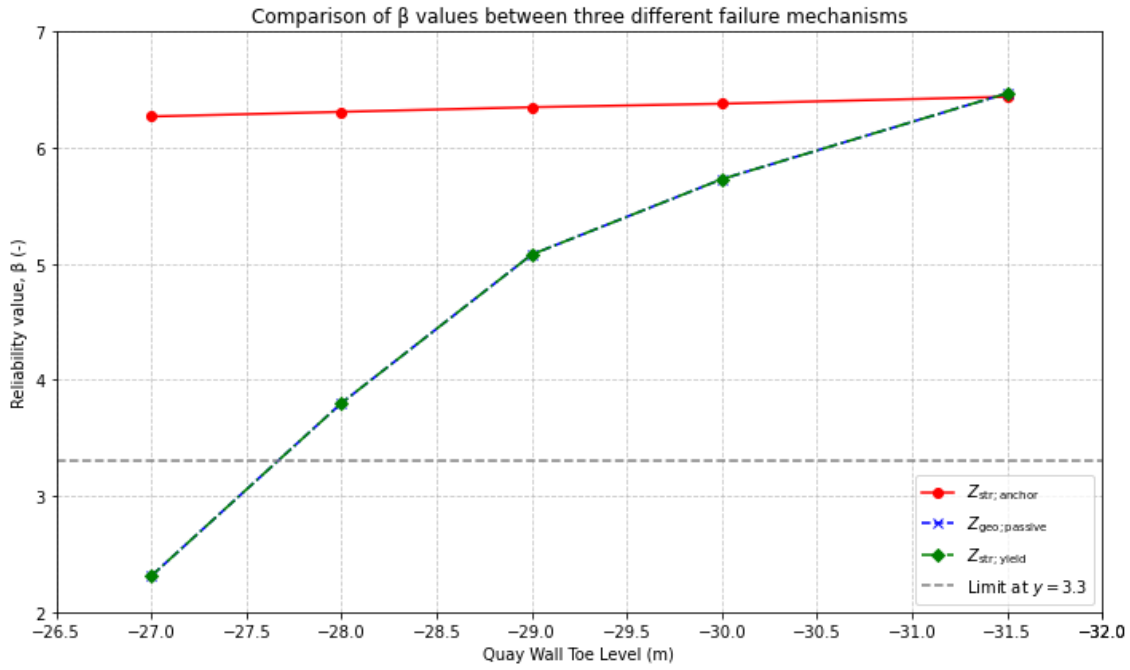

Figure 6.2: Calculation of all failure mechanism equations for different quay wall toe level.

Upon conducting an in-depth analysis of all three failure equations, it becomes evident that the more critical equation demanding optimization is Equation (b), (c), as indicated in Table (5.1), which correspond to $Z_{\text{GEO;passive}}$ and $Z_{\text{STR; yield}}$. This conclusion arises by Figure (6.2), where in the case of Equation (a) ($Z_{\text{STR; anchor}}$) even adjusting the retaining height of the structure, β value does not significantly changes close to the limit value. In its starting value of $F_{\text{rd;anchor}} = 1980.00kN$, anchor force has been designed in a way that if one anchor fails, it does not result in the failure of the anchor wall. Anchor Force needs to be reduced significantly from its initial limit value of 1980.00 kN to approach the failure limit value β, so in order to fail it would need a double optimization in the sense that both the retaining height as well as the anchor force would need to optimized. Another noteworthy observation in the results is the consistency between the β values obtained from Equation (b) and (c). These values remain nearly identical across various retaining heights, suggesting that failures occur simultaneously for both equations.

In order to discern the impact of additional stochastic variables in our study, we will present a comparative analysis of the change of β with increasing complexity, meaning that in steps an analysis will be conducted with 1. material stochastic variables as stochastic, structural and geometry stochastic variables as deterministic (Simple), 2. material and structural variables as stochastic, geometry variables as deterministic (Load Inclusion), 3. all variables as stochastic (Water Head Inclusion). The partial factors are going to be extracted only on step 3, where all the variables are been included, whereas steps 1,2 only be used as an identification of how β value changes due to the inclusion of more stochastic variables for all three failure equation mechanisms.

In the next sections, each failure equation will be presented separately:

- $Z_{\text{GEO;passive}}$ Failure Equation
- $Z_{\text{STR;yield}}$ Failure Equation
- $Z_{\text{STR; anchor}}$ Failure Equation

6.1.1.1 $Z_{GEO;passive}$ Failure Equation

As indicated in Figure (6.3) in the pursuit of achieving the correct partial factors, it is essential to aim for a toe level around -28.00 m, falling within the range of -27.50 m to -28.00 m. Instead of carefully searching for an exact value to meet the limit, engineering judgment comes into play. As a result, the final toe level is chosen as -28.00 m based on a pragmatic assessment of the situation.

It is worth noting based on the Table (6.1), and also Figure (6.3) that the most "safe" approach (highest β) appears to be the Load inclusion. This observation could be attributed to the inherent variability in the loads, contributing to a design point with a higher β value, especially considering that the loads are subject to change. Also the first two

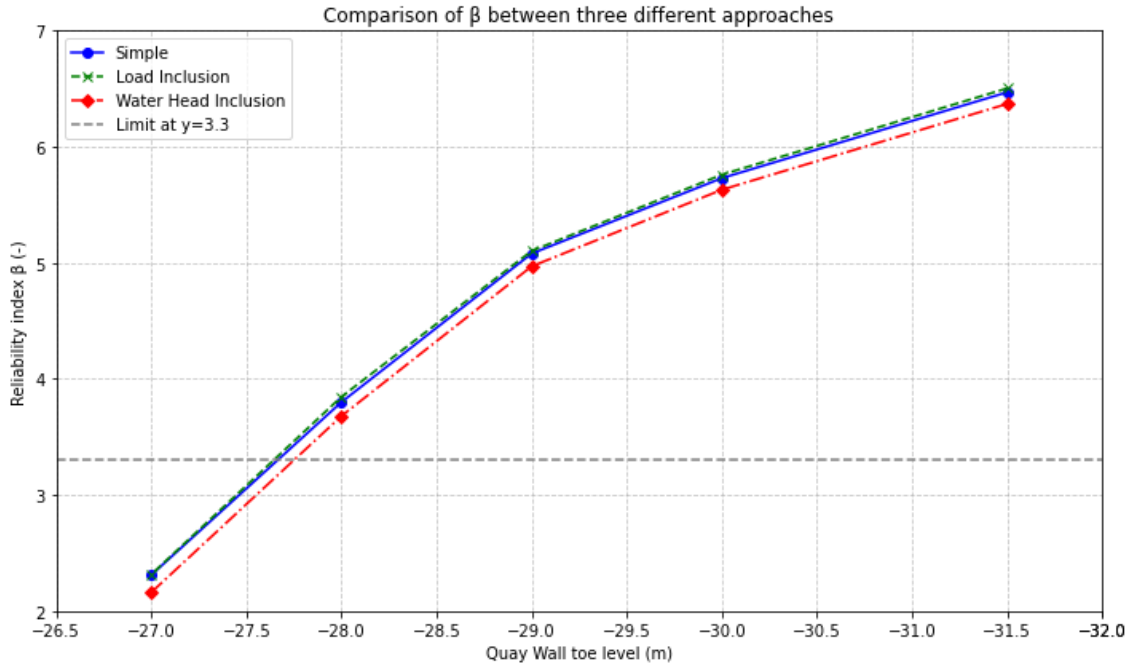

Figure 6.3: Progressive change of reliability index, β, for $Z_{\text{GEO;passive}}$

Table 6.1: Comparison of β values between three different approaches.

Quay Wall Toe Level (m NAP)	Simple (β)	Load Inclusion (β)	Water Head Inclusion (β)
-31.50	6.470	6.504	6.370
-30.00	5.730	5.760	5.630
-29.00	5.080	5.103	4.970
-28.00	3.800	3.846	3.680
-27.00	2.310	2.315	2.160

approaches (Simple and Load inclusion) appear to have their values very close with each other with their values hardly discernible at most points in the Figure. Though it appears how important it really is the inclusion of more stochastic parameters, notably here the inclusion of the geometry stochastic parameters, when the water levels are included, which appears to be the most "unsafe" one. This can be linked to the standard deviation associated with the water levels, and the acknowledgment that a greater water level difference than the established one may result in a lower β value.

In the context of solving the partial factors problem, it is essential to identify the most influential parameters for the reliability analysis. This analysis aims to reveal any discernible patterns and provide insights into the results before deriving the partial factors. Given the variations in the parameters that exert the most influence on the design, we will focus on the ten most influential parameters for the concluded quay wall toe level of -28.00 m. It is important to mention that the importance factor is essentially a^2, which provides a measure to quantify the significance of a stochastic variable.

Table 6.2: Importance factors for uncorrelated and correlated FORM analysis at a quay wall toe depth of -31.50 meters ($Z_{GEO;passive}$) with water head inclusion parameters

-31.50 m							
Uncorrelated				Correlated			
Layer/Force	Variable	a	Imp. Factor	Layer/Force	Variable	a	Imp. Factor
Sand 3	ϕ	0.679	0.462	Sand 3	ϕ	0.842	0.709
Sand 3	γ_{sat}	0.506	0.256	Sand 3	δ	0.840	0.706
Clay 1	γ_{sat}	0.292	0.085	Sand 3	γ_{sat}	0.507	0.257
Sand 2	γ_{sat}	0.286	0.081	Sand 3	γ_{unsat}	0.506	0.256
Sand 2	ϕ	0.225	0.051	Sand 2	ϕ	0.338	0.114
Clay 2	γ_{sat}	0.139	0.019	Sand 2	δ	0.337	0.114
Clay 3	γ_{sat}	0.103	0.011	Clay 1	γ_{sat}	0.293	0.086
Sand 1	γ_{sat}	-0.091	0.008	Clay 1	γ_{unsat}	0.292	0.085
Water level	OWL	0.078	0.006	Sand 2	γ_{sat}	0.286	0.082
Water level	GWL	-0.077	0.005	Sand 2	γ_{unsat}	0.286	0.082

Table 6.3: Importance factors for uncorrelated and correlated FORM analysis at a quay wall toe depth of -30.00 meters ($Z_{GEO;passive}$) with water head inclusion parameters

-30.00 m							
Uncorrelated				Correlated			
Layer/Force	Variable	a	Imp. Factor	Layer/Force	Variable	a	Imp. Factor
Sand 3	ϕ	0.648	0.420	Sand 3	ϕ	0.791	0.626
Sand 3	γ_{sat}	0.458	0.210	Sand 3	δ	0.789	0.623
Sand 2	γ_{sat}	0.332	0.110	Sand 3	γ_{sat}	0.459	0.211
Clay 1	γ_{sat}	0.331	0.110	Sand 3	γ_{unsat}	0.458	0.210
Sand 2	ϕ	0.261	0.068	Sand 2	ϕ	0.393	0.154
Clay 2	γ_{sat}	0.155	0.024	Sand 2	δ	0.392	0.154
Clay 3	γ_{sat}	0.114	0.013	Sand 2	γ_{sat}	0.333	0.111
Sand 1	γ_{sat}	-0.095	0.009	Clay 1	γ_{sat}	0.333	0.111
Water level	OWL	0.089	0.008	Sand 2	γ_{unsat}	0.332	0.110
Water level	GWL	-0.085	0.007	Clay 1	γ_{unsat}	0.331	0.110

Analyzing the outcomes of Table (6.2), Table (6.3), Table (6.4), and Table (6.5), which are based on FORM analysis results for both uncorrelated and correlated calculations we observe that at a depth of -31.50 meters, the predominant influence comes from Sand 3, which spans from -26.00 m to the model's bottom. The key factors within this layer are the angle of internal friction (ϕ) and (γ_{sat}). Notably, the water levels, both the outer water level (OWL) and ground water level (GWL), also emerge as significant variables.

Shifting our focus to a toe level of -28 meters, these influential parameters remain consistent, especially for Sand 3 and, notably, ϕ. It is worth noting that ϕ experiences a decrease in its importance factor value (a^2) from 0.462 to 0.229 when transitioning from -31.50 to -28.00 meters.

In the context of correlated variables, a similar pattern emerges. Here, δ and γ_{sat} exhibit strong correlations, with ϕ and γ_{unsat} even though γ_{unsat} should not be so influential because it is only present in one soil layer. These results appear to be directly linked to the

Table 6.4: Importance factors for uncorrelated and correlated FORM analysis at a quay wall toe depth of -29.00 meters ($Z_{GEO;passive}$) with water head inclusion parameters

-29.00 m							
Uncorrelated				Correlated			
Layer/Force	Variable	a	Imp. Factor	Layer/Force	Variable	a	Imp. Factor
Sand 3	ϕ	0.626	0.392	Sand 3	ϕ	0.755	0.570
Sand 3	γ_{sat}	0.424	0.180	Sand 3	δ	0.753	0.567
Sand 2	γ_{sat}	0.362	0.131	Sand 2	ϕ	0.426	0.181
Clay 1	γ_{sat}	0.356	0.127	Sand 2	δ	0.425	0.181
Sand 2	ϕ	0.283	0.080	Sand 3	γ_{sat}	0.424	0.180
Clay 2	γ_{sat}	0.165	0.027	Sand 3	γ_{unsat}	0.424	0.180
Clay 3	γ_{sat}	0.120	0.014	Sand 2	γ_{sat}	0.363	0.132
Sand 1	γ_{sat}	-0.095	0.009	Sand 2	γ_{unsat}	0.362	0.131
Water level	OWL	0.088	0.007	Clay 1	γ_{sat}	0.357	0.127
Water level	GWL	-0.088	0.007	Clay 1	γ_{unsat}	0.356	0.127

Table 6.5: Importance factors for uncorrelated and correlated FORM analysis at a quay wall toe depth of -28.00 meters ($Z_{GEO;passive}$) with water head inclusion parameters

-28.00 m							
Uncorrelated				Correlated			
Layer/Force	Variable	a	Imp. Factor	Layer/Force	Variable	a	Imp. Factor
Sand 3	ϕ	0.479	0.229	Sand 3	ϕ	0.575	0.331
Sand 2	γ_{sat}	0.454	0.206	Sand 3	δ	0.573	0.328
Clay 1	γ_{sat}	0.442	0.196	Sand 2	ϕ	0.537	0.288
Sand 2	ϕ	0.357	0.128	Sand 2	δ	0.536	0.287
Sand 3	γ_{sat}	0.321	0.103	Sand 2	γ_{sat}	0.455	0.207
Clay 2	γ_{sat}	0.202	0.040	Sand 2	γ_{unsat}	0.454	0.206
Clay 3	γ_{sat}	0.146	0.021	Clay 1	γ_{sat}	0.444	0.197
Sand 1	γ_{sat}	-0.119	0.014	Clay 1	γ_{unsat}	0.442	0.195
Water level	OWL	0.110	0.012	Sand 3	γ_{sat}	0.321	0.103
Clay 3	ϕ	0.107	0.011	Sand 3	γ_{unsat}	0.321	0.103

slip failure line of the structure, considering the prevailing failure mechanism, specifically $Z_{GEO;passive}$.

Table (6.6) provides a comprehensive comparison of partial factors for various geotechnical parameters and structural parameters, including uncorrelated and correlated partial factors. Not all soil layers contribute the same to the exertion of the partial factors. In essence, the partial factors are predominantly influenced by specific soil layers with high importance factors. The partial factors have been calculated using the Equations by Section (5.3.2).

It should be stated that partial factors in Eurocode are uncorrelated, so a direct comparison of the results should be made with the uncorrelated partial factors, though considering that the statistical determination of the correlation factors from the region of the port of Rotterdam, the correlated partial factors are also valid. Using correlated partial factors can provide a more realistic representation in the system. Since, physically

Table 6.6: Partial factors for the failure equation $Z_{\text{GEO;passive}}$ with water head inclusion parameters (-28 m).

$Z_{\text{GEO;passive}}$	β :	3.68						
Variable	Soil layer	SI	$X_{k;i}$	$X_{d;i}$		Partial Factors		
-	-	-	-	Uncorr.	Corr.	Uncorr.	Corr.	EC
γ_{unsat}	Sand 1	kN/m^3	18.50	18.91	18.90	0.98	0.98	1.00
γ_{sat}	Clay 1	kN/m^3	16.50	16.38	15.15	1.09	1.10	1.00
ϕ	Sand 2	°	30.00	27.92	26.25	1.07	1.14	1.15
c	Clay 2	kPa	10.02	8.53	9.09	1.17	1.10	1.15
δ	Sand 2	°	20.00	20.78	17.51	0.96	1.14	1.15
k_1, k_2, k_3	Clay 1 (K_{b3})	kN/m^3	1447.52	1274.76	1080.50	1.14	1.34	1.30
Variable	Force	SI	$F_{k;i}$	$F_{d;i}$		Partial Factors		
-	-	-	-	Uncorr.	Corr.	Uncorr.	Corr.	EC
Loads Perm.	$F_{\text{selfweight28}}$	kN	519.57	524.37	524.33	1.01	1.01	1.00
Loads Var.	$Q_{\text{surcharge}}$	kN/m^2	100.00	104.53	102.88	1.03	1.05	1.00

correlated partial factors acknowledge that certain uncertainties or variations in different parameters are not independent but are related. Also, in most cases the correlated partial factors result in more conservative designs, considering the joint effects of correlated uncertainties. Considering the selection of a correct set of partial factors which are project relevant, the highest values of partial factors, either uncorrelated or correlated, should be chosen as a conservative solution.

The characteristic as well as the design values appear with two decimals in Table (6.6). Considering the calculation for γ_{unsat}, even though there had been higher values from other soil layers, Sand 1 had been selected since it is the only layer that has a part of its soil stratigraphy above water level.

A crucial observation is that, despite certain variables having higher importance factors, the determination of the final partial factors are not exerted by them. This is notable for most of the results of the analysis. Clay 1 and Sand 2 appear as the most notable variables with the participation in two partial factors, whereas Sand 3 does not appear at the calculation even though it had the highest importance factor. This could be a consequence of Sand 2 being the layer that appears most at the stratigraphy as well being the soil layer at the final excavation toe from the outer water side. Clay 1 could be of similar consequences, considering that it appears after Sand 2 at the outer water side and been the clay layer with the highest height.

Considering the parameters, where the partial factors are lower than, this implies that they have a lower variability or smaller fluctuations.

Compared to Eurocode guidelines, which recommend a partial factor of 1 for both unsaturated and saturated soil unit weights, our analysis has brought to light a significant discrepancy. Therefore, the analysis highlights the need to introduce a partial factor for the saturated unit weight of the soil layers, γ_{sat}, in the present case study. This adjustment aims to enhance the accuracy of the failure mechanism equation by better reflecting real-world

conditions. It is essential to note that these findings are based on a single benchmark case, and their generalization to a broader context may not be appropriate.

Similarly, with regards to the (ϕ) parameter, Eurocode guidelines suggest a partial factor of 1.15. In our analysis both uncorrelated and correlated partial factors closely approximate this specified value. Notably, this alignment becomes particularly evident when the correlated approach is applied, resulting in identical values for the ϕ parameter. The ϕ parameter emerges as a critical variable in this analysis due to its significant influence factor within the study.

For cohesion (c), the Eurocode recommends a partial factor of 1.15. In our analysis the values appear to be on the same scale, close to the value of EC especially for the uncorrelated approach.

In the context of the angle of shearing resistance of interfaces (δ), the Eurocode prescribes a partial factor of 1.15. Nevertheless, in our analysis, through the correlated approach this can be identified as a close value of 1.14 is the result of the analysis. It is worth noting that the increase in correlated factors appears to be directly correlated with ϕ, emphasizing the significance of considering both variables simultaneously.

Regarding the value of subgrade reaction, the Eurocode recommends a partial factor of 1.30. In our study, uncorrelated partial factors is lower than the value, whereas correlated partial factors exhibit a value a bit higher. So in this applied case an increased partial factor could be identified.

For permanent and variable loads, the Eurocode recommends specific partial factors of 1.00 and 1.00, respectively. Our findings reveal a close alignment of the partial factors for both permanent and variable loads with the Eurocode's recommendations. Even though on the case of the variable loads, the calculated values are a bit higher than the value of 1.00.

6.1.1.2 $Z_{STR;yield}$ Failure Equation

As indicated again in a similar case as Subsection (6.1.1.1), Figure (6.4) in the pursuit of achieving the correct partial factors, a value as close as possible to the target value of β = 3.30 should be selected. As a result, the final toe level is chosen as -28.00 m again.

Table 6.7: Comparison of β values between three different approaches.

Quay Wall Toe Level (m NAP)	Simple (β)	Load Inclusion (β)	Water Head Inclusion (β)
-31.50	6.492	6.520	6.382
-30.00	5.735	5.762	5.646
-29.00	5.090	5.112	4.987
-28.00	3.814	3.859	3.697
-27.00	2.326	2.330	2.182

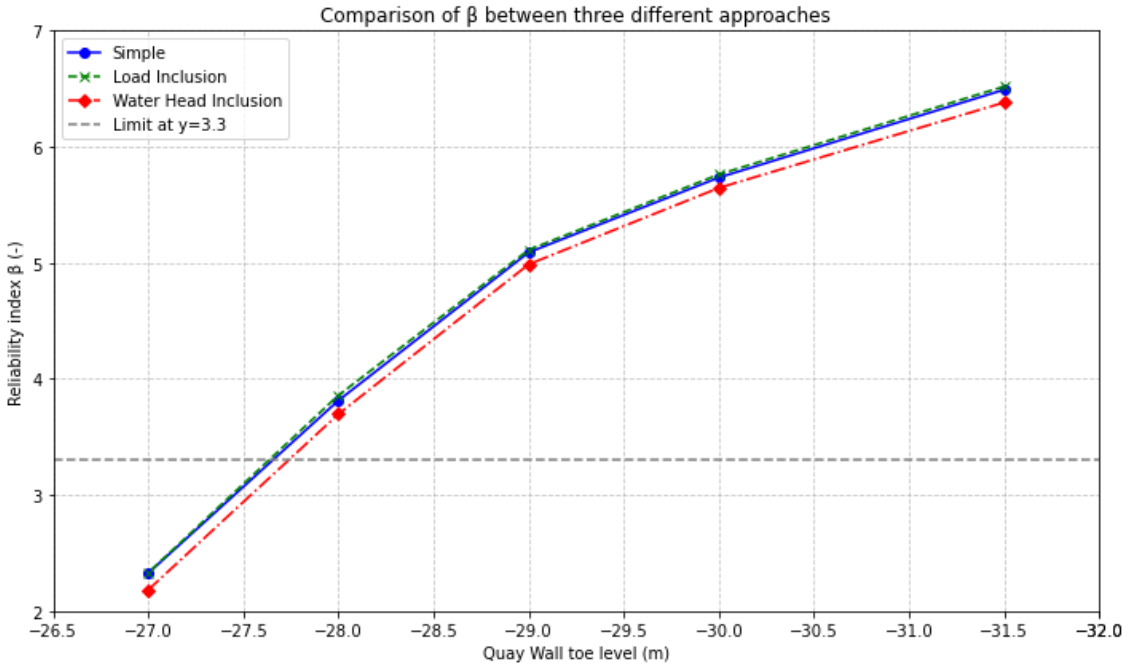

Figure 6.4: Progressive change of reliability index, β, for $Z_{\text{STR;yield}}$

It is worth noting based on the Table (6.7), and also Figure (6.4) that the most "safe" approach (highest β) appears to be the Load inclusion, where the structural loads are considered as Gumbel distributions. Also the first two approaches (Simple and Load inclusion) appear to have their values very close with each other with their values hardly discernible at most points in the Figure (6.4). Though as it has been stated already, a conclusion by Table (6.1), Table (6.7) and Figure (6.3) and the Figure (6.4) it is hardly discernible the difference in the values of β with the previous case of the $Z_{\text{GEO;passive}}$. An indication that both failure mechanisms are similar.

Again, it is essential to identify the most influential parameters for the model with the highest number of stochastic variables (Water Head Inclusion) across various final toe levels. The focus will shift again on ten most influential parameters for 4 different quay wall toe levels, namely -31.50 m, -30.00 m, -29.00 m, -28.00 m which is concluded as the final quay wall toe level.

It is important to compare the values of, Table (6.2), Table (6.3), Table (6.4), and Table (6.5), Table (6.8), Table (6.9), Table (6.10), and Table (6.11). The variables have almost identical values, which can contribute to the conclusion that both failure mechanism equations fail at the same moment. So similar conclusions can be drawn for both failure mechanism equations.

Table 6.8: Importance factors for uncorrelated and correlated FORM analysis at a quay wall toe depth of -31.50 meters ($Z_{STR;yield}$) with water head inclusion parameters

-31.50 m							
Uncorrelated				Correlated			
Layer/Force	Variable	a	Imp. Factor	Layer/Force	Variable	a	Imp. Factor
Sand 3	ϕ	0.677	0.458	Sand 3	ϕ	0.838	0.702
Sand 3	γ_{sat}	0.503	0.253	Sand 3	δ	0.836	0.699
Clay 1	γ_{sat}	0.294	0.087	Sand 3	γ_{sat}	0.504	0.254
Sand 2	γ_{sat}	0.289	0.087	Sand 3	γ_{unsat}	0.503	0.253
Sand 2	ϕ	0.228	0.052	Sand 2	ϕ	0.343	0.118
Clay 2	γ_{sat}	0.139	0.019	Sand 2	δ	0.342	0.117
Clay 3	γ_{sat}	0.103	0.011	Clay 1	γ_{sat}	0.342	0.117
Sand 1	γ_{sat}	-0.092	0.008	Clay 1	γ_{unsat}	0.294	0.086
Water level	GWL	-0.084	0.007	Sand 2	γ_{unsat}	0.290	0.084
Water level	OWL	0.076	0.006	Sand 2	γ_{sat}	0.289	0.084

Table 6.9: Importance factors for uncorrelated and correlated FORM analysis at a quay wall toe depth of -30.00 meters ($Z_{STR;yield}$) with water head inclusion parameters

-30.00 m							
Uncorrelated				Correlated			
Layer/Force	Variable	a	Imp. Factor	Layer/Force	Variable	a	Imp. Factor
Sand 3	ϕ	0.639	0.409	Sand 3	ϕ	0.785	0.616
Sand 3	γ_{sat}	0.461	0.213	Sand 3	δ	0.783	0.613
Sand 2	γ_{sat}	0.337	0.114	Sand 3	γ_{sat}	0.461	0.213
Clay 1	γ_{sat}	0.336	0.113	Sand 3	γ_{unsat}	0.461	0.213
Sand 2	ϕ	0.264	0.070	Sand 2	ϕ	0.398	0.158
Clay 2	γ_{sat}	0.157	0.025	Sand 2	δ	0.397	0.158
Clay 3	γ_{sat}	0.115	0.013	Sand 2	γ_{sat}	0.338	0.114
Sand 1	γ_{sat}	-0.096	0.009	Clay 1	γ_{sat}	0.337	0.114
Water level	GWL	-0.086	0.007	Clay 1	γ_{unsat}	0.337	0.114
Water level	OWL	0.086	0.007	Sand 2	γ_{unsat}	0.336	0.113

Table 6.10: Importance factors for uncorrelated and correlated FORM analysis at a quay wall toe depth of -29.00 meters ($Z_{STR;yield}$) with water head inclusion parameters

-29.00 m							
Uncorrelated				Correlated			
Layer/Force	Variable	a	Imp. Factor	Layer/Force	Variable	a	Imp. Factor
Sand 3	ϕ	0.623	0.388	Sand 3	ϕ	0.750	0.563
Sand 3	γ_{sat}	0.421	0.177	Sand 3	δ	0.748	0.560
Sand 2	γ_{sat}	0.365	0.133	Sand 2	ϕ	0.431	0.186
Clay 1	γ_{sat}	0.358	0.128	Sand 2	δ	0.430	0.185
Sand 2	ϕ	0.287	0.082	Sand 3	γ_{sat}	0.421	0.177
Clay 2	γ_{sat}	0.165	0.027	Sand 3	γ_{unsat}	0.421	0.177
Clay 3	γ_{sat}	0.121	0.015	Sand 2	γ_{sat}	0.366	0.134
Sand 1	γ_{sat}	-0.096	0.009	Sand 2	γ_{unsat}	0.365	0.133
Water level	OWL	0.089	0.008	Clay 1	γ_{sat}	0.359	0.129
Water level	GWL	-0.088	0.008	Clay 1	γ_{unsat}	0.358	0.128

Table 6.11: Importance factors for uncorrelated and correlated FORM analysis at a quay wall toe depth of -28.00 meters ($Z_{\text{STR;yield}}$) with water head inclusion parameters

-28.00 m							
Uncorrelated				Correlated			
Layer/Force	Variable	a	Imp. Factor	Layer/Force	Variable	a	Imp. Factor
Sand 3	ϕ	0.482	0.232	Sand 3	ϕ	0.579	0.335
Sand 2	γ_{sat}	0.457	0.209	Sand 3	δ	0.576	0.332
Clay 1	γ_{sat}	0.445	0.198	Sand 2	ϕ	0.540	0.292
Sand 2	ϕ	0.359	0.129	Sand 2	δ	0.539	0.291
Sand 3	γ_{sat}	0.322	0.104	Sand 2	γ_{sat}	0.458	0.210
Clay 2	γ_{sat}	0.203	0.041	Sand 2	γ_{unsat}	0.457	0.209
Clay 3	γ_{sat}	0.147	0.022	Clay 1	γ_{sat}	0.447	0.200
Sand 1	γ_{sat}	-0.119	0.014	Clay 1	γ_{unsat}	0.445	0.198
Water level	OWL	0.110	0.012	Sand 3	γ_{sat}	0.322	0.104
Clay 3	ϕ	0.106	0.011	Sand 3	γ_{unsat}	0.322	0.104

In the next step, the partial factors are going to be calculated. Table (6.12) provides the values of the partial factors. The final values are almost identical to Table (6.6).

Table 6.12: Partial factors for the failure equation $Z_{\text{STR;yield}}$ with water head inclusion parameters (-28 m).

$Z_{\text{STR;yield}}$	β :	3.70						
Variable	Soil layer	SI	$X_{k;i}$	$X_{d;i}$		Partial Factors		
-	-	-	-	Uncorr.	Corr.	Uncorr.	Corr.	EC
γ_{unsat}	Sand 1	kN/m^3	18.50	18.91	18.91	0.98	0.98	1.00
γ_{sat}	Clay 1	kN/m^3	16.50	15.14	15.14	1.09	1.09	1.00
ϕ	Sand 2	°	30.00	27.89	26.20	1.08	1.15	1.15
c	Clay 2	kPa	10.02	8.53	9.09	1.18	1.10	1.15
δ	Sand 2	°	20.00	20.78	17.47	0.96	1.14	1.15
k_1, k_2, k_3	Clay 1 (K_{b3})	kN/m^3	1447.52	1274.76	1078.40	1.14	1.34	1.30
Variable	Force	SI	$F_{k;i}$	$F_{d;i}$		Partial Factors		
-	-	-	-	Uncorr.	Corr.	Uncorr.	Corr.	EC
Loads Perm.	$F_{\text{selfweight28}}$	kN	519.57	524.37	524.33	1.01	1.01	1.00
Loads Var.	$Q_{\text{surcharge}}$	kN/m^2	100.00	104.53	102.88	1.03	1.05	1.00

Based on the analysis and the indication it has become apparent that these two failure mechanisms are almost identical for the input of the current stochastic variables.

6.1.1.3 $Z_{STR;anchor}$ Failure Equation

By excluding all structural uncertainties associated with the anchor, our primary focus will center around determining the maximum force applied to the anchor. In the third failure mechanism equation, denoted as Equation (a) in Table (5.1) the emphasis will be on the analysis of anchor failure based on F_{anchor}. Starting from the starting value of setting the limit value $F_{\text{rd;anchor}} = 1980.00$ kN, which was also included on Figure (6.2) as $Z_{STR;\text{anchor}}$, arises already an indication on a dual optimization of the design in order to get to the target value of 3.30. The meaning of the dual optimization is that not only there would a need to reduce the retaining height (quay wall toe level), but also reduce $F_{\text{rd;anchor}}$ to a value where it will fail. After iterative process, $F_{\text{rd;anchor}}$ is finalized on a value of 1650.00 kN. The results of the analysis are reported on Table (6.13), and also Figure (6.5). Except the three cases, which were reported as before, also the basic case where the limit value $F_{\text{rd;anchor}} = 1980.00$ kN is been presented.

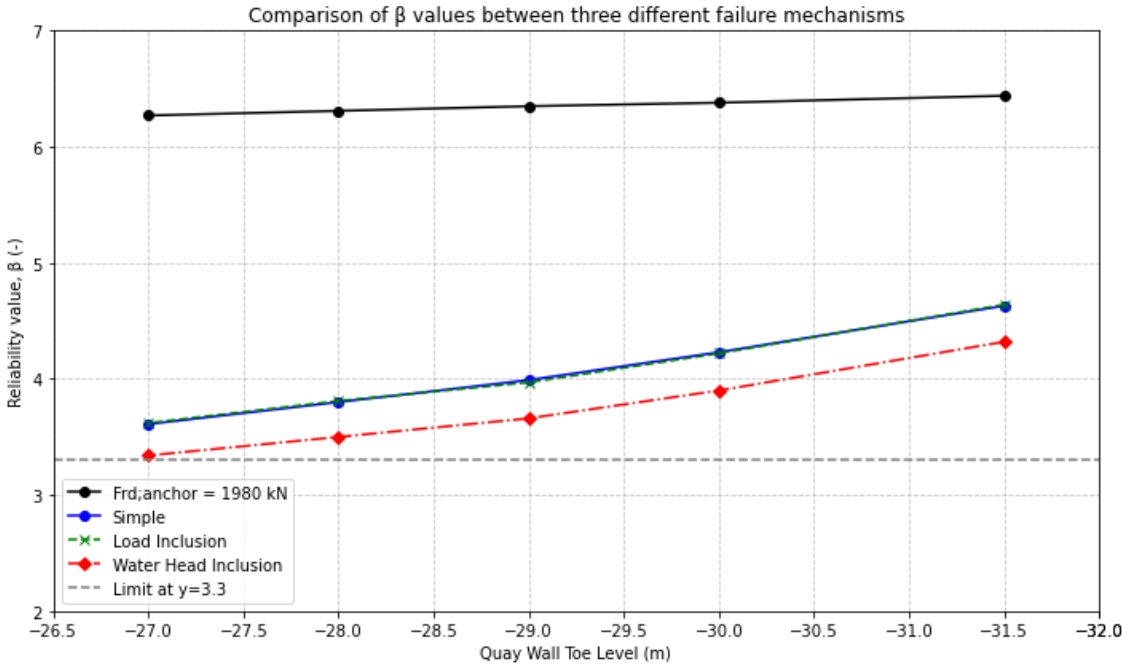

Figure 6.5: Progressive change of reliability index, β, for $Z_{STR;\text{anchor}}$

Table 6.13: Comparison of β values between four different approaches.

Quay Wall Toe Level (m NAP)	$F_{rd;\text{anchor}} = 1980\,\text{kN}(\beta)$	Simple (β)	Load Inclusion (β)	Water Head Inclusion (β)
-31.50	6.440	4.630	4.642	4.323
-30.00	6.383	4.232	4.223	3.901
-29.00	6.354	3.992	3.971	3.660
-28.00	6.312	3.803	3.812	3.501
-27.00	6.273	3.614	3.621	3.342

Again commenting on the results, it is apparent that the Simple approach is again close to the Load Inclusion one. Though in this case opposed to the previous two cases,

Load Inclusion appears to be less "safer". It should be stated though that the three decimals precision is sufficiently high, and in practical terms, the distinctions between the two approaches for all three failure mechanisms are negligible. Also there appears to be a contrast between the two previous failure mechanism equations and this, in the sense that there appears to a notable difference between the values of Simple and Load Inclusion in comparison to the Water Head Inclusion, where it appears that for this equation the inclusion of the water heads as stochastic variables is more important. This can be attributed to the fact that a higher water head may result in increased lateral soil pressure on the anchor, influencing its stability. Throughout the entire depth range, we encounter an approximately value difference of 0.30 in reliability index values. The final quay wall toe level is been set at -28.00 m again.

As before, it will be made an attempt to characterize the change of the most influential parameters as the retaining height decreases. Again the depicted parameters are going to be the ones that include the variation in the water level heads.

Table 6.14: Importance Factors for Uncorrelated and Correlated FORM Analysis at a quay wall toe depth of -31.5 meters ($Z_{STR;\text{anchor}}$) with water head inclusion parameters

-31.5 m							
Uncorrelated				Correlated			
Layer/Force	Variable	a	Imp. Factor	Layer/Force	Variable	a	Imp. Factor
Sand 2	ϕ	0.611	0.373	Sand 2	ϕ	0.713	0.508
Water level	GWL	-0.387	0.150	Sand 2	δ	0.711	0.506
Sand 2	γ_{sat}	0.368	0.136	Water level	GWL	-0.387	0.150
Clay 1	γ_{sat}	0.302	0.091	Sand 2	γ_{sat}	0.368	0.135
Sand 1	ϕ	0.227	0.051	Sand 2	γ_{unsat}	0.368	0.135
Sand 3	ϕ	0.219	0.048	Clay 1	γ_{sat}	0.303	0.092
Sand 1	γ_{sat}	-0.198	0.039	Clay 1	γ_{unsat}	0.302	0.091
Water level	OWL	0.180	0.032	Sand 3	ϕ	0.270	0.073
Sand 3	γ_{sat}	0.161	0.026	Sand 3	δ	0.269	0.072
Clay 1	ϕ	0.135	0.018	Clay 1	ϕ	0.269	0.072

In contrast to the prior two failure equation mechanisms, where the results were almost identical the findings from this analysis reveal significant disparities. However, a discernible pattern persists, with the parameters ϕ and γ_{sat}, and the differences in water levels being the primary driving forces in the analysis. This has also been observed in Figure (6.5). In the uncorrelated case, an interesting observation is the emergence of F_{bollard} at -30 m and -29 m depths. This suggests that F_{bollard} likely ranks just below the top 10 most influential parameters, as its "a" values plateau at 0.135. Notably, when F_{bollard} does come into play, its "a" values are either 0.123 or 0.13. The noteworthy influence of F_{bollard} can be attributed to its applied force, close to the installation depth of the anchor, thus causing a pullout failure or change the stability of the system.

In this failure equation, the soil friction angle (ϕ) of Sand 2 emerges as the most influential parameter. Sand 2 is the most dominant soil layer in the design and is identified

Table 6.15: Importance Factors for Uncorrelated and Correlated FORM Analysis at a quay wall toe depth of -30 meters ($Z_{STR;\text{anchor}}$) with water head inclusion parameters

-30 m							
Uncorrelated				Correlated			
Layer/Force	Variable	a	Imp. Factor	Layer/Force	Variable	a	Imp. Factor
Sand 2	ϕ	0.656	0.430	Sand 2	ϕ	0.751	0.564
Sand 2	γ_{sat}	0.367	0.135	Sand 2	δ	0.749	0.561
Water level	GWL	-0.349	0.122	Sand 2	γ_{sat}	0.367	0.135
Clay 1	γ_{sat}	0.292	0.085	Sand 2	γ_{unsat}	0.367	0.135
Sand 1	ϕ	0.247	0.061	Water level	GWL	-0.349	0.122
Sand 1	γ_{sat}	-0.206	0.042	Clay 1	γ_{sat}	0.293	0.086
Water level	OWL	0.192	0.037	Clay 1	γ_{unsat}	0.292	0.085
Sand 3	ϕ	0.147	0.022	Clay 1	ϕ	0.273	0.075
Clay 1	ϕ	0.146	0.021	Clay 1	δ	0.272	0.074
Force	F_{bollard}	0.123	0.015	Sand 1	γ_{sat}	-0.206	0.042

Table 6.16: Importance Factors for Uncorrelated and Correlated FORM Analysis at a quay wall toe depth of -29 meters ($Z_{STR;\text{anchor}}$) with water head inclusion parameters

-29 m							
Uncorrelated				Correlated			
Layer/Force	Variable	a	Imp. Factor	Layer/Force	Variable	a	Imp. Factor
Sand 2	ϕ	0.669	0.448	Sand 2	ϕ	0.759	0.576
Sand 2	γ_{sat}	0.359	0.129	Sand 2	δ	0.757	0.573
Water level	GWL	-0.358	0.128	Sand 2	γ_{sat}	0.359	0.129
Clay 1	γ_{sat}	0.281	0.079	Sand 2	γ_{unsat}	0.359	0.129
Sand 1	ϕ	0.253	0.064	Water level	GWL	-0.358	0.128
Sand 1	γ_{sat}	-0.208	0.043	Clay 1	γ_{sat}	0.282	0.080
Water level	OWL	0.198	0.039	Clay 1	γ_{unsat}	0.281	0.079
Clay 1	ϕ	0.150	0.022	Clay 1	ϕ	0.271	0.073
Force	F_{bollard}	0.130	0.016	Sand 1	γ_{sat}	-0.208	0.043

as also the "weakest" sand layer of the design. This observation holds significant importance, as any reduction in strength in Sand 2 leads to a larger mobilization of the active wedge, consequently increasing the load on the anchor. Sand 3, is not identified here as the dominant parameter, which could be expected since in an anchor failure mechanism, slip surface line failure mechanism is not the most dangerous mechanism and in general Layer 3 simply hardly contributes to the development of the anchor force. Also in this case, Sand 1 is identified, which could indicate how important is the fact that the installation level of anchor is located at this soil layer. Additionally, the ground water level on the landward side, as opposed to the seaward side, exerts substantial influence on the model. This is consistent with the fact that the water level difference exerts a significant lateral force onto the wall.

The direct correlations between δ and ϕ firstly and secondly γ_{unsat} and γ_{sat} contribute to their elevated importance, implying that any changes in these variables can significantly

Table 6.17: Importance factors for uncorrelated and correlated FORM analysis at a quay wall toe depth of -28 meters ($Z_{STR;\text{anchor}}$) with water head inclusion parameters

-28 m							
Uncorrelated				Correlated			
Layer/Force	Variable	a	Imp. Factor	Layer/Force	Variable	a	Imp. Factor
Sand 2	ϕ	0.611	0.373	Sand 2	ϕ	0.713	0.508
Water level	GWL	-0.387	0.150	Sand 2	δ	0.711	0.506
Sand 2	γ_{sat}	0.368	0.136	Water level	GWL	-0.387	0.150
Clay 1	γ_{sat}	0.302	0.091	Sand 2	γ_{sat}	0.368	0.135
Sand 1	ϕ	0.227	0.052	Sand 2	γ_{unsat}	0.368	0.135
Sand 3	ϕ	0.219	0.048	Clay 1	γ_{sat}	0.303	0.092
Sand 1	γ_{sat}	-0.198	0.039	Clay 1	γ_{unsat}	0.302	0.091
Water level	OWL	0.180	0.032	Sand 3	ϕ	0.270	0.073
Sand 3	γ_{sat}	0.161	0.026	Sand 3	δ	0.269	0.072
Clay 1	ϕ	0.135	0.018	Clay 1	ϕ	0.269	0.072

Table 6.18: Partial factors for the failure equation $Z_{STR;\text{anchor}}$ with water head inclusion parameters (-28 m).

$Z_{STR;\text{anchor}}$	β :	3.50						
Variable	Soil layer	SI	$X_{k;i}$	$X_{d;i}$		Partial Factors		
-	-	-	-	Uncorr.	Corr.	Uncorr.	Corr.	EC
γ_{unsat}	Sand 1	kN/m^3	18.50	19.17	19.17	0.96	0.96	1.00
γ_{sat}	Sand 2	kN/m^3	19.50	18.40	18.40	1.06	1.06	1.00
ϕ	Sand 2	°	30.00	25.23	24.51	1.19	1.22	1.15
c	Clay 3	kPa	10.02	8.77	8.91	1.14	1.13	1.15
δ	Sand 2	°	20.00	20.76	16.35	0.96	1.22	1.15
k_1, k_2, k_3	Sand 2 (K_{b3})	kN/m^3	5428.18	4780.33	4239.90	1.14	1.28	1.30
Variable	Force	SI	$F_{k;i}$	$F_{d;i}$		Partial Factors		
-	-	-	-	Uncorr.	Corr.	Uncorr.	Corr.	EC
Loads Perm.	$F_{\text{selfweight28}}$	kN	519.57	524.37	524.33	1.01	1.01	1.00
Loads Var.	$Q_{\text{surcharge}}$	kN/m^2	100.00	104.53	102.88	1.03	1.05	1.00

impact the analysis. This observation underscores the importance of understanding and accounting for variable correlations when conducting reliability assessments.

Now, in determining the partial factors, a similar approach to the previous two failure mechanism equations has been employed.

Similar patterns to the previous failure mechanism reappear in Table (6.18). The only difference lies in the fact that the value of partial factor of ϕ has been significantly increased compared to the previous failure equations and is higher than the Eurocode for both the uncorrelated and the correlated partial factors, and it is depicted as the most influential parameter. Also, the correlations δ can be identified as highly influential in the design, given its complete alignment with the value of ϕ.

Again in compliance with Eurocode guidelines, which recommend a partial factor of 1 for both unsaturated and saturated soil unit weights, our analysis has indicated again a higher value. As a result, our analysis has introduced the necessity of a partial factor for γ_{sat} for the current case study.

Considering ϕ, the results of the analysis again indicate a higher value in both the uncorrelated and correlated partial factors, which could introduce the necessity for a higher value than 1.15 for this current case study.

Considering cohesion, c, the values are very closely aligned with the partial factor of 1.15.

In the context of δ, through the direct correlation with ϕ a similar conclusion could be drawn, for the correlated partial factors, whereas the uncorrelated partial factors the value is lower than 1, which implies that it has a lower variability or smaller fluctuations when considered independently.

For the modulus of subgrade reaction, both the uncorrelated and the correlated partial factors are lower than the prescribed value of EC, though the correlated partial factor is very close to 1.30.

Considering the permanent and the variable loads, the values appear to be completely the same as the two previous failure mechanisms. The design values for all three failure mechanisms are the same. This might be an unforeseen conclusion, given that the design point value, which is uncorrelated, relies on an equation where the variations in the reliability index are relevant, even though these variations can be observed up to the fourth decimal.

6.1.2 Implementation of increased model uncertainty

In the context of design evolution and the assessment of heightened model uncertainty, we introduced a parameter denoted as $\theta_{m;i}$ for all the different failure mechanism equations. Model uncertainty has been implemented as a log-normal distribution considering that the uncertainty is multiplicative as having been stated in the failure mechanism equations. This addition aimed to provide a more comprehensive understanding of the results, particularly when analyzing β and interpreting the figures. This realism is crucial in representing the inherent variability apparent in engineering projects.Moreover, comparing the current analysis, where model uncertainty is considered, with the previous case where model uncertainty is assumed to be zero, can provide insightful conclusions. A coefficient of variation of 0.1 was employed, which appears to be a reasonable value.

For the analysis only the third scenario will be analyzed where all the parameters are been included as stochastic (Water head Inclusion).

In Figure (6.6) we delve into the impact of the model uncertainty on the reliability of the system. Considering that on the Figure (6.6) all the three failure mechanism equations are been included, conclusions can be drawn on these three failure mechanism equations. Considering the graphs where the uncertainty is not taken into account, it becomes apparent that the reliability values are much higher. As indicated before $Z_{\text{GEO;passive}}$ and $Z_{\text{STR;yield}}$ have very close reliability index values. Considering $Z_{STR;\text{anchor}}$, $F_{rd;\text{anchor}}$ is equal to

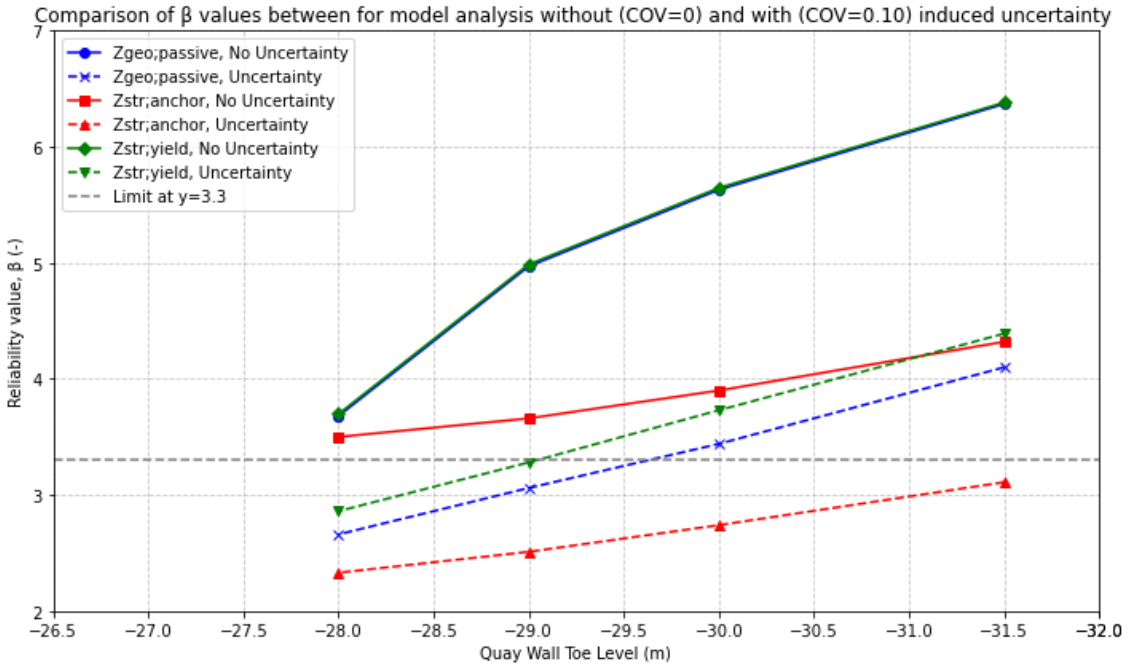

Figure 6.6: Progressive change of reliability index, β, for all three failure mechanism equations with and without induced uncertainty

1650.00 kN. Also the "safe" quay wall toe level can be set at -28.00 m, when considering the current three failure mechanisms.

One observation is that for $Z_{\text{GEO;passive}}$, $Z_{\text{STR;yield}}$ when there is no uncertainty the values of β are closely alligned, whereas with the induced uncertainty, the values have a relative difference.

Considering the transition from the no uncertainty to uncertainty, it can be discerned that the reliability index values, fall below the target limit value of 3.30 at the previous safe quay wall toe level value of -28.00 m. It becomes evident that a design approach solely based on optimization, without accounting for inherent model uncertainty, may not be the best choice. For $Z_{STR;\text{anchor}}$, the value of β is below the limit even at the maximum quay wall toe level of -31.50 m. $Z_{\text{STR;yield}}$ appears to be "safe", when the toe level is adjust to -29.10 m, while $Z_{\text{GEO;passive}}$ when it is adjusted to a value of -29.75 m. So the final quay wall toe level would be selected to be set at -30.00 m in order for the two latter failure mechanism equations to be "safe". This indicate a first difference from the no uncertainty case, where the quay wall toe level was set at -28.00 m.$Z_{\text{STR;yield}}$ in order to be safe would need to be modified, in a similar way as the previous case of a dual optimization (adjust $F_{rd;\text{anchor}}$ on the selected quay wall toe level). After iterative increasing the resistance of the anchor the final force for $F_{rd;\text{anchor}}$ = 1800.00 kN. The results appear in Figure (6.7).

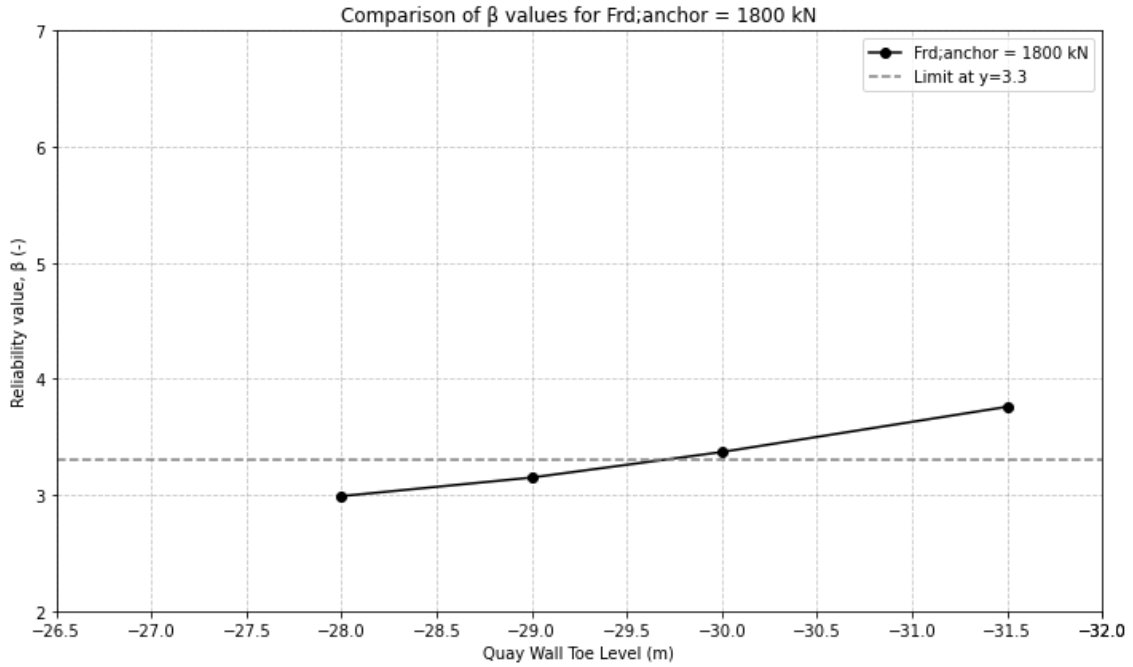

Figure 6.7: Progressive change of reliability index, β, $Z_{STR;\text{anchor}}$

When considering the essential factors that influence the design, it becomes evident that the influence of the 10 important parameters changes significantly. The biggest major difference is the inclusion of the uncertainty factor, $\theta_{m;i}$. The 10 most important parameters for the quay wall toe level of -30.00 m is going to be presented.

Table 6.19: Importance factors for uncorrelated and correlated FORM analysis at a quay wall toe depth of -30 meters ($Z_{STR;\text{anchor}}$) with water head inclusion parameters

-30 m							
Uncorrelated				Correlated			
Layer/Force/Unc.	Variable	a	Imp. Factor	Layer/Force/Unc.	Variable	a	Imp. Factor
Uncer.Factor	$\theta_{m;\text{F}}$	-0.725	0.526	Uncer.Factor	$\theta_{m;\text{F}}$	-0.725	0.526
Sand 2	ϕ	0.478	0.228	Sand 2	ϕ	0.558	0.311
Sand 2	γ_{sat}	0.288	0.083	Sand 2	δ	0.556	0.309
Clay 1	γ_{sat}	0.218	0.047	Sand 2	γ_{unsat}	0.288	0.083
Sand 1	ϕ	0.175	0.031	Sand 2	γ_{sat}	0.288	0.083
Water level	OWL	0.137	0.019	Clay 1	γ_{unsat}	0.218	0.048
Sand 1	γ_{sat}	-0.134	0.018	Clay 1	γ_{sat}	0.218	0.048
Clay 1	ϕ	0.109	0.012	Clay 1	ϕ	0.204	0.042
Force	F_{bollard}	0.098	0.010	Clay 1	K_{o1}	0.144	0.021

The conclusions derived from the importance factors in Table (6.19), Table (6.20), and Table (6.21) are primarily influenced by the uncertainty factor, which serves as the predominant parameter shaping the results.

The conclusions that can be drawn by the importance factors on Table (6.19), Table (6.20) and Table (6.21) are influenced on the uncertainty factor, $\theta_{m;i}$, which serves as an important parameter in shaping the results. The failure mechanism on the anchor, $Z_{STR;\text{anchor}}$, appears to be the one less influenced by the uncertainty whereas, $Z_{\text{GEO;passive}}$

Table 6.20: Importance factors for uncorrelated and correlated FORM analysis at a quay wall toe depth of -30.00 meters ($Z_{\text{STR;yield}}$) with water head inclusion parameters

-30.00 m							
Uncorrelated				Correlated			
Layer/Force/Unc.	Variable	a	Imp. Factor	Layer/Force/Unc.	Variable	a	Imp. Factor
Uncer.Factor	$\theta_{m;\text{MobM}}$	-0.780	0.608	Uncer.Factor	$\theta_{m;\text{MobM}}$	-0.780	0.608
Sand 3	ϕ	0.391	0.015	Sand 3	ϕ	0.462	0.213
Sand 3	γ_{sat}	0.245	0.045	Sand 3	δ	0.461	0.212
Sand 2	γ_{sat}	0.212	0.044	Sand 2	ϕ	0.284	0.081
Clay 1	γ_{sat}	0.209	0.042	Sand 2	δ	0.284	0.01
Sand 2	ϕ	0.206	0.009	Sand 3	γ_{sat}	0.246	0.061
Sand 3	K_{b3}	-0.097	0.008	Sand 3	γ_{unsat}	0.245	0.060
Clay 2	γ_{sat}	0.092	0.006	Sand 2	γ_{sat}	0.212	0.045
Sand 2	γ_{sat}	-0.076	0.005	Sand 2	γ_{unsat}	0.212	0.045
Water level	OWL	0.073	0.004	Clay 1	γ_{unsat}	0.209	0.044

Table 6.21: Importance factors for uncorrelated and correlated FORM analysis at a quay wall toe depth of -30.00 meters ($Z_{\text{GEO;passive}}$) with water head inclusion parameters

-30.00 m							
Uncorrelated				Correlated			
Layer/Force/Unc.	Variable	a	Imp. Factor	Layer/Force/Unc.	Variable	a	Imp. Factor
Uncer.Factor	$\theta_{m;\text{MobP}}$	-0.813	0.662	Uncer.Factor	$\theta_{m;\text{MobP}}$	-0.813	0.662
Sand 3	ϕ	0.373	0.139	Sand 3	ϕ	0.441	0.195
Sand 3	γ_{sat}	0.236	0.056	Sand 3	δ	0.439	0.192
Clay 1	γ_{sat}	0.187	0.0349	Sand 2	ϕ	0.251	0.063
Sand 2	γ_{sat}	0.187	0.0349	Sand 2	δ	0.251	0.063
Sand 2	ϕ	0.182	0.033	Sand 3	γ_{sat}	0.237	0.056
Sand 3	K_{b3}	-0.088	0.008	Sand 3	γ_{unsat}	0.236	0.056
Clay 2	γ_{sat}	0.086	0.007	Clay 1	γ_{sat}	0.188	0.035
Sand 2	γ_{sat}	-0.070	0.005	Clay 1	γ_{unsat}	0.187	0.035
Water level	OWL	0.068	0.005	Sand 2	γ_{unsat}	0.187	0.035

appears to be the one most influenced. Another difference than the previous case with no uncertainty included is the identification of subgrade reaction on the most dominant parameters. Both of the previous statements can be identified on the importance factors of the tables.

Table (6.22), Table (6.23), and Table (6.24) present an attempt to calculate partial factors considering model uncertainty, specifically for the final toe level of -30 m.

Notably, the partial factors incorporating model uncertainty are consistently lower when compared to those in Table (6.6), Table (6.12), and Table (6.18). This reduction in partial factors can be attributed to the elevated importance factor of the uncertainty factor, $\theta_{m;i}$, in each failure mechanism equation. Consequently, this reduces the significance of other stochastic parameters' importance factors. Similar to the previous section, same patterns emerge, such as the close resemblance of values between $Z_{\text{GEO;passive}}$ and $Z_{\text{STR;yield}}$. Moreover, for these two failure mechanisms, all partial factors for parameters exhibit lower values than those in the Eurocode, except for a well-fitting c and a higher value for γ_{sat}.

Table 6.22: Partial factors for the failure equation $Z_{\text{GEO;passive}}$ with water head inclusion parameters (-30 m).

$Z_{\text{GEO;passive}}$	β :	3.44						
Variable	Soil layer	SI	$X_{k;i}$	$X_{d;i}$		Partial Factors		
-	-	-	-	Uncorr.	Corr.	Uncorr.	Corr.	EC
γ_{unsat}	Sand 1	kN/m^3	18.50	18.72	18.72	0.99	0.99	1.00
γ_{sat}	Sand 3	kN/m^3	19.50	18.71	18.71	1.04	1.04	1.00
ϕ	Sand 3	°	35.00	33.93	33.29	1.03	1.05	1.15
c	Clay 2	kPa	10.02	8.75	8.95	1.15	1.12	1.15
δ	Sand 3	°	23.33	25.00	22.21	0.93	1.05	1.15
k_1, k_2, k_3	Clay 1 (K_{b3})	kN/m^3	1447.52	1274.75	1194.4	1.14	1.21	1.30
Variable	Force	SI	$F_{k;i}$	$F_{d;i}$		Partial Factors		
-	-	-	-	Uncorr.	Corr.	Uncorr.	Corr.	EC
Loads Perm.	$F_{\text{selfweight30}}$	kN	527.18	534.56	527.30	1.01	1.00	1.00
Loads Var.	$Q_{\text{surcharge}}$	kN/m^2	100.00	104.53	102.88	1.05	1.03	1.00

Table 6.23: Partial factors for the failure equation $Z_{\text{STR;yield}}$ with water head inclusion parameters (-30 m).

$Z_{\text{STR;yield}}$	β :	3.73						
Variable	Soil layer	SI	$X_{k;i}$	$X_{d;i}$		Partial Factors		
-	-	-	-	Uncorr.	Corr.	Uncorr.	Corr.	EC
γ_{unsat}	Sand 1	kN/m^3	18.50	18.76	18.76	0.99	0.99	1.00
γ_{sat}	Sand 3	kN/m^3	19.50	18.61	18.61	1.05	1.05	1.00
ϕ	Sand 3	°	35.00	33.45	32.72	1.05	1.07	1.15
c	Clay 2	kPa	10.02	8.73	8.98	1.15	1.12	1.15
δ	Sand 3	°	23.33	25.00	21.83	0.93	1.07	1.15
k_1, k_2, k_3	Clay 1 (K_{b3})	kN/m^3	1447.52	1274.76	1177.06	1.14	1.23	1.30
Variable	Force	SI	$F_{k;i}$	$F_{d;i}$		Partial Factors		
-	-	-	-	Uncorr.	Corr.	Uncorr.	Corr.	EC
Loads Perm.	$F_{\text{selfweight30}}$	kN	527.18	534.56	527.30	1.01	1.00	1.00
Loads Var.	$Q_{\text{surcharge}}$	kN/m^2	100.00	104.53	102.88	1.05	1.03	1.00

Table 6.24: Partial factors for the failure equation $Z_{\text{STR;anchor}}$ with water head inclusion parameters (-30 m).

$Z_{\text{STR;anchor}}$	β :	3.33						
Variable	Soil layer	SI	$X_{k;i}$	$X_{d;i}$		Partial Factors		
-	-	-	-	Uncorr.	Corr.	Uncorr.	Corr.	EC
γ_{unsat}	Sand 1	kN/m^3	18.50	18.91	18.91	0.98	0.98	1.00
γ_{sat}	Sand 2	kN/m^3	18.00	17.14	17.13	1.05	1.05	1.00
ϕ	Sand 2	°	30.00	27.22	26.49	1.10	1.13	1.15
c	Clay 3	kPa	10.02	8.77	8.90	1.14	1.13	1.15
δ	Sand 2	°	20.00	20.78	17.67	0.96	1.13	1.15
k_1, k_2, k_3	Sand 2 (K_{b3})	kN/m^3	5428.18	4780.33	4342.20	1.14	1.25	1.30
Variable	Force	SI	$F_{k;i}$	$F_{d;i}$		Partial Factors		
-	-	-	-	Uncorr.	Corr.	Uncorr.	Corr.	EC
Loads Perm.	$F_{\text{selfweight30}}$	kN	527.18	534.56	527.30	1.01	1.00	1.00
Loads Var.	$Q_{\text{surcharge}}$	kN/m^2	100.00	104.53	102.88	1.05	1.03	1.00

In the case of $Z_{STR;\text{anchor}}$, the values approach those in the Eurocode when considering correlated partial factors. Again the higher partial factors between the uncorrelated and correlated are been selected.

6.2 Cost Estimation & CO_2 Emissions

In order to give a more complete approach to the whole scope of the problem, a rough cost estimation has been conducted in order to evaluate the difference in materials, primarily in tons of steel. The most distinct approach is to reduce the total wall height of the structure. To complement this approach, also the CO_2 emissions of the construction material have been calculated for the starting construction project, where the toe is at -31.5 m and at -28 m. Regarding CO_2 emissions, the values include production, realisation, equipment, demolition (kg CO_2), the values have been estimated with a tool created at Royal Haskoning DHV (Vreman and de Vries, 2022) in Table (6.26), Table (6.27), Table (6.28). A comparison was also established from a rough estimation coming from bibliography. It does not include the costs of engineering, bottom protection, fendering and dredging in front of the quay.

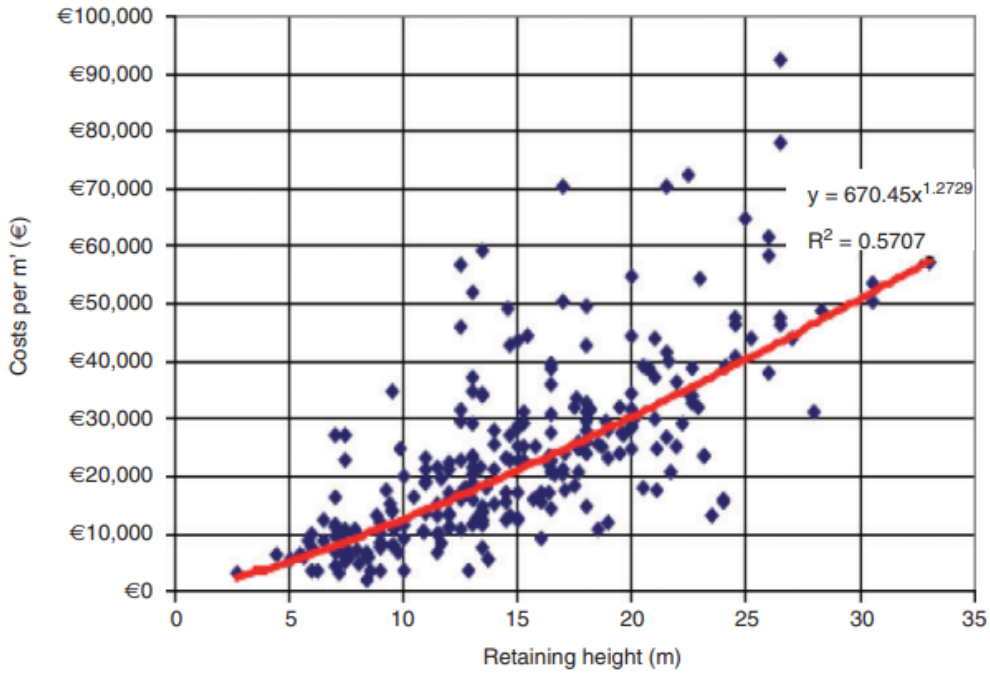

Figure 6.8: Relationship between retaining height and costs. Source: Adapted from (de Gijt J.G, 2010)

In our analysis, we aim to extract valuable insights from Figure (6.8), taking into account the existing retaining height of 18.25 meters. One noticeable trend is that the cost per square meter tends to increase as the retaining height rises. The increase in cost with rising retaining heights can be ascribed to a multitude of influential factors. With

an increased retaining height, the material quantities also increase, involving larger wall profiles, enhanced foundation requirements, and additional structural elements. Foremost among these is the intensified demand for resources and power in the construction process, essential for reaching deeper into the underlying soil layers. This heightened requirement necessitates the utilization of specialized equipment, including longer piles and enhanced structural support, which invariably results in elevated project costs. Additionally, the extension of project timelines further contributes to the cumulative expenses.

Taking into account the two optimization scenarios: one without model uncertainty and the other with included uncertainty. Figure (6.8) would need to be expanded, to follow the trend line. For the three cases: (a) Current construction, (b) Optimized design with 10 % model uncertainty (c) Optimized design with no model uncertainty. Though the retaining high is the same for all cases, only a resulted cost can be estimated for the retaining height of 18.25 m. By the Figure (6.8), the cost per m' is around 28.000 € and the resulted cost is 511,000 €. For 100 m of quay wall the final value is 51,100,000 €.

In the next pages the results from the tool are going to be presented again for the three total wall heights. In Table (6.26), Table (6.27), Table (6.28) it is easily detectable the factors that have been included and one that could differentiate from the value of 51,100,000 € is the lack of the installation costs, only focusing on raw material costs and expanding them in also the CO_2 emissions. The unit price stem from values by the tool based on the date of the publish 11/03/2022, so the values are not up to date, but it can serve as a valuable tool to compare the values. An important point to note is that the value of steel changes every day, so an assumption is already there, since the oil price is changing and there are huge variations through the calendar year. The final results are depicted comparatively in Table 6.25.

Table 6.25: Material cost calculations for different total wall heights (Tool) (100 m of quay wall)

Total Wall Height	Result Cost (€) (100 m)	Material Cost per m^2	CO_2 Emission Total (kg CO_2)	CO_2 Emission per m^2 (kg CO_2)
35.50 m	1,592,143 (-)	15,924	1,531,200 (-)	15,312
34.00 m	1,533,643 (3.7% ↓)	15,336	1,492,084 (2.5% ↓)	14,921
32.00 m	1,457,143 ((8.5% ↓)	14,571	1,437,142 (6% ↓)	14,371

When lowering the total wall height from 35.50 meters to 34.00 meters, the following changes occur: Firstly, the cost in euros decrease from 1,592,143 to 1,533,643, resulting in a substantial cost reduction of 58,500.00 euros. Additionally, this reduction in total wall height leads to a decrease in CO_2 emissions from 1,531,200 kg to 1,492,084 kg, resulting in a substantial reduction of 39,116.00 kg in CO_2 emissions. In the case of lowering the total wall height from 35.50 meters to 32 meters without any associated uncertainty, further cost and emissions reductions are realized. The cost in euros decreases from 1,592,143 to 1,457,143, resulting in a substantial cost reduction of 135,000 euros. Similarly, the CO_2 emissions decrease from 1,531,200 kg to 1,437,142 kg, leading to a reduction of 94,058 kg

in CO_2 emissions. These changes underscore the impact of total wall height adjustments on both cost and environmental considerations. A crucial distinction to note is that the second table exclusively focuses on the raw material costs, without factoring in installation expenses.

Table 6.26: Cost Estimation and CO_2 Total Emissions with quay wall toe at -31.5 m

Description	Quantity	Unit	Unit Price (€)	Total Price (€)	CO_2 ITEM	CO_2 emission total (kg CO_2)
Supplying pipe pile 1420-20 mm, length 35.5 m, total 37 pieces	908	ton	**€ 1,500.00**	**€ 1,362,000**	Steel profile, non-galvanized	**1,249,598**
Diameter	1,420.00	mm	-	-	-	-
Wall thickness	20	mm	-	-	-	-
Length	35.5	m	-	-	-	-
Intermediate sheet type	AZ 18-10-10	-	-	-	-	-
Intermediate sheets	2	st	-	-	-	-
H.O.H. Distance	2,694.00	mm	-	-	-	-
Quantity	37	st	-	-	-	-
Supply and installation of sheet pile lock C9	**1,683.50**	**m**	**€ 55.00**	**€ 92,593**	Steel sheet pile - Interlock C9, 9.3 kg/m	**30,063**
Supplying pipe pile 1420-20 mm, length 35.5 m, total 37 pieces	**131**	**ton**	**€ 1,050.00**	**€ 137,550**	Steel sheet pile	**251,539**
Type	AZ18-10-10	-	-	-	-	-
Weight per single sheet	77.8	kg/m	-	-	-	-
Length	22.25	m	-	-	-	-
Single (1), double (2), or triple (3) intermediate sheet	2	st	-	-	-	-
Number of struts	37	st	-	-	-	-
Number of single sheets	74	st	-	-	-	-
Final Costs	-	-	-	**€1,592,143**	-	**1,531,200**

Table 6.27: Cost Estimation and CO_2 Total Emissions with quay wall toe at -30.00 m (10% uncertainty)

Description	Quantity	Unit	Unit Price (€)	Total Price (€)	CO_2 ITEM	CO_2 emission total (kg CO_2)
Supplying pipe pile 1420-20 mm, length 34.00 m, total 37 pieces	869	ton	**€ 1,500.00**	**€ 1,303,500**	Steel profile, non-galvanized	**1,208,380**
Diameter	1,420.00	mm	-	-	-	-
Wall thickness	20	mm	-	-	-	-
Length	34	m	-	-	-	-
Intermediate sheet type	AZ 18-10-10	-	-	-	-	-
Intermediate sheets	2	st	-	-	-	-
H.O.H. Distance	2,694.00	mm	-	-	-	-
Quantity	37	st	-	-	-	-
Supply and installation of sheet pile lock C9	**1,683.50**	**m**	**€ 55.00**	**€ 92,593**	Steel sheet pile - Interlock C9, 9.3 kg/m	**30,287**
Supplying pipe pile 1420-20 mm, length 34.00 m, total 37 pieces	**131**	**ton**	**€ 1,050.00**	**€ 137,550**	Steel sheet pile	**253,417**
Type	AZ18-10-10	-	-	-	-	-
Weight per single sheet	77.8	kg/m	-	-	-	-
Length	22.25	m	-	-	-	-
Single (1), double (2), or triple (3) intermediate sheet	2	st	-	-	-	-
Number of struts	37	st	-	-	-	-
Number of single sheets	74	st	-	-	-	-
Final Costs	-	-	-	**€1,533,643**	-	**1,492,084**

Table 6.28: Cost Estimation and CO_2 Total Emissions with quay wall toe at -28 m (no uncertainty)

Description	Quantity	Unit	Unit Price (€)	Total Price (€)	CO_2 ITEM	CO_2 emission total (kg CO_2)
Supplying pipe pile 1420-20 mm, length 32 m, total 37 pieces	818	ton	**€ 1,500.00**	**€ 1,227,000**	Steel profile, non-galvanized	**1,125,739**
Diameter	1,420.00	mm	-	-	-	-
Wall thickness	20	mm	-	-	-	-
Length	32	m	-	-	-	-
Intermediate sheet type	AZ 18-10-10	-	-	-	-	-
Intermediate sheets	2	st	-	-	-	-
H.O.H. Distance	2,694.00	mm	-	-	-	-
Quantity	37	st	-	-	-	-
Supply and installation of sheet pile lock C9	**1,683.50**	**m**	**€ 55.00**	**€ 92,593**	Steel sheet pile - Interlock C9, 9.3 kg/m	**30,063**
Supplying pipe pile 1420-20 mm, length 32 m, total 37 pieces	**131**	**ton**	**€ 1,050.00**	**€ 137,550**	Steel sheet pile	**251,539**
Type	AZ18-10-10	-	-	-	-	-
Weight per single sheet	77.8	kg/m	-	-	-	-
Length	22.25	m	-	-	-	-
Single (1), double (2), or triple (3) intermediate sheet	2	st	-	-	-	-
Number of struts	37	st	-	-	-	-
Number of single sheets	74	st	-	-	-	-
Final Costs	-	-	-	**€1,457,143**	-	**1,407,341**

6.3 Incorporating Optimization into the Current Construction

In the effort to enhance profitability and functionality at the Port of Rotterdam, various strategic approaches can be explored. These strategies aim to extract the maximum advantage from the existing structures, whether it involves accommodating larger vessels or enhancing cargo handling to augment revenue streams. Four distinctive scenarios have been examined with a common goal of realizing the construction's full potential. Transitioning to probabilistic design can offer these additional benefits.

To establish the failure equation mechanisms as per Table (5.1), the results are going to be presented, without and with the model uncertainty, $\theta_{m;i}$, separately which will also contribute to a comparison of both results. The value of which is again 0.10. Considering the results by the previous sections, the induced uncertainty should be taken into account for the correct interpretation of the results. Considering the value $F_{\text{rd;anchor}}$ is going to be capped at 1980 kN of the original design. An essential consideration is the integral role played by water levels in the process of optimizing the design. The COV of Q_1 is assumed 0.13, similar to the first case, and reaches a COV of 0.10 at Q_{50}. The loads are increased in steps, by changing the characteristic value for each case.

6.3.1 Universal increase of loads in structure

In the first case, a universal increase of the loads in the structure was explored, in Table (6.30), the specific values of the loads used are presented:

Table 6.29: Universal Increase in Stochastic Structural Variables

Universal Increase 1x			
$Q_{\text{surcharge}}$	kN/m^2	100	104.49
Q_{crane}	kN/m^2	40	41.80
F_{bollard}	kN	-155	-95.97
Universal Increase 2x			
Variable Name	SI	Char. Value	Mean
$Q_{\text{surcharge}}$	kN/m^2	200	208.98
Q_{crane}	kN/m^2	80	83.60
F_{bollard}	kN	-310	-191.94
Universal Increase 2.5x			
Variable Name	SI	Char. Value	Mean
$Q_{\text{surcharge}}$	kN/m^2	250	261.22
Q_{crane}	kN/m^2	100	104.49

Table 6.29 – Continued

Variable Name	SI	Char. Value	Mean
$F_{bollard}$	kN	-387.5	-239.93
Universal Increase 3x			
Variable Name	SI	Char. Value	Mean
$Q_{surcharge}$	kN/m^2	300	313.47
Q_{crane}	kN/m^2	120	125.39
$F_{bollard}$	kN	-465	-287.91

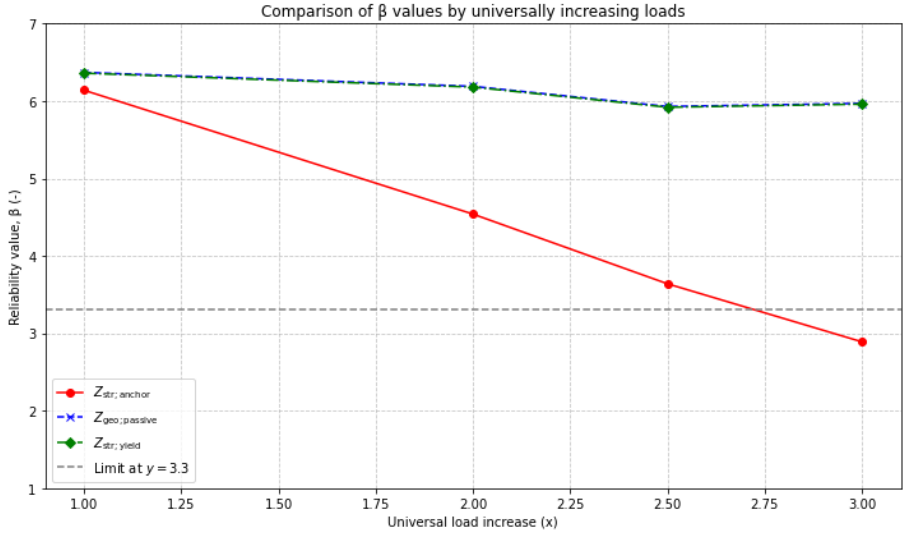

Figure 6.9: Impact of universal increase in load to structural integrity of quay wall, with no model uncertainty.

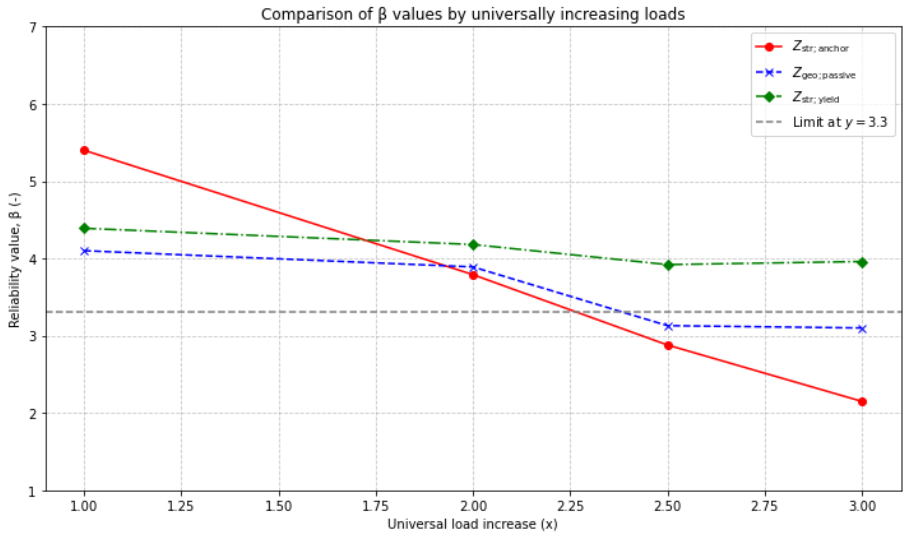

Figure 6.10: Impact of universal increase in load to structural integrity of quay wall, with induced model uncertainty.

As indicated in Figure (6.9) and Figure (6.10), it can be discerned that for the case of the $Z_{\text{geo;passive}}$ and $Z_{\text{str;yield}}$, the universal load increase is not so influential to the reliability index as it is for the $Z_{\text{str;anchor}}$. Anchor failure is more likely to occur than the other two failure mechanisms and it is more difficult to detect. $Z_{\text{geo;passive}}$ failure exhibits warning signs, which are underwater, so it is also difficult to detect, but it can be detected by extensive active mobilisation by apron settlement. $Z_{\text{str;yield}}$ failure exhibits again warning signs by the yield of the quay wall , but $Z_{\text{str;anchor}}$ lacks a discernible warning system. The anchor exhibits a ductile failure mechanism that occurs when the anchor exceeds its pullout capacity. Considering the failure mechanisms that have been taken into account, it can be concluded that a safe universal increase of all structural loads would involve multiplying the original load by 2.8 when the model uncertainty is not taken into account, whereas for a value of 2.25 when the model uncertainty is taken into account. The increased universal load can be visualized as extra container loads that could be stored (cargo) or the bigger ships that could be accommodated that would exert higher forces in the bollards.

6.3.2 Increase of bollard force in structure

In this subsection, we investigate the influence of solely focusing on increasing the bollard force by an *n*x value. Again the Gumbel distribution characteristic values as well as mean values are going to be depicted.

Table 6.30: Bollard Force Increase in Stochastic Structural Variables

Bollard Increase 1x			
Variable Name	SI	Char. Value	Mean
F_{bollard}	kN	-155	-95.97
Bollard Increase 2x			
Variable Name	SI	Char. Value	Mean
F_{bollard}	kN	-310	-191.94
Bollard Increase 3x			
Variable Name	SI	Char. Value	Mean
F_{bollard}	kN	-465	-287.91
Bollard Increase 4x			
Variable Name	SI	Char. Value	Mean
F_{bollard}	kN	-620	-383.89
Bollard Increase 4.5x			
Variable Name	SI	Char. Value	Mean
F_{bollard}	kN	-697.5	-431.87

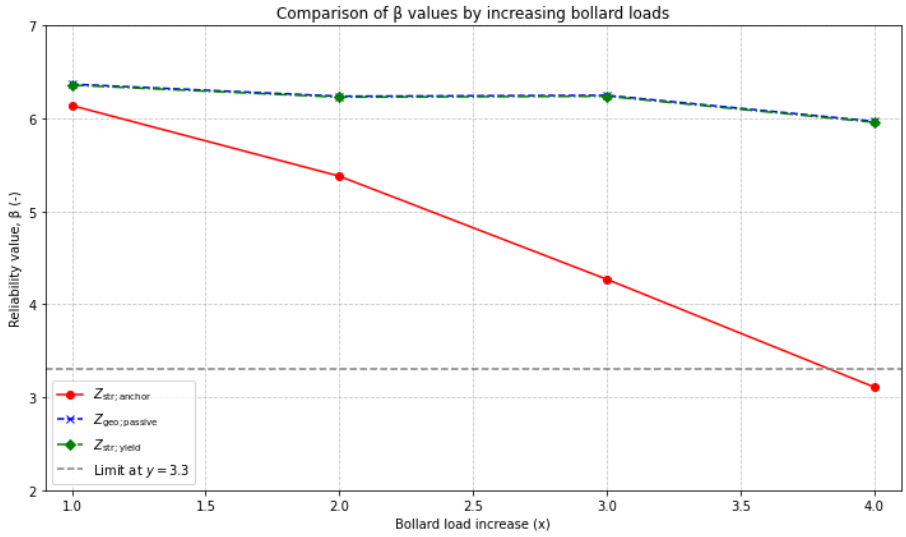

Figure 6.11: Impact of bollard loading increase to structural integrity of quay wall, with no model uncertainty.

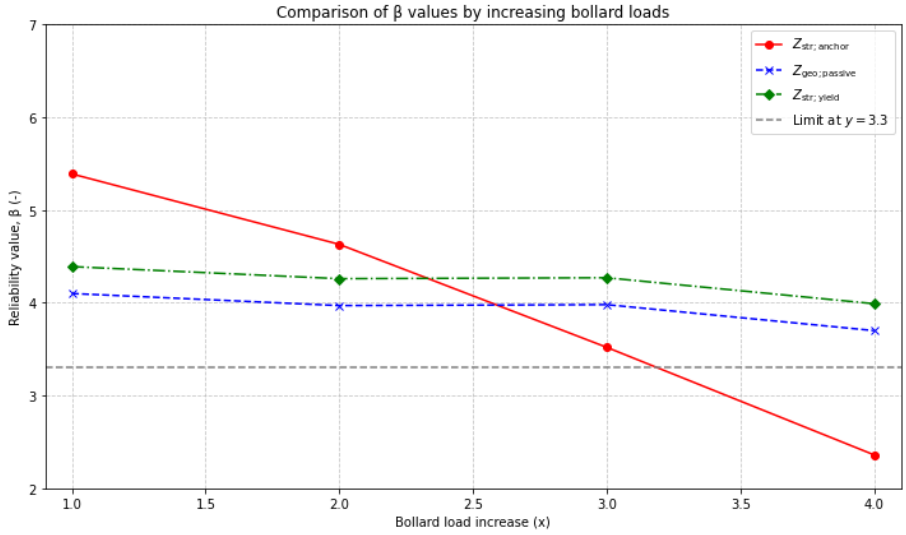

Figure 6.12: Impact of bollard loading increase to structural integrity of quay wall, with induced model uncertainty.

In this case, it is imperative that again the $Z_{\text{str;anchor}}$ failure, is the most dangerous failure mechanism at -31.5 meters. Also since the bollard has only been increased alone, the value of the bollard could be increased safely to a value of 3.75 times with no model uncertainty and 3.15 times with induced model uncertainty.

6.3.3 Increase of surcharge loads ("terrain loads") in structure

In this subsection, we investigate the influence of solely increasing the terrain load by a factor of n. We again depict the Gumbel distribution characteristic values and mean values.

Table 6.31: Terrain Load Increase in Stochastic Structural Variables

Terrain Load Increase 1x			
Variable Name	SI	Char. Value	Mean
$Q_{surcharge}$	kN/m^2	100	104.49
Q_{crane}	kN/m^2	40	41.80
Terrain Load Increase 2x			
Variable Name	SI	Char. Value	Mean
$Q_{surcharge}$	kN/m^2	200	208.98
Q_{crane}	kN/m^2	80	83.60
Terrain Load Increase 3x			
Variable Name	SI	Char. Value	Mean
$Q_{surcharge}$	kN/m^2	300	313.47
Q_{crane}	kN/m^2	120	125.39
Terrain Load Increase 4x			
Variable Name	SI	Char. Value	Mean
$Q_{surcharge}$	kN/m^2	400	417.96
Q_{crane}	kN/m^2	160	167.18
Terrain Load Increase 5x			
Variable Name	SI	Char. Value	Mean
$Q_{surcharge}$	kN/m^2	500	522.44
Q_{crane}	kN/m^2	200	208.98
Terrain Load Increase 6x			
Variable Name	SI	Char. Value	Mean
$Q_{surcharge}$	kN/m^2	600	626.93
Q_{crane}	kN/m^2	240	250.77

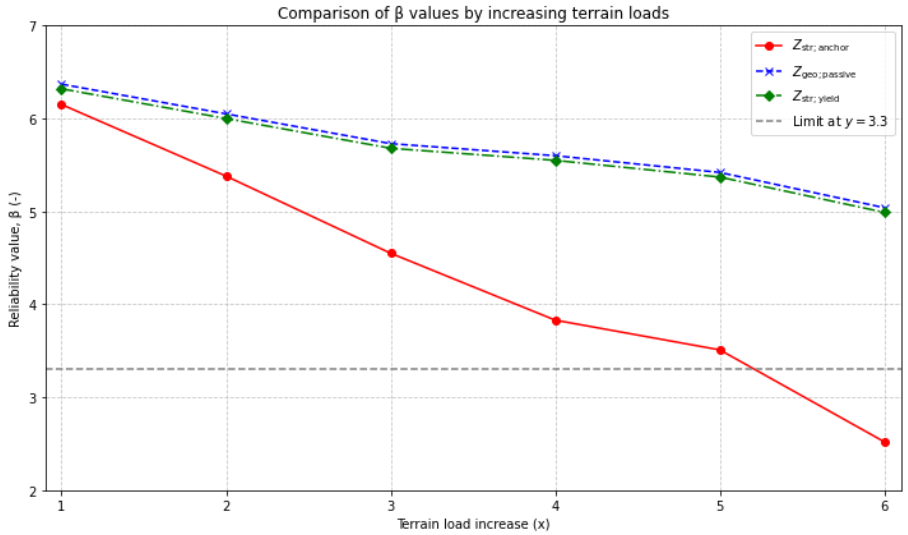

Figure 6.13: Impact of terrain loading increase to structural integrity of quay wall, with no model uncertainty.

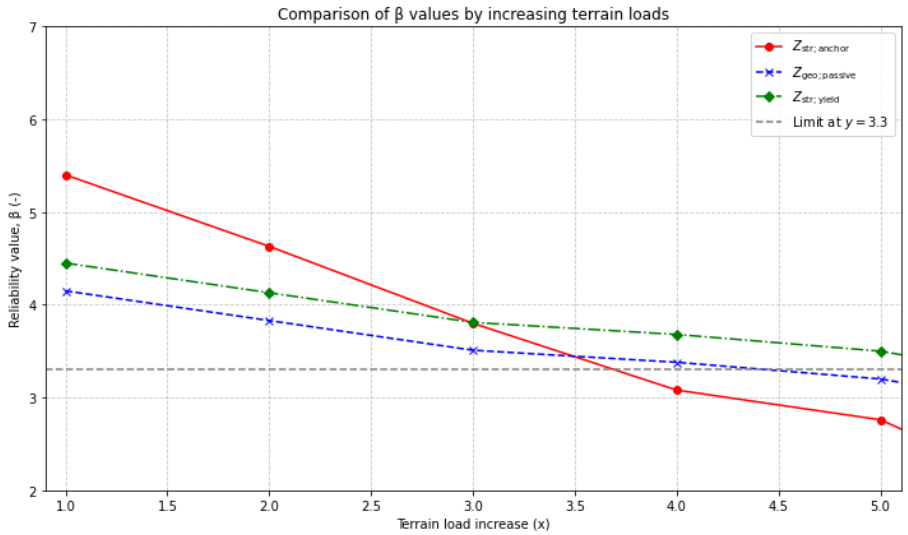

Figure 6.14: Impact of terrain loading increase to structural integrity of quay wall, with induced model uncertainty.

It is safe to assume that the terrain load can be increased up to 5.2 times until failure, when no model uncertainty is taken into account, whereas this falls to a value of 3.65, when model uncertainty is induced in the model.

6.3.4 Deepen the quay wall on the sea side

Finally, perhaps the most important case would be to deepen the quay wall on the sea side, so basically excavating from the starting depth of -14.25 meters and gradually increasing by 1 meter to track the difference in the reliability index.

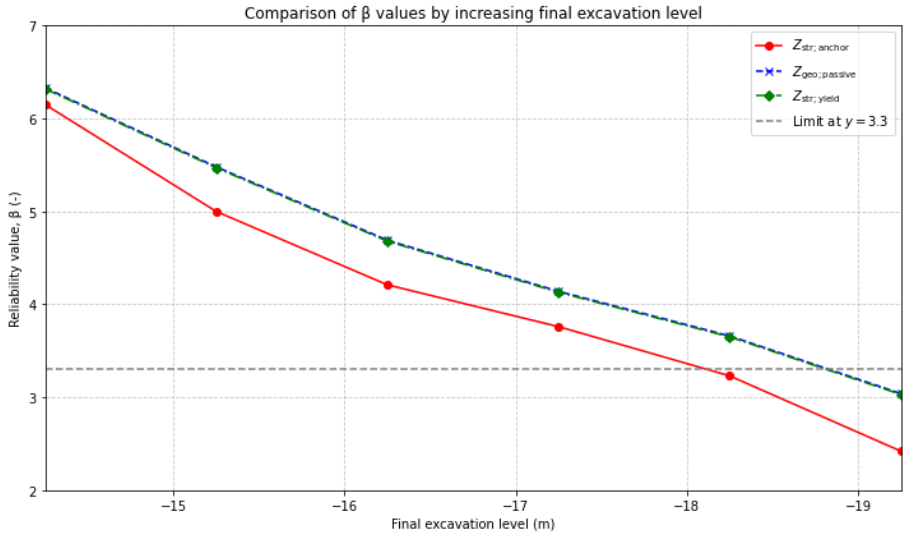

Figure 6.15: Impact on final excavation level increase to structural integrity of quay wall, with no model uncertainty.

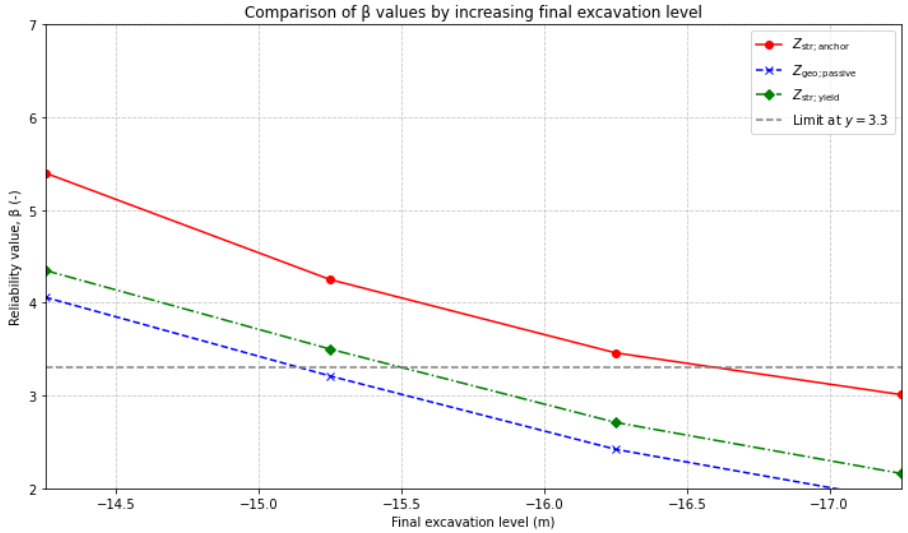

Figure 6.16: Impact on final excavation level increase to structural integrity of quay wall, with induced model uncertainty.

It is illustrated that focusing on these 3 failure mechanism equations, the final depth of the quay wall on the sea side could increase by 3.75 meters, when no model uncertainty is taken into account. Though when the model uncertainty is applied, the final excavation can be increased by 0.85 meters.

7

Conclusions and Recommendations for future research

In the final chapter, the outcomes of the research are been discussed as well as recommendations for future studies. The objective of the thesis was to analyze the impact of soil parameter uncertainties and partial factors on quay wall design, with the ultimate goal of improving design efficiency, safety, and sustainability while minimizing costs.

7.1 Conclusions

The primary objectives of this thesis encompassed four distinct research questions, each formulated to guide our comprehensive investigation into modern Quay Wall design optimization. These research inquiries serve as cornerstones for the research conducted, providing a structured approach to our analysis:

1. **How can reliability-based analysis be used to optimize a modern Quay Wall design, and what are the key considerations in reliability-based design?**

   Reliability-based analysis is a crucial tool for optimizing quay wall designs. This thesis has examined the most critical factors in the design process. By incorporating reliability-based design, a deeper understanding of the structure can be achieved, which could provide optimizations in safety and sustainability.

   By this approach the inherent uncertainty in both geotechnical and structural aspects of quay wall design is been acknowledged, which can end up in more resilient and adaptable designs of structures. In this thesis, the primary focus was into geotechnical uncertainty, considering a broad scope that incorporates all soil parameters as stochastic variables. To better understand the soil-structure interaction of quay walls.

   The key considerations for incorporating reliability-based analysis into modern Quay Wall design revolve around gathering extensive geotechnical and structural data

required for problem setup. This approach, which is informed by existing research and the insights of the design company, is an integral part of current design practices. One crucial factor is the need for a wealth of geotechnical and structural information to formulate the problem effectively. Due to the heightened complexity, it is essential to strike a balance between ensuring maximum accuracy by considering numerous parameters and streamlining the process to meet project timelines and maintain cost-effectiveness. Additionally, it is crucial to pay close attention to the coefficient of variation for stochastic variables and their correlations. Even stochastic soil variables that did not have a high importance factor on the case design when they are uncorrelated, through their correlations with other stochastic variables they can be fundamental in the derivation of partial factor, which can be higher than the current design code specifications. Eurocode employs uncorrelated partial factors. However given that in the current case study the correlations between the parameters stem from statistical determination of correlation factors the use of correlated partial factors is also valid. By incorporating correlated partial factors a more realistic representation in the system can be offered. Thus, understanding and managing these relationships are essential to prevent errors in the analysis. As reliability based design approach is incorporated into engineering practices, the challenge of computational speed becomes evident. Running an analysis on D-Sheet Piling can provide rapid results, but the transition to reliability analysis using Probabilistic Toolkit is more resource-intensive. Therefore, addressing the computational demands is crucial for the successful integration of reliability-based analysis into design practices.

2. **How can a semi/full probabilistic design approach be implemented, and establish a repository for reliability index values, β?**

   This thesis comprehensively explored various probabilistic design approaches, necessitating an initial decision regarding whether to adopt a Level II (semi-probabilistic design) or a Level III (fully probabilistic design) approach. Extensive literature review and practical experimentation led to the realization that exclusively pursuing a comprehensive Level III design would prove excessively time-consuming. The reliance on Monte Carlo approaches alone was deemed impractical due to encountered errors, particularly the generation of "not a value" (NAN) results, which pointed to issues in assessing limit state values. It is worth noting that the Probabilistic Toolkit was still in beta version at the time of the research, and addressing this issue could be related to the software development stage.

   Through the literature review, it became evident that the First Order Reliability Method (FORM), classified as a Level II method, stood out as an appropriate approach for evaluating limit state functions linked to the two failure equations under investigation. The preference for $FORM$ primarily stems from its significantly

shorter computational time when compared to Level III methods, like Monte Carlo simulations.

Nevertheless, it is crucial to acknowledge the limitations of the $FORM$ method, particularly its reduced accuracy when dealing with non-normal distributions and non-linear limit states. Given that the thesis involved scenarios characterized by non-linear and non-normally distributed cases, the failure probabilities estimated through $FORM$ should be regarded as approximations of the exact failure probabilities. To mitigate this, a Level III approach can be considered for more accurate evaluations.

Based on the results and the experience gained from numerous simulations, it can be concluded that $FORM$ yielded notable outcomes. In most cases, reliability index value, β, converged successfully on a differential reliability less than 0.01, suggesting minimal error at the design points. The number of iterations varied, with some runs being time-consuming, involving up to 400 iterations. The most time-consuming iterations were associated with the $Z_{GEO;passive}$ and $Z_{STR;yield}$ failure equation. As an illustrative example, with all six cores active on a laptop, $Z_{GEO;passive}$ with six soil layers converged in approximately 30 minutes to two hours, while $Z_{STR;anchor}$ required between 20 to 40 minutes.

3. **How do the results obtained from the probabilistic design approach compare to the current EC partial factors approach, and what are the differences in the design results obtained from the two approaches?**

   Partial factors in the Eurocode are uncorrelated. Therefore, when comparing the results, it is best to directly assess them against the uncorrelated partial factors. However, given the statistical determination of correlation factors from the region around the port of Rotterdam, it is valid to consider the correlated partial factors as well. Utilizing correlated partial factors can offer a more realistic portrayal of the system. Correlated partial factors tend to be more conservative. In order to be on the safe side, the higher value of partial factor between the uncorrelated and correlated value is going to be determined the one to be adopted for the current structure. If partial factors are below 1, it suggests a conservative estimation of the parameter.

   In Table 7.1 , the final partial factors are been illustrated determined for all three failure mechanisms that the quay wall has been subjected to. The predominant failure mechanism is $Z_{\text{GEO;passive}}$ and $Z_{STR;yield}$, given that for $Z_{STR;\text{anchor}}$, the limit value of $F_{\text{rd;anchor}}$ is based on the previous two failure mechanisms. It is important to note that these partial factor values represent the maximum ratios and are not uniform across all soil layers and materials. As discussed in the preceding chapter, probabilistic design calculations primarily depend on three to four key soil parameters based on the importance factors.

Table 7.1: Partial factors for all failure equation mechanisms in models with all variables as stochastic (no model uncertainty)

Failure Mechanism:	$Z_{GEO;passive}$		$Z_{STR;yield}$		$Z_{STR;anchor}$		
Variable	**Partial Factors**						
-	**Uncorr.**	**Corr.**	**Uncorr.**	**Corr.**	**Uncorr.**	**Corr.**	**EC**
γ_{unsat}	0.98	0.98	0.98	0.98	0.96	0.96	1.00
γ_{sat}	1.09	1.10	1.09	1.09	1.06	1.06	1.00
ϕ	1.07	1.14	1.08	1.15	1.19	1.22	1.15
c	1.17	1.10	1.18	1.10	1.14	1.13	1.15
δ	0.96	1.14	0.96	1.14	0.96	1.22	1.15
k_1, k_2, k_3	1.14	1.34	1.14	1.34	1.14	1.28	1.30
Load Permanent, un	1.01	1.01	1.01	1.01	1.01	1.01	1.00
Load Variable, un	1.03	1.01	1.03	1.01	1.03	1.05	1.00

It is important that the absence of other benchmark cases for the analysis can not directly indicate the global applicability of the conclusions, but the conclusions are specific for the current case study. Also the model has not be subjected to all the available failure mechanism equations, thus the conclusions are based on the current three. Also a remark is based on the assumption that the quay wall toe level was set at -28.00 m and the value is not exactly 3.30 at the target set value of RC1, especially for$Z_{\text{GEO;passive}}$ and $Z_{STR;yield}$ the respective β are close to RC2 target value of 3.80. If the quay wall toe level at a higher point (-27.8m) the partial factor values would be lower as the result of the lower reliability index value and more aligned with the values of RC1. This could indicate an extra conservatism, which is already included in the Eurocode.

For unsaturated unit weight, γ_{unsat}, it can be identified that the value of Eurocode is a good fit, considering that the value is lower than 1. For this parameter, as it has been stated is based on the only soil layer, which extends above groundwater level.

For saturated unit weight, γ_{sat}, it can be identified that a partial factor, should be included. Since for all three failure equation mechanisms the value is higher 1, which the most notables $Z_{\text{GEO;passive}}$ and $Z_{STR;yield}$, with values close to 1.10.

For angle of internal friction, ϕ, $Z_{\text{GEO;passive}}$ and $Z_{STR;yield}$ appear to be well-fitted to Eurocode value, considering the correlated partial factors, though on the uncorrelated partial factors are much lower. $Z_{STR;\text{anchor}}$ on the other side, has a higher value than the Eurocode for both its uncorrelated and correlated values.

For effective cohesion, c, it can be identified that $Z_{\text{GEO;passive}}$ and $Z_{STR;yield}$ have higher uncorrelated partial factors and lower correlated partial factors than the Eurocode respectively. For $Z_{STR;\text{anchor}}$ the values for both the uncorrelated and the correlated cases are a bit lower than EC value, but well-fit.

For angle of shearing resistance, δ, $Z_{\text{GEO;passive}}$ and $Z_{STR;yield}$ appear again to be fitted to the value by the Eurocode, whereas the value value is lower than 1 in the uncorrelated case. Considering $Z_{STR;\text{anchor}}$ a similar trend appears for the uncorrelated case, whereas the correlated value is higher than the Eurocode. It is important to be stated, that since δ has a direct correlation with ϕ, the correlated values are the same for both.

For subgrade reaction modulus, k_1, k_2, k_3, $Z_{\text{GEO;passive}}$ and $Z_{STR;yield}$ is a bit higher than the value of EC for the correlated partial factors whereas for $Z_{STR;\text{anchor}}$ the value is a bit lower. Across all three failure mechanisms the same value can be identified for the uncorrelated case, which is lower than 1.30.

In terms of permanent and variable loads, the values consistent across all three failure mechanisms on the permanent load case, with the value almost the same as EC value. Considering the variable loads, in the uncorrelated case the values are consistent again, with a value higher than 1.00. For $Z_{\text{GEO;passive}}$ and $Z_{STR;yield}$ the correlated value is lowered close to 1, whereas for $Z_{STR;\text{anchor}}$ the value is increased to 1.05. It can be identified that for permanent loads unfavorable the value is almost the same.

Table 7.2: Partial factors for all failure equation mechanisms in models with all variables as stochastic (model uncertainty)

Failure Mechanism:	$Z_{GEO;passive}$		$Z_{STR;yield}$		$Z_{STR;anchor}$		
Variable	**Partial Factors**						
-	**Uncorr.**	**Corr.**	**Uncorr.**	**Corr.**	**Uncorr.**	**Corr.**	**EC**
γ_{unsat}	0.99	0.99	0.99	0.99	0.98	0.98	1.00
γ_{sat}	1.04	1.04	1.05	1.05	1.05	1.05	1.00
ϕ	1.03	1.05	1.05	1.07	1.10	1.13	1.15
c	1.15	1.12	1.15	1.12	1.14	1.13	1.15
δ	0.93	1.05	0.96	1.07	0.96	1.13	1.15
k_1, k_2, k_3	1.14	1.21	1.14	1.23	1.14	1.25	1.30
Load Permanent, un	1.01	1.00	1.01	1.00	1.01	1.00	1.00
Load Variable, un	1.05	1.03	1.05	1.03	1.05	1.03	1.00

In the case where the model uncertainty is taken into account, the quay wall toe level is set at -30.00 , though in this case the value is much closer to the target value of RC1 for the cases of $Z_{\text{GEO;passive}}$ and $Z_{STR;yield}$, with their values 3.44 and 3.33 respectively. In the case when the model uncertainty is taken into account, the values of the partial factors are in general lower compared to the no model uncertainty case. This can be attributed to the uncertainty factor which has a high importance factor for all three failure mechanisms. Therefore the values have a higher deviation to the Eurocode values compared to the previous case.

4. **How can we improve the current design during the design phase to achieve cost optimization? Furthermore, what alternatives are available for further refining the existing structure to maximize optimization potential?**

The analysis has revealed that analyzing the results of the three failure mechanism equations, it is possible to reduce the toe level of the quay wall in the case study by 3.50 meters when the model uncertainty is at 0% and 1.50 meters when the model uncertainty is at 10%. It is important to state that these results do not the take vertical bearing capacity into account, which can be governing for the results. The financial implications, specifically the material costs (steel), and the corresponding reduction in the carbon footprint have been quantified. It is important to note that this calculation does not factor in installation costs, which could further affect these values.

Furthermore, the research explores a range of alternatives for transitioning to probabilistic design. This involves increasing the loads by a factor 'n' for three distinct scenarios and investigating the deepening of the quay wall on the sea side as a final option, where the structure functional capacity can be enhanced.

In order to grasp completely the topic, the following sub-questions were also answered:

a. How were the partial factors derived in the Eurocode for quay walls, and what simplifications were used in the derivation process?

   The safety factors for sheet pile walls have been established through a comprehensive study conducted by Fugro/Geodelft (2004). In the case of quay walls, the foundational study conducted by Wolters (2012) served as the basis for determining safety factors.

   Derivation of partial factors in the Eurocode for quay walls is a process, with many different aspects which has its roots on the principles of load and resistance factor design. This approach applies partial factors to loads and material resistances, with the aim to keep structural safety in the construction while addressing uncertainties. The Eurocode encompasses both ultimate and serviceability limit states, offering a comprehensive safety philosophy calibrated to target specific levels of reliability. Reliability analysis plays a pivotal role in estimating the probabilities of failure for distinct structural components and limit states.

   Eurocode simplifies various aspects to enhance practicality in its application. Some of these simplifications involve treating materials as homogeneous, assuming uniformity in soil layers. Load models are also simplified by not considering all possible load combinations. Additionally, certain statistical assumptions are made, such as considering a constant yield strength for steel. Furthermore, Eurocode does not ac-

count for time-dependent effects, like steel corrosion. Expert consultation, structural testing, and historical data validation are essential aspects of the derivation process.

b. Which are the most influential parameters in the design, how are they correlated?

It is important to highlight that the most influential parameters in a reliability analysis of a quay wall are not globally the same, but are subjected to the case study and are site specific. In light of this, the most influential parameters in the current research, for $Z_{\text{GEO;passive}}$ and $Z_{STR;yield}$, are ϕ (influences the mobilized shear resistance of the soil), γ (influences lateral earth pressure and the mobilized resistance), and the water levels considering their resulted importance factors after the analysis. Furthermore, the parameter δ emerges through correlations as highlighted in the correlation index table. Notably, the most influential parameter is discernible within the soil layer's ϕ value where slip surface failure may occur.

Shifting our focus to the second equation, $Z_{STR;anchor}$, the same parameters hold significant influence (high importance factor). The paramount parameter can be identified as the ϕ and γ values within the soil layer, Sand 2, which leads to a larger mobilization of the active wedge, consequently increasing the load on the anchor.

Considering the correlations between the variable it is important to imply that they are based on Table (5.12). These are site specific correlations for Port of Rotterdam. Taking into account this assumption ,ϕ and γ, are moderately positively correlated with each other, with a correlation coefficient of 0.5. This indicates that when one variable increases by a certain amount, the other variable tends to increase by a moderate amount.

c. What achievable improvements can be made to engineering practice to enhance reliability design in quay walls?

Enhancing the reliability of quay wall design is of paramount importance, as it directly impacts the long-term performance, safety, and economic viability of these critical maritime structures. As a geotechnical engineer, I firmly believe that for achieving this goal it is essential to begin with thorough site investigation and soil characterization. Over time, specific sites, like the Port of Rotterdam, continue to be reused for various construction projects. Accumulating a comprehensive database of soil information for these sites becomes invaluable for future designs, enabling engineers to make informed decisions and mitigate potential geotechnical challenges. This wealth of knowledge serves as a foundation for informed decision-making and ensures that each new project benefits from the insights gained from past endeavors. In practice, combining advanced techniques like Cone Penetration Testing (CPT), geophysical surveys, and seismic testing in these areas can provide a multifaceted view of the site's geotechnical conditions. These methods offer valuable insights into

potential geohazards that may affect the site, along with detailed information on soil properties and the often non-linear stratigraphy beneath the surface. This approach minimizes the uncertainties associated with critical parameters and sets a solid foundation for the design process. Moreover, while the current research may not have delved into it, a level III probabilistic design approach, such as the Monte Carlo method, offers a path to achieve the highest level of design accuracy. Consequently, the resulting design is not only more precise but also takes into account the unique characteristics and challenges of the specific quay wall being constructed. In essence, enhancing quay wall design reliability is a multidimensional endeavor that begins with a strong foundation of site investigation and progresses through the application of advanced probabilistic design methods. By adopting these practices, quay walls are not merely constructed; they are engineered to meet precise reliability goals.

d. How much is the limit of enhancing the design to provide more sustainable solutions?

Reliability based design has been proven for the current case study to be an effective way to reduce the unnesessary use of materials/resources, and CO2 emmissions in the environment impact, as highlighted in the Cost Estimation & CO_2 Emissions section. When the model uncertainty is taken into account the material costs for 100 m of quay wall the resulted costs are been reduced by 3.7% while the total CO_2 emissions are reduced by 2.5%. While when the model uncertainty is not taken into account, the costs of the material are been reduced by 8.5% and the emissions by 6%. Additionally, the second part of the case study had the focus to incorporate optimization into the current structure. The examination of four scenarios aimed to unlock the full potential of the structure by (a) universal increase of loads in structure, (b) increase of bollard force in structure, (c) increase of terrain loads in structure and (d) deepen the quay wall on the sea side for both incorporated and not incorporated model uncertainty. The results are presented in Table 7.3.

Table 7.3: Increase of a 'x' factor for all different scenarios

Scenario	No Model Uncertainty	Model Uncertainty
(a)	2.8	2.25
(b)	3.75	3.15
(c)	5.2	3.65
(d)	3.75	0.85

In general the limit by which enhanced designs can provide more sustainable solution is a complex and ever-evolving subject. It is dependent on various factors, including the characteristics of the project, the available technology, financial considerations, and societal priorities. It is evident that achieving a high degree of safety in design places a strong emphasis on evaluating potential consequences, which acted as

also the basis of the thesis, where the project should be categorized in an RC/CC category. Though, in the context of quay walls, a partial failure may entail minimal to negligible consequences when compared to the catastrophic loss of human lives resulting from structural failure (cost of human life compared to partial structure failure cost).

Government regulations and policies wield significant influence in delineating the frontiers of sustainability. As environmental awareness grows (Sustainable Development Goals), regulations tend to become more detailed, driving the demand for increasingly sustainable designs. To learn about sustainability in structural safety, it might be necessary to start with pilot projects. These pilot constructions can serve as valuable testbeds, allowing engineers to gather insights, learn from real-world experiences, and continually refine their practices for future projects.

7.2 Recommendations for future research

In extension of the current work done, in this thesis a set of recommendations are going to be set for future research:

1. Extending the current research to encompass the remaining failure mechanism equations ($Z_{\text{STR;yield;land}}$, $Z_{\text{STR;yield;water}}$ where both account for ultimate limit state for the steel stress in combi-wall and $Z_{STR;\text{ buckling}}$) which accounts for ultimate limit state for the buckling stress in combi-wall a logical progression. Also, incorporating all variables within the failure mechanism equations as stochastic rather than deterministic. This approach entails treating each variable as a random parameter with associated uncertainties, offering a more comprehensive analysis of the quay wall's behavior under various conditions.

2. As this analysis has been conducted on the assumption that the model behavior is elastic in D-Sheet Piling. Rerun the analysis on the assumption of plastic model behavior and compare the results.

3. Exploring the reliability calculation method involving response surfaces is worth further investigation. This methodology relies on response surfaces to predict model responses, essentially reducing the computational effort.

4. While it may not yet be implemented in practical design, given the inherent variability and subsurface conditions, an approach to account for different sheet pile structures along a cross-section can have huge benefits. This can offer not only further cost optimization but also valuable insights into the complex soil-structure interactions and the interactions of different quay wall structures (different structural properties) within the project.

5. A comprehensive, fully probabilistic Level III design is essential for reassessing the outcomes of current practices and highlighting disparities in the calculations. It is advisable to explore the potential differences between the FORM equation and the Monte Carlo approach as a means of quantifying these variations. Understanding these differences is crucial for refining the probabilistic design methodology and ensuring its accuracy in practical applications.

6. Considering an alternative approach involving the usage of Plaxis in the analysis could be more time-consuming, it offers more accurate results compared to D-Sheet Piling. This trade-off between time and accuracy should be carefully evaluated to determine the most suitable analysis method for the specific project requirements

7. While it may not be the most suitable choice for a thesis topic, an extension focused on the application of 3D software, such as Plaxis 3D, for reliability assessment holds promise. In this way also the spatial variability in the out of plane direction can be included as part of the analysis. This research avenue offers the potential for more accurate outputs, enhancing the reliability of quay wall designs and contributing valuable insights for real-world construction projects in the future.

Background Design Information

A.1 Soil Classification and Properties

type of soil		characteristic mean value of the soil parameters												
name	admixture	consistency [1]	γ [2] [kN/m^3]	γ_{sat} [kN/m^3]	q_c [3] [6] [MPa]	C'_p [6]	C'_s	C_c [6]	C_a [5]	C_{sw} [6]	E_{100} [6] [7] [MPa]	ϕ' [6] [°]	c' [kPa]	f_{undr} / c_u [kPa]
Gravel	little silty	loose medium dense	17 18 19 or 20	19 20 21 or 22	15 25 30	500 1,000 1,200 or 1,400	– – –	0.008 0.004 0.003 or 0.002	0 0 0	0.003 0.002 0.001 or 0	75 125 150 or 200	32.5 35 37.5 or 40	–	–
	very silty	loose medium dense	18 19 20 or 21	20 21 22 or 22.5	10 15 25	400 600 1,000 or 1,500	– – –	0.009 0.006 0.003 or 0.002	0 0 0	0.003 0.002 0.001 or 0	50 75 125 or 150	30 32.5 35 or 40	–	–
Sand	clean	loose medium dense	17 18 19 or 20	19 20 21 or 22	5 15 25	200 600 1,000 or 1,500	– – –	0.021 0.006 0.003 or 0.002	0 0 0	0.007 0.003 0.001 or 0	25 75 125 or 150	30 32.5 35 or 40	–	–
	little silty/clayey very silty/clayey		18 or 19 18 or 19	20 or 21 20 or 21	12 8	450 or 650 200 or 400	– –	0.008 or 0.005 0.019 or 0.009	0 0	0.003 or 0.001 0.006 or 0.001	25 or 35 20 or 30	27 or 32.5 25 or 30	–	–
Silt [4]	little sandy	soft medium stiff	19 20 21 or 22	19 20 21 or 22	1 2 3	25 45 70 or 100	650 1,300 1,900 or 2,500	0.168 0.084 0.049 or 0.030	0.004 0.002 0.001	0.056 0.028 0.017 or 0.005	2 5 10 or 20	27.5 or 30 27.5 or 32.5 27.5 or 35	0 2 5 or 7.5	50 100 200 or 300
	very sandy		19 or 20	19 or 20	2	45 or 70	1,300 or 2,000	0.092 or 0.055	0.002	0.031 or 0.005	5 or 10	27.5 or 35	0 or 2	50 or 100
Clay	clean	soft medium stiff	14 17 19 or 20	14 17 19 or 20	0.5 1.0 2.0	7 15 25 or 30	80 160 320 or 500	1.357 0.362 0.168 or 0.126	0.013 0.006 0.004	0.452 0.121 0.056 or 0.042	1 2 4 or 10	17.5 17.5 17.5 or 25	0 10 25 or 30	25 50 100 or 200
	little sandy	soft medium stiff	15 18 20 or 21	15 18 20 or 21	0.7 1.5 2.5	10 20 30 or 50	110 240 400 or 600	0.759 0.237 0.126 or 0.069	0.009 0.005 0.003	0.253 0.079 0.042 or 0.014	1.5 3 5 or 10	22.5 22.5 22.5 or 27.5	0 10 25 or 30	40 80 120 or 170
	very sandy		18 or 20	18 or 20	1.0	25 or 140	320 or 1,680	0.190 or 0.027	0.004	0.063 or 0.025	2 or 5	27.5 or 32.5	0 or 2	0 or 10
	organic	soft medium	13 15 or 16	13 15 or 16	0.2 0.5	7.5 10 or 15	30 40 or 60	1.690 0.760 or 0.420	0.015 0.012	0.550 0.250 or 0.140	0.5 1.0 or 2.0	15 15	0 or 2 0 or 2	10 25 or 30
Peat	not preloaded	soft	10 or 12	10 or 12	0.1	5 or 7.5	20 or 30	7.590 or 1.810	0.023	2.530 or 0.600	0.2 or 0.5	15	2 or 5	10 or 20
	medium preloaded	medium	12 or 13	12 or 13	0.2	7.5 or 10	30 or 40	1.810 or 0.900	0.016	0.600 or 0.300	0.5 or 1.0	15	5 or 10	20 or 30
Variation coefficient			0.05		–	0.25						0.10	0.20	

Table A.1: Correlation between soil classification and corresponding soil properties. Source: Adapted from NEN (2016)

A.2 CPT Information

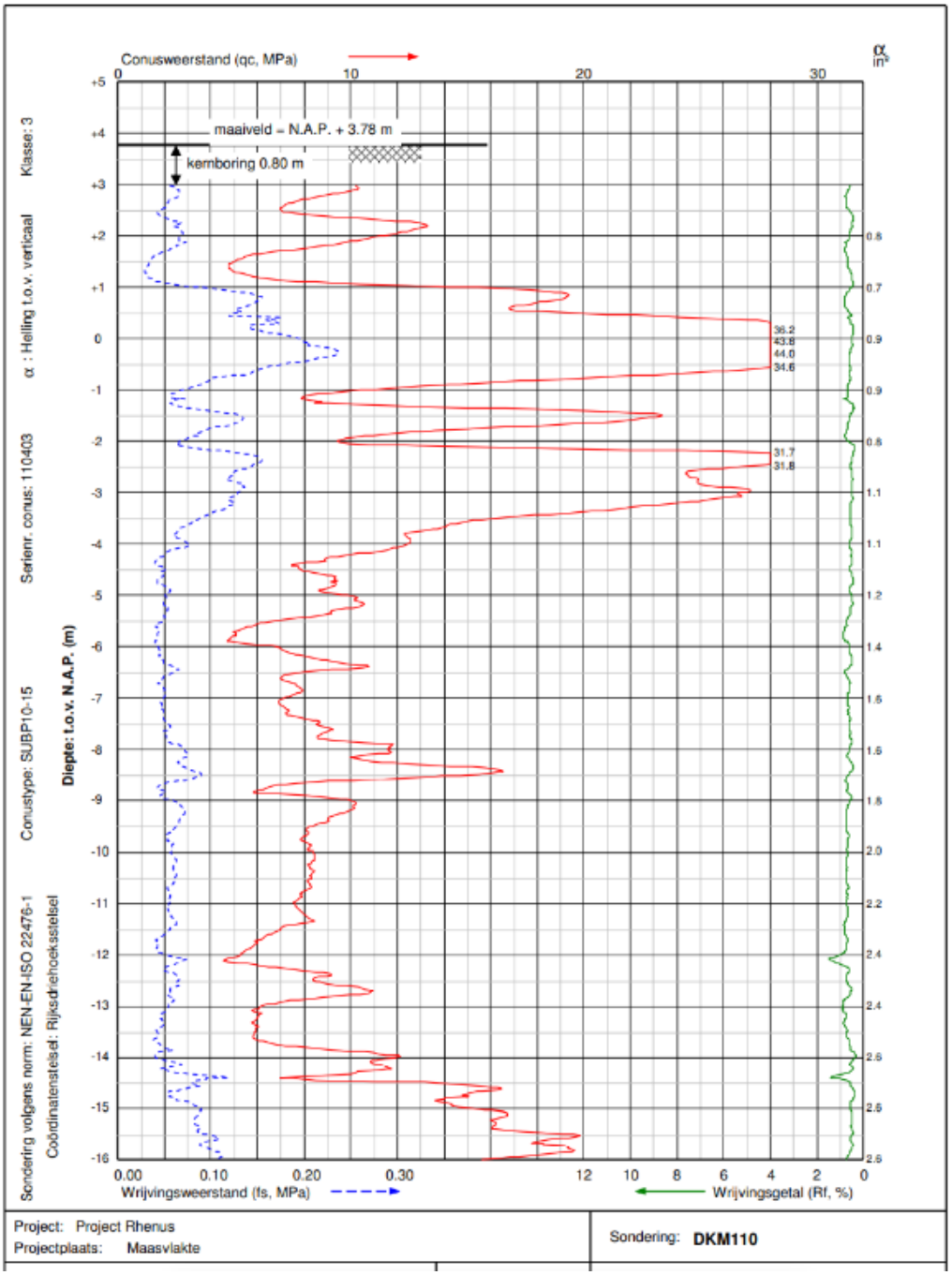

Figure A.1: CPT DKM110 results 1/3

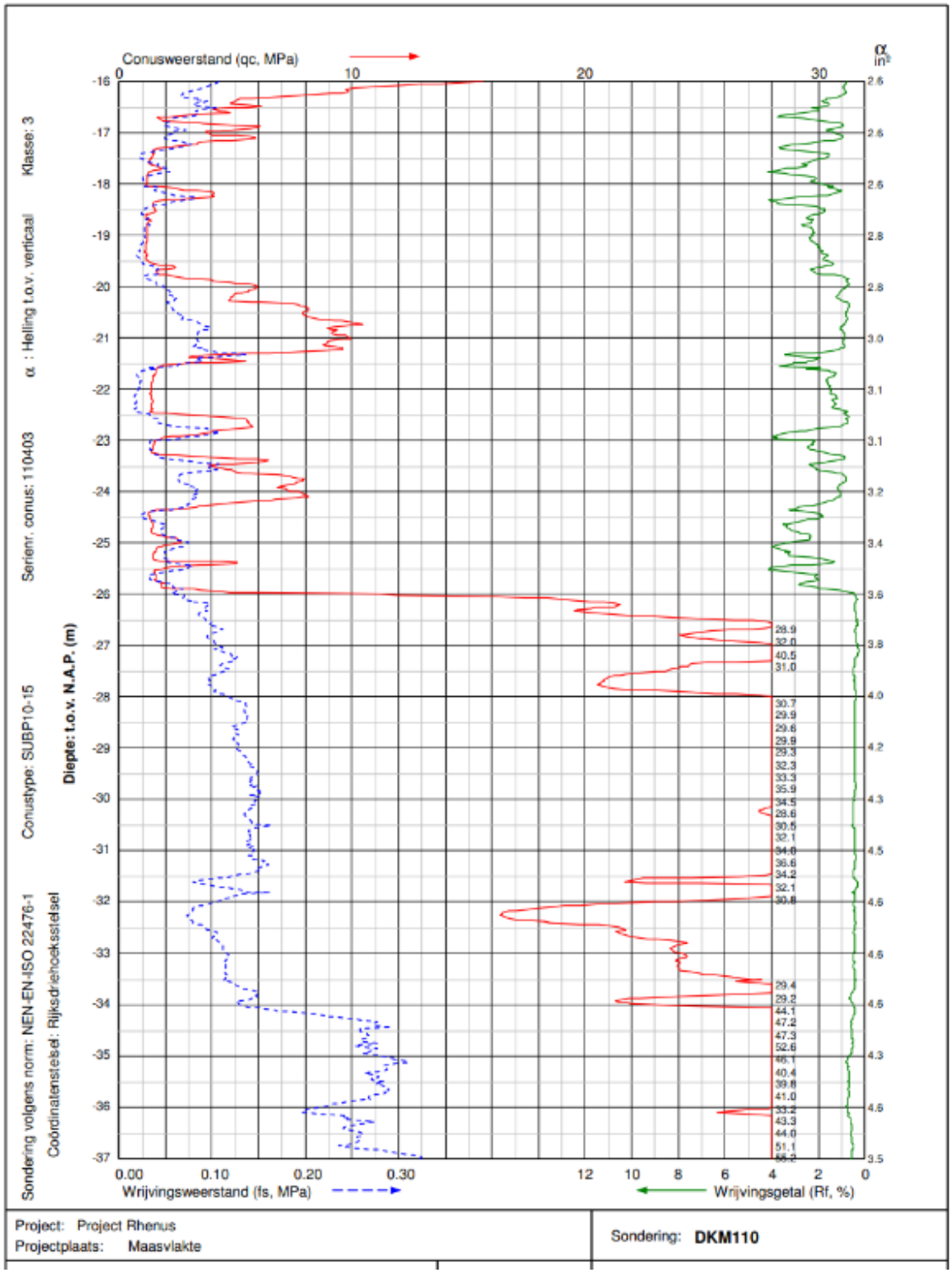

Figure A.2: CPT DKM110 results 2/3

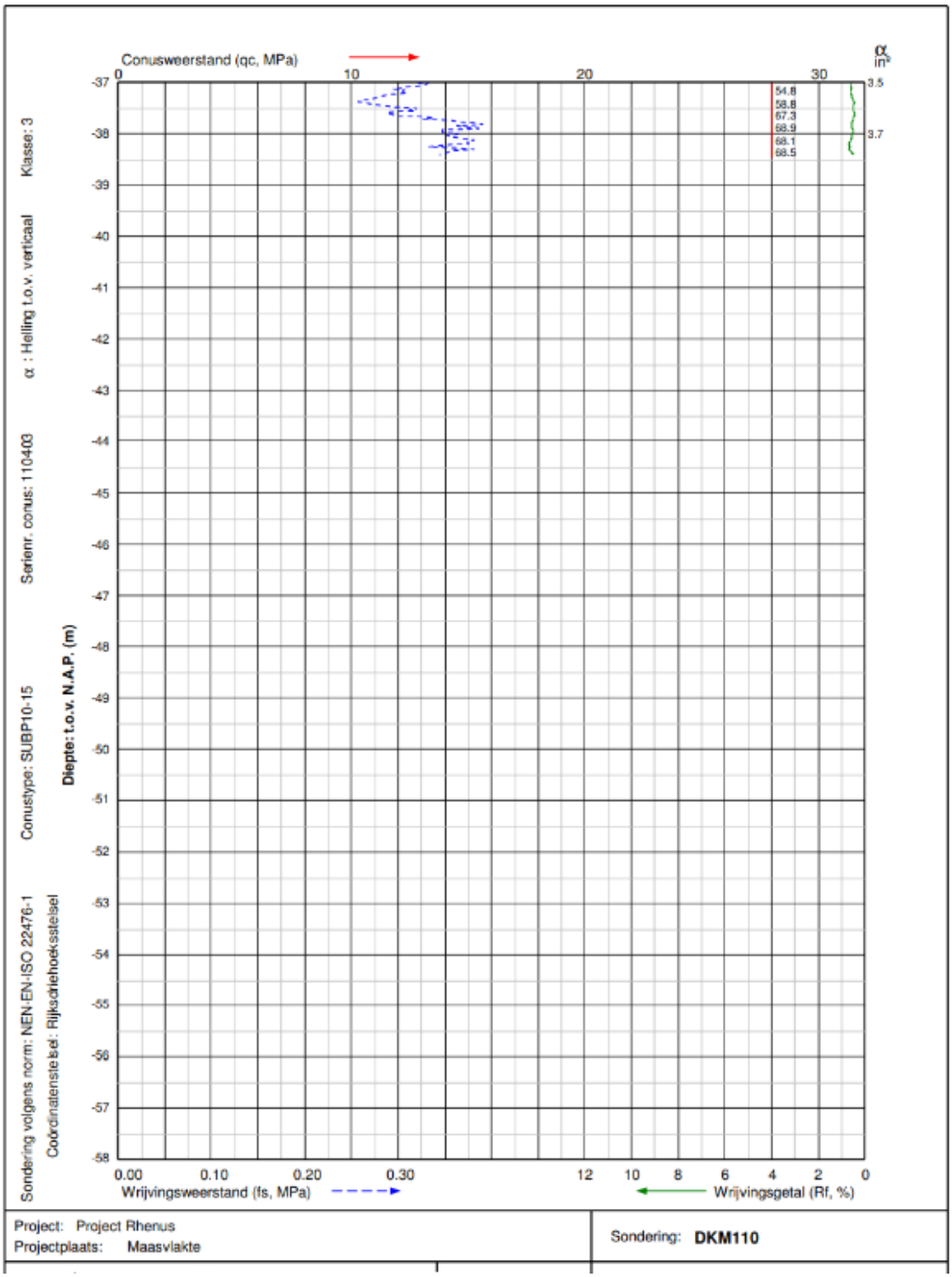

Figure A.3: CPT DKM110 results 3/3

A.3 Comparative analysis of two modelling methods

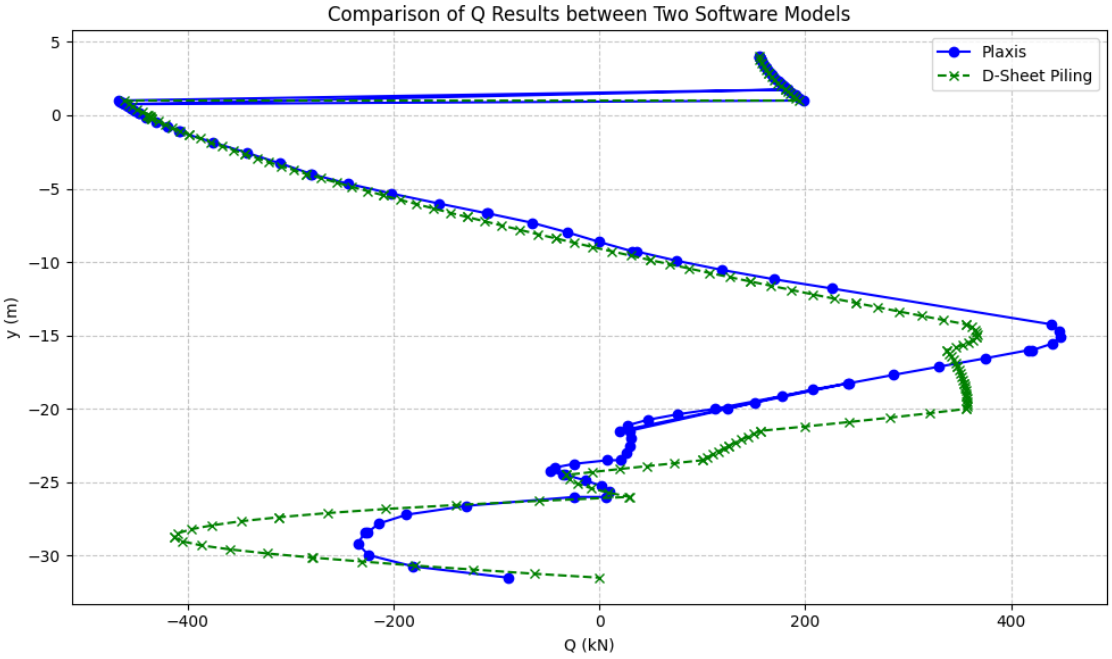

(a) Comparative results for Q for load combination B for D-Sheet Piling and Plaxis.

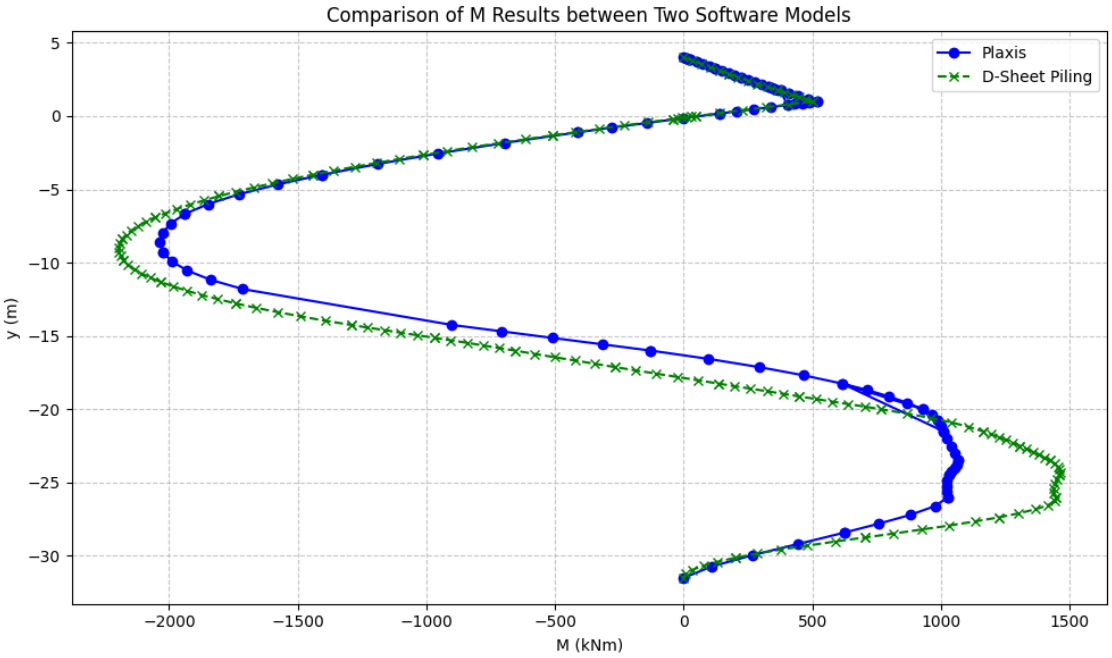

(b) Comparative results for M for load combination B for D-Sheet Piling and Plaxis.

Figure A.4: Comparison of structural components of quay wall for load combination B.

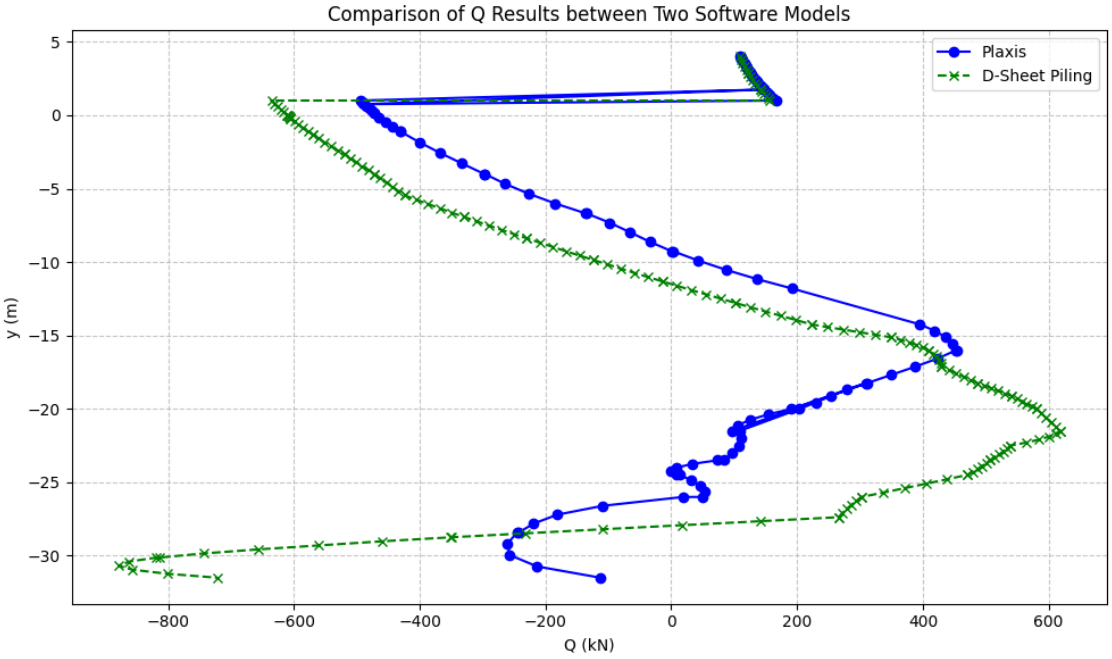

(a) Comparative results for Q for load combination C for D-Sheet Piling and Plaxis.

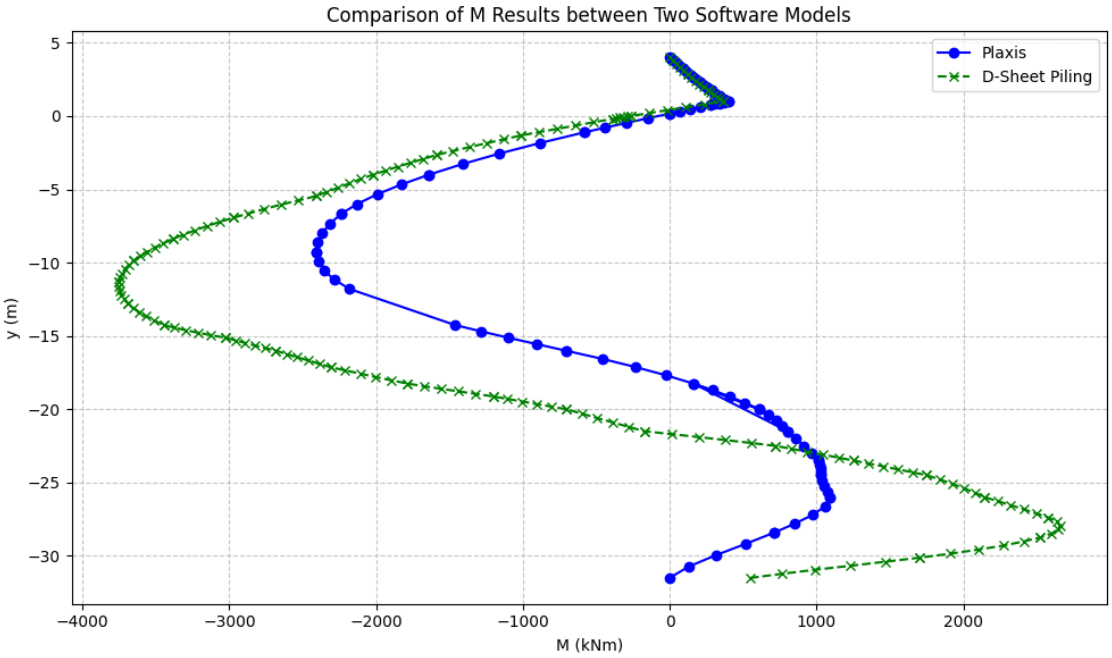

(b) Comparative results for M for load combination C for D-Sheet Piling and Plaxis.

Figure A.5: Comparison of structural components of quay wall for load combination C.

References

AASHTO (1993). *AASHTO Guide for Design of Pavement Structures, 1993*. AASHTO Guide for Design of Pavement Structures. The Association.

Adel, N. (2018). Load testing of a quay wall: An application of bayesian updating. Master's thesis, Delft University of Technology, Delft, The Netherlands.

Allaix, D. L., Ozer, E., Steenbergen, R., Schweckendiek, T., and van der Krogt, M. (2022). Richtlijn bewezen sterkte damwanden en kademuren eindrapport. Technical Report TNO-2022-R11621-11206387-002-GEO-0002, TNO.

ArcelorMittal (n.d.). AZ 18-10/10. Accessed on March 25, 2023.

Ayyub, B. M. and McCuen, R. H. (2003). *Probability, Statistics, and Reliability for Engineers and Scientists*. CRC Press.

Baecher, G. and Christian, J. (2003). *Reliability and Statistics in Geotechnical Engineering*. Wiley.

Benjamin, J. R. and Cornell, A. (1970). *Probability, statistics and decision for civil engineers*. McGraw-Hill Book Company.

Bentley Advancing Infrastructure (2022). *PLAXIS 2D - Material Models Manual*.

Blum, H. (1931). *Einspannungsverhältnisse bei bohlwerken*. Wil. Ernst und Sohn, Berlin, Germany. (in German).

Brinkgreve, R. (2005). Selection of soil models and parameters for geotechnical engineering application. In Yamamuro, J. and Kaliakin, V., editors, *Soil Constitutive Models*, pages 69–98, United States. American Society of Civil Engineers (ASCE). null ; Conference date: 24-01-2005 Through 26-01-2005.

Brinkgreve, R. B. (2022). *Lecture Notes on the Behavior of Soils and Rocks*.

CEN (2004). *Eurocode 2: Design of concrete structures - Part 1-1: General rules and rules for buildings*. Publication date: December 1, 2004. Status: Active. Page Count: 230. ICS Code (Concrete structures): 91.080.40. ICS Code (Technical aspects): 91.010.30.

CUR (2005). *Handbook Quay Walls*. CUR, Gouda, The Netherlands.

CUR (2012). *CUR-publication 166, Sheet pile structures*. CUR, Gouda, The Netherlands, 6th edition. Part 1 and 2, in Dutch only.

De Gijt, J. (1999). Kademuren, verleden, heden en toekomst, ingenieursbureau gemeentewerken rotterdam.

De Gijt, J. (2010). *A History of Quay Walls, Techniques, types, costs and future*. PhD thesis.

De Gijt, J., Horst, H. v. d., Heijndijk, P., and Schaik, C. v. (1993). Quaywall design and construction in the port of rotterdam (1993). PIANC-bulletin no. 80-62, April.

De Gijt, J., Kleef, I., Taneja, P., and Ligteringen, H. (2010). Development of container handling in the port of rotterdam.

De Gijt, J. G. and Broeken, M. L. (2013). *Quay Walls: Second Edition*, volume 1. CRC Press, sbrcurnet publication, 211e edition.

de Gijt J.G (2010). *A History of Quay Walls*. PhD thesis, Technische Universiteit Delft.

Deltares (2020). *D-Sheet Piling, User Manual*. Available online at: URL_of_the_manual.

Deltares (2023). *Probabilistic Toolkit User Manual*. Deltares, Boussinesqweg 1, 2629 HV Delft, The Netherlands, 2.0 edition.

Diermanse, F., Jongejan, R., and Leeuw, A. D. (2016). Wbi - onzekerheden. Technical Report 1220080-001, Rijkswaterstaat - WVL.

ERTC10: Evaluation of Eurocode 7 (2021). Second generation of eurocode 7, Improvements and Challenges[Webinar]. International society for soil mechanics and geotechnical engineering. https://vimeo.com/619946919.

Fenton, A. G., Naghibi, F., Dundas, D., Bathurst, J., and Griffiths, D. V. (2016). Reliability-based geotechnical design in 2014 canadian highway bridge design code. *Canadian Geotechnical Journal*, 53:236–251.

Fugro/Geodelft (2004). *Probabilistische Berekeningen Onderdeel 7.1Bc*.

Gouw, D. T.-L. (2014). Common mistakes on the application of plaxis 2d in analyzing excavation problems.

Griffiths, D. V. and Fenton, G. A. (2007). *Probabilistic Methods in Geotechnical Engineering*. SpringerWienNewYork.

Gulvanessian, H. (2001). En1990 eurocode - basis of structural design. *Proceedings of The Institution of Civil Engineers-civil Engineering - PROC INST CIVIL ENG-CIVIL ENG*, 144:8–13.

Hemel, M.-J., Korff, M., and Peters, D. J. (2022). Analytical model for laterally loaded pile groups in layered sloping soil. *Marine Structures*, 84:103229.

Heténi, M. and Hetbenyi, M. I. (1946). *Beams on Elastic Foundation: Theory with Applications in the Fields of Civil and Mechanical Engineering*, volume 16. University of Michigan Press, Ann Arbor, MI.

HTG (2015). *Recommendations of the Committee for Waterfront Structures Harbours and Waterways: EAU 2012*. John Wiley & Sons, 9 edition.

ISO (1998). General principles on reliability for structures. International Standard ISO/IS2394.

JCSS (2006). *JCSS Probabilistic Model Code, Section 3.7: Soil properties*.

Jonkman, S., Steenbergen, R., Morales-Napoles, O., Vrouwenvelder, A., and Vrijling, J. (2018). *Probabilistic Design: Risk and Reliability Analysis in Civil Engineering*. TU Delft, Department Hydraulic Engineering. Collegedictaat CIE4130.

Kanning, W., Teixeira, A., van der Krogt, M., and Rippi, K. (2017). Derivation of the semi-probabilistic safety assessment rule for inner slope stability. Project Report 1230086-009, Deltares, The Netherlands. Calibration STBI 2016.

Korff, M. (2018). Syllabus for cie4363 deep excavations. Lecture notes for the course CIE4363 Deep excavations in the Master of GeoEngineering at Delft University of Technology. August 2018.

Low, B. K. and Phoon, K.-K. (2015). Reliability-based design and its complementary role to eurocode 7 design approach. *Computers and Geotechnics*, 65:30–44.

Lunne, T. and Christophersen, H. (1983). Interpretation of cone penetrometer data for offshore sands. In *Proc. of the Offshore Technology Conference*, Richardson, Texas. Paper No. 4464.

Mahmood, Z., Qureshi, M. U., Memon, Z. A., and Imran Latif, Q. B. a. (2022). Ultimate limit state reliability-based optimization of mse wall considering external stability. *Sustainability*, 14(9).

Meijer, E. (2006). Comparative analysis of design recommendations for quay walls. Master's thesis, Your University's Name.

Meulen, F. (2016). Environmental compensation for port extension: The case of rotterdam harbor and nature compensation, policy and practice. *Renewable Energy and Sustainable Development*, 2:147–153.

NEN (2016). Netherlands standard nen 9997-1: Geotechnical design of structures - part 1: General rules. Standard NEN 9997-1, Nederlands Normalisatie Instituut (NEN), The Hague, Netherlands.

NEN (2017). (nen 9997-1+c2:2017) geotechnisch ontwerp van constructies - deel 1: Algemene regels (geotechnical design of structures - part 1: General rules), in dutch.

NEN (2019). Nen-en 1990+a1+a1/c2:2019. eurocode: Grondslagen voor het constructief ontwerp. Technical Report Report Number, NEN, Delft, The Netherlands.

OCDI (2020). *Technical Standards and Commentaries for Port and Harbour Facilities in Japan*. OCDI.

Perumalsamy, K., Venkatesh, M., and Sundaravadivelu, R. (2015). Soil structure interaction analysis of a dry dock. *Aquatic Procedia*, 4.

Phoon, K. K. and Retief, J. V. (2016). *Reliability of Geotechnical Structures in ISO239*. CRC Press.

Port of Rotterdam (2023). Havenbedrijf Rotterdam N.V. - Samenvatting Jaarverslag 2022. https://reporting.portofrotterdam.com/FbContent.ashx/pub_1011/downloads/v230309104726/Highlights-annual-report-2022-Port-of-Rotterdam-Authority%20goed.pdf.

Post, M., Schweckendiek, T., Roubos, A., and van de Greef, J. (2021). Reliability analysis of quay walls: Exploring a metamodeling approach for more robustness and efficiency. Technical Report 11204256-052-GEO-0003, Deltares.

Rippi, A. and Texeira, A. (2016). Reliability-based assessment of a retaining wall using fem. In *25th European Young Geotechnical Engineers Conference*, Sibiu, Romania.

Roubos, A. and Gijt, d. J. (2013). IABSE 2013, Rotterdam.

Roubos, A. A. (2019). *Enhancing Reliability-Based Assessments of Quay Walls*. PhD thesis, Delft University of Technology.

Roubos, A. A., Allaix, D., Schweckendiek, T., Steenbergen, R. D. J. M., and Jonkman, S. N. (2020). Time-dependent reliability analysis of service-proven quay walls subject to corrosion-induced degradation. *Reliability Engineering & System Safety*.

Sanglerat, G. (1972). *The Penetrometer and Soil Exploration*. Developments in Geotechnical Engineering. Elsevier Science.

Schanz, T., Vermeer, P., and Bonnier, P. (2019). The hardening soil model: Formulation and verification. *Beyond 2000 in Computational Geotechnics*, 16:281–296.

Schneider, H. R. and Schneider, M. A. (2013). Dealing with uncertainties in ec7. In Arnold, P., editor, *Modern Geotechnical Design Codes of Practice*, pages 87–100. IOS Press, Amsterdam.

Schweckendiek, T., Vrouwenvelder, A. C. W. M., Calle, E. O. F., Jongejan, R. B., and Kanning, W. (2012). Partial factors for flood defenses in the netherlands: modern geotechnical codes of practice – development and calibration. In Arnold, P. et al., editors, *Special Geotechnical Publication*. Taylor Francis.

Teixeira, A., Rippi, K., Schweckendiek, T., Brinkman, H., Nuttall, J., Hellebrandt, L., and Courage, W. (2016). Soil-structure interaction – reliability analysis of a retaining wall, 2015. Technical report, Deltares & TNO.

Thoft-Christensen, P. and Baker, M. J. (1982). *Structural Reliability Theory and Its Applications*. Springer Book Archive. Springer Berlin, Heidelberg, 1 edition.

Vreman, C. and de Vries, P. (2022). Co2 emissions calculator for maritime projects. Copyright: ©Royal HaskoningDHV, 2022.

Wel, T. J. v. d. (2018). Reliability-based assessment of quay walls. Master's thesis, Delft University of Technology, Delft, The Netherlands.

Wolters, H. J. (2012). Reliability of quay walls using finite element analysis. Master's thesis, Delft University of Technology, Delft, The Netherlands.

Zekri, A., Ghalandarzadeh, A., Ghasemi, P., and Aminfar, M. H. (2014). Experimental study of remediation measures of anchored sheet pile quay walls using soil compaction. *Journal of Soil Dynamics and Earthquake Engineering*, 67:106–117.